Ca' Foscari
University
of Venice

Master's Degree programme

in Sustainable Chemistry and Technologies
"Second Cycle (D.M. 270/2004)"

Final Thesis

Synthesis and characterization of gold nanorods

Supervisor
Ch. Prof. Patrizia Canton

Graduand
Asia Saorin
Matriculation Number 846281

Academic Year
2017/ 2018

Summary

1 INTRODUCTION

1.1 Nanotechnology

Working within the nano scale (1-100nm) give rises to new physical, chemical, and biological properties of the materials, which are different from both the ones of bulk materials and of individual constituents (atoms or molecules) (Eustis and El-Sayed 2006b).

Chemical and physical properties of matter are, to a large extent, determined by the type of motion the electrons can perform. The kind of the material and the space accessible to the electrons (i.e. degree of confinement) are the factors which determine the electronic motion. In the nanometres scale the spatial effects becomes crucial and, for this reason, nanomaterials show peculiar properties. Since these properties are given by restrictions to the electron motion, they also strongly depend on the shape of the materials as well as dimension and chemical composition (X. Huang, Neretina, and El-Sayed 2009).

Hence a great feature of nanomaterials is the possibility to vary their properties without the need to change their chemical composition but only their shape or size. One example is the colour of noble metal nanoparticles, which is found to be dependent on the shape and size of the nanoparticle and dielectric constant of the surrounding medium (Vincenzo Amendola, Roberto Pilot, Marco Frasconi and Iatì 2017).

Thanks to the small size of nanomaterials, they have a high surface to volume ratio, which is particular interesting in some applications such as catalysis.

Considering the fields of nanomaterial applications, one of the most interesting and studied is within the framework of biological systems. Examples of this kind of applications is the use of nanostructures as drug delivery agents, labelling agents and sensors (Eustis and El-Sayed 2006b).

However, the need for accurate designed structures has led to a huge research in their way of synthesis. Thanks to this effort in the development of new synthetic routes the availability of nanoscale materials is huge, so their applications are possible in many fields and are increasing.

1.2 Gold nanoparticles

Gold nanoparticles (Au NPs) have been widely studied and applied, they are attractive for biomedical use in sensing, drug delivery, cancer therapy, cellular imaging but also they are particular attractive in other research fields such as electronics, catalysis, chemical analysis (Vincenzo Amendola, Roberto Pilot, Marco Frasconi and Iatì 2017).

In the nanotechnology scenario, Au NPs raised great interest due mainly to three reasons(Vincenzo Amendola, Roberto Pilot, Marco Frasconi and Iatì 2017):

1) high chemical and physical stability which allows biocompatibility;
2) easy surface functionalization with organic and biological molecules;
3) numerous optical properties related to surface plasmons.

As an example of the Au NPs stability, there still exists some very old specimens, one of the oldest is represented by a gold-plated Egyptian ivory dating back to the 8th century BC. In this object Au NPs accidentally formed a purple staining by the diffusion of gold from a thin foil into the porous ivory substrate(Vincenzo Amendola, Roberto Pilot, Marco Frasconi and Iatì 2017).

Thanks to the high biocompatibility, colloidal gold has been used for curative purposes since Middle Ages, moreover, it seems that the alchemists' elixir of youth was a gold colloidal solutions called "aurum potabile"(Moores and Goettmann 2006).

Manufactures have been attracted by bright red colour of Au NPs since ancient times, they started to take advantage of Au NPs optical properties for glass and ceramics since ancient times. One of the most fascinating example Au NPs can be found in Lycurgus cup (crafted by Romans in the 4th century) . This cup has the unique properties of changing colour depending on the direction of the illumination.

Michael Faraday was the first scientist to relate the optical properties of Au NPs to their smaller size, during a lecture at the Royal Institute in London entitled "Experimental Relations of Gold (and Other Metals) to Light" in 1852 (Moores and Goettmann 2006).

Many different shapes of Au NPs have been synthesized, among them nanorods are particular interested and have attracted great attention due to their interesting optical properties, the large number of synthetic methods available, the possibility to reach high monodispersity and finally the rational control over the aspect ratio that allows to easily tune their optical properties.

1.3 Surface plasmon resonance in Au NPs

The mean free path for gold d electrons is about 50nm (Eustis and El-Sayed 2006b). In the case of metal particles, surface effects become important and give rise to particular properties when the size of the particle is smaller or comparable to the electron mean free path. Hence, for Au NPs smaller than 50 nm no scattering is expected from the bulk, so all the interactions are expected to be with the surface(X. Huang, Neretina, and El-Sayed 2009).

Collective oscillations of these free electrons in metals are called plasmons and occurred at a well-defined frequency. Plasmon can be described as a negatively charged electron cloud coherently displaced from its equilibrium positions around a lattice made of positively charged ions(Vincenzo Amendola, Roberto Pilot, Marco Frasconi and Iatì 2017).

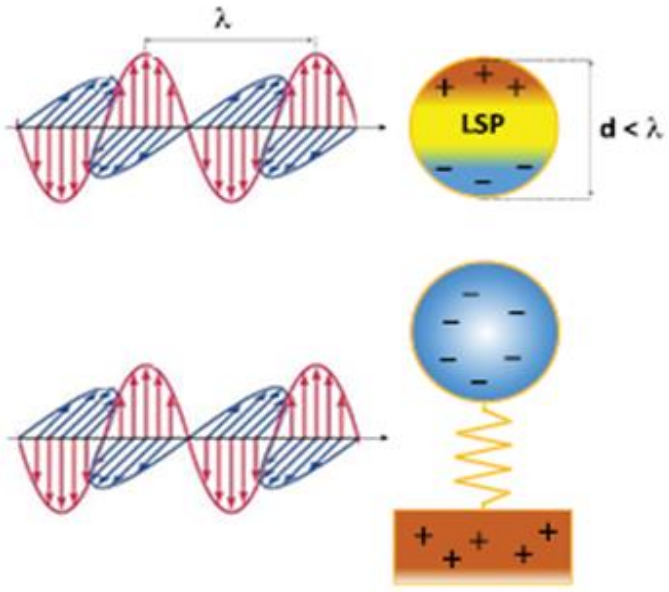

Figure 1Above illustration of a LSPR excited by light in a spherical nanoparticle, below LSPR is represented as a spring-mass harmonic oscillator where free electron density is the equivalent mass

The electrical field of an electromagnetic radiation with a wavelength much larger than metallic nanoparticles can set up standing resonant conditions with the plasmons, while this excitation of plasmon by the electric field of light is not allowed in bulk matter (Moores and Goettmann 2006). As depicted in Figure 1, when the wave front of the light passes, the electron density in the particles is polarized, this coherent displacement of electrons from the positively charged lattice generating a restoring force that pulls the polarized electron back to the lattice. Plasmon in a NPs than be considered as a mass-spring harmonic oscillator driven by the energy resonant light wave, where the electron cloud oscillates like a simple dipole in parallel direction to the electric field of the electromagnetic radiation. In this model the mass of the spring is represented by the electron density and the constant of the spring is set by the coulomb restoring force between the lattice atoms and the electrons, this simple model is often utilized to gain semi-quantitative understanding of plasmonic system.

Plasmons in NPs with size smaller than light wavelength are non-propagating excitations, and since their oscillation is distributed over the whole particle volume they are called localized surface plasmons (LSPs)(Vincenzo Amendola, Roberto Pilot, Marco Frasconi and Iatì 2017).

Considering gold nanospheres (Au NSs) with size much smaller than the wavelength of the light, the metal polarizability can be used to express the distortion of the electron cloud in response to the electric field (Vincenzo Amendola, Roberto Pilot, Marco Frasconi and Iatì 2017).

$$\alpha(\lambda) = 3\varepsilon_m(\lambda)V_{NP}\frac{\varepsilon(\lambda) - \varepsilon_m(\lambda)}{\varepsilon(\lambda) + \chi\varepsilon_m(\lambda)} \qquad (1)$$

λ: light wavelength; ε_m: dielectric constant of the non-absorbing surrounding medium; V_{NP} : nanoparticles volume ; χ: geometrical factor ($\chi = 2$ in the case of sphere); $\varepsilon(\lambda)$: frequency (ω) dependent complex dielectric function

For obtaining the dielectric permittivity in metals, the first developed model was the Drude Model

1.3.1 Drude model

In this model electrons are considered as free particles of a gas (plasma) and it uses the classical statistical distribution of Boltzmann to describe them. This model is an oversimplification of the system and has some limits, but it is an easy tool to understand the plasmon resonance. Dielectric permittivity is described by a complex function of the external electric field's frequency (Moores and Goettmann 2006):

$$\varepsilon(\omega) = \varepsilon' + i\varepsilon'' = \varepsilon_\infty - \frac{\omega_p^2}{\omega_+^2\Gamma^2} + i\frac{\omega_P^2\Gamma}{\omega(\omega^2+\Gamma^2)} \approx \varepsilon_\infty - \frac{\omega_p^2}{\omega^2} - \frac{i\Gamma\omega_p^2}{\omega^3} \qquad (2)$$

ε_∞: polarization background of the ion core (in the case of metals it is related to the intraband transitions)

Γ :Dumping parameter, since Drude model is a classical approach this parameter represents carriers scattering. When NP size is comparable to the mean free path of the carriers γ is bigger than for the corresponding bulk material because the carriers scattering with the surface is relevant.

ω_p Plasma frequency

$$\omega_p^2 = \frac{n_e e^2}{\varepsilon_0 m^*} \qquad (3)$$

n_e carrier density

m* carrier effective mass: stands for the effective mass of the electron (taking into account the presence of a positively charge background)

1.3.2 Necessary conditions for localised surface plasmon resonance in NP

Only light with frequency in resonance with the oscillation of the plasmons is able to excite the LSPs, if this occurs, localized surface plasmon resonance take place. To show localized surface plasmon resonance a NP needs to be bigger than a couple of nanometres and smaller than 1/5 of the LSP's wavelength. In that case, inside the NP the dielectric polarization can be assumed as uniform and the electronic structure of the particle can be regarded as the one in bulk material (quasistatic approximation). These approximations allow to describe the coherent response of free carriers with the laws of electrostatics and therefore, as already seen, the electron cloud distortion caused by an incident light radiation can be expressed by polarizability of the metal α (equation 1)(Vincenzo Amendola, Roberto Pilot, Marco Frasconi and Iatì 2017).

From equation 1 is possible to calculate the extinction cross-section σ of a particle, for a spherical Au NP it is:

$$\sigma_{Ext} = \frac{18\pi[\varepsilon_m(\lambda)]^3 b}{\lambda} V_{NP} \frac{i\varepsilon''(\lambda)}{[\varepsilon'(\lambda)+2\varepsilon_m(\lambda)]^2} \qquad (4)$$

From equation 4 is clear that:

1) The plasmonic properties of any material are defined by its ε(ω)
2) σ_{Ext} scale with particle volume
3) σ_{Ext} is maximum when the denominator is minimized, namely the LSP is excited at the frequency where:

$$\varepsilon'(\omega) = -\chi\, \varepsilon_m \qquad (5)$$

the equation 5 is called the Frolich condition, It is a clear explanation of the reason why the LSPR can be tuned by changing the dielectric constant of the surrounding medium ($\varepsilon_m(\lambda)$), anyway, also NPs size, shape and composition can strongly affect the SPR (χ is the geometrical factor) (Vincenzo Amendola, Roberto Pilot, Marco Frasconi and Iatì 2017).

1.3.3 Calculate the surface plasmon resonance: GNRs and NSs

Silver, copper and gold spherical nanoparticles show a strong SPR band in the visible region, while other metal have broad and weak bands in the UV region. A red shift is obtained for hollow or core/shell structures and anisotropic structures like GNRSs or triangular structures (X. Huang, Neretina, and El-Sayed 2009).

Mie was the first to calculate the surface plasmon resonance for a small sphere interacting with an electromagnetic field by solving Maxwell's equation under the appropriate boundary conditions (Eustis and El-Sayed 2006b). This first and simple theory allow to calculate (under certain condition) LSPR of Au NSs, however in this theory the only material-related functions and constants are the dielectric constant of the surrounding medium and the complex dielectric function of the metal. The surrounding medium refers to the capping material that prevents nanoparticles aggregation(Link, Mohamed, and El-Sayed 1999).

Nowadays, the modern method for calculating SPR use the discrete dipole approximation(DDA)[1] and allow the calculation for arbitrary geometry such as GNRs. Using the DDA Gans was able to extend Mie theory for the explanation of optical properties of ellipsoid particles, namely prolate and oblate particles averaged over all orientations. In the case of nanorods, they show to have two plasmon resonances, one at around 520nm due to transverse oscillation of the electrons (TSPR) and the other at longer wavelength due to longitudinal plasmon resonance (LSPR). The latter one is easily tuned by change the aspect ratio of the nanorods (R=l/d), namely changing the ratio between the particle diameter and length. On the contrary, TSPR do not depend to the aspect ratio and it is at the same wavelength as the plasmon resonance of the spheres. In order to obtain LSPR red shifted higher aspect ratio have to be reached (Yousaf and Ali 2007; Link, Mohamed, and El-Sayed 1999).

Another model used to describe the optical properties of metal nanoparticles is the Maxwell Garnett theory. It computes the effective (complex) dielectric function of the composite material, namely the metallic nanoparticles and the surrounding medium, and from the calculated dielectric function it is possible to derive the refractive index and the absorption. In this theory is possible to introduce the dependence to the shape of the particles by the introduction of a screening parameter (Link, Mohamed, and El-Sayed 1999).

Differences between localised surface plasmon resonance of GNSs and Au NSs are depicted in Figure 2. From the figure it can be seen that the interaction between the electric field (E) of incident

1 The DDA simulates the metal particle as an array of N point dipoles of known polarizability tensor organised on a cubic lattice to represent the NP shape(Vincenzo Amendola, Roberto Pilot, Marco Frasconi and Iatì 2017).

polarized light (propagating along K direction) and the particles generates collective oscillation of conduction band electrons with respect to the positively charged metallic core.

In the case of NSs the SPR band lies in the visible region, while GNR shows two bands. The more intense band for GNRSs in the NIR corresponds to LSPR so it is due to the electron oscillations along the long axis. The weak band in the visible region and at the same wavelength as NSs' SPR corresponds to electron oscillations along the short axis(X. Huang, Neretina, and El-Sayed 2009).

It has been found that in aqueous solutions, the absorption maximum of LSPR λ_{max} is linearly proportional to R by the following relationship(X. Huang, Neretina, and El-Sayed 2009):

$$\lambda_{max} = 95R + 420 \qquad (6)$$

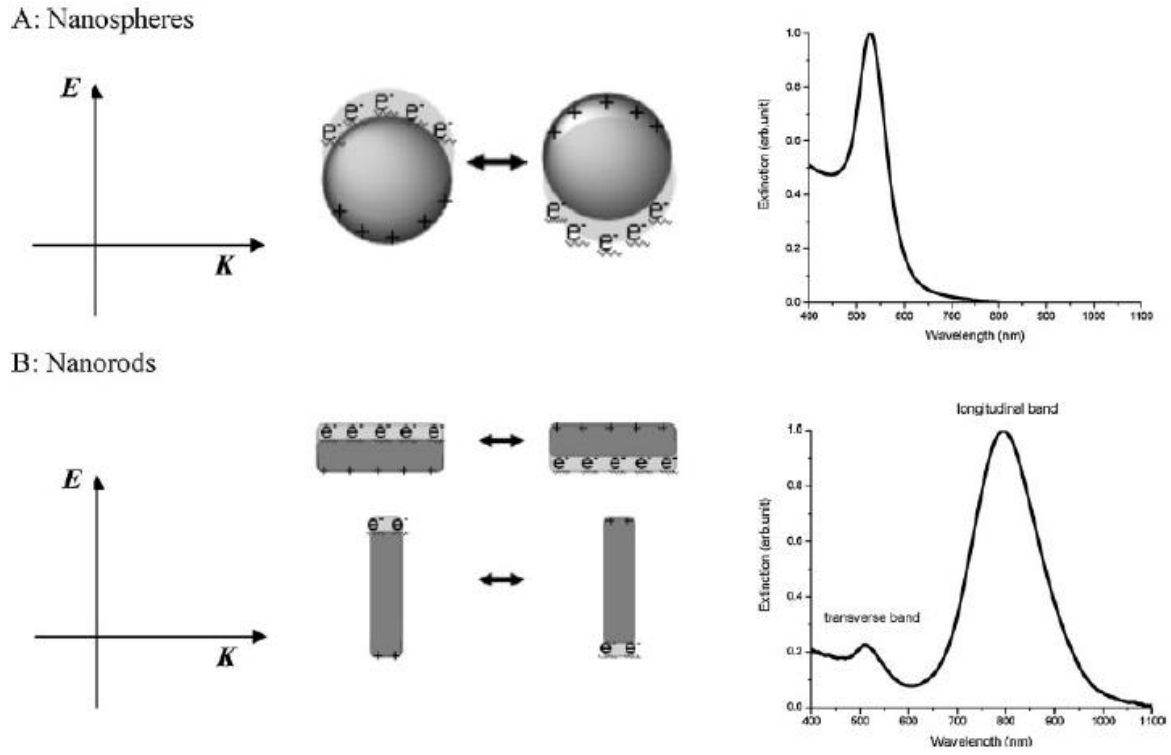

Figure 2 Schematic illustration of the interaction of polarized light and gold nanospheres taken from(X. Huang, Neretina, and El-Sayed 2009)

1.3.4 Losses in plasmonic nanoparticles

The persistence of plasmonic oscillations is limited in time by losses.

In noble-metal nanoparticles' plasmon decay occurs via two different ways(Sönnichsen et al. 2002) (as reported in Figure 2). The total relaxation rate Γ can be expressed as:

$$\Gamma = \Gamma_{nr} + \omega^2 \Gamma_r \qquad (7)$$

1) Γr Radiative decay (scattering): producing elastically scattered radiation (Sönnichsen et al. 2002). As it can be seen from equation 7, this term is multiplied for a ω^2 factor, meaning that it rapidly decreases its contribution to the total relaxation rate while lowering the SPR frequency.

2) Γ_{nr} Non-radiative decay (absorption): electronic relaxation processes, transformation of particle plasmons into electron-hole excitation. Both intraband and interband (IB) are part of this decay. Intraband are excitations within the conduction band, while interband are excitations due to transition between d bands and the conduction band. Intraband transitions are an unavoidable consequence of coupling light to free carriers and are modelled in the Drude function, differently interband transitions are avoidable if you work at frequencies away from the bandgap energy (Sönnichsen et al. 2002).
Electron–electron scattering, electron–defects scattering, and additional damping effects due to surface effects are linked to the decay into electron-hole excitations both intraband and IB (Landau mechanism).
The final effect of non-radiative decay is the release of heat in the surroundings of the particle(Vincenzo Amendola, Roberto Pilot, Marco Frasconi and Iatì 2017).

The bandwidth of SPR of a single particle is larger for faster loss of coherence(Vincenzo Amendola, Roberto Pilot, Marco Frasconi and Iatì 2017).

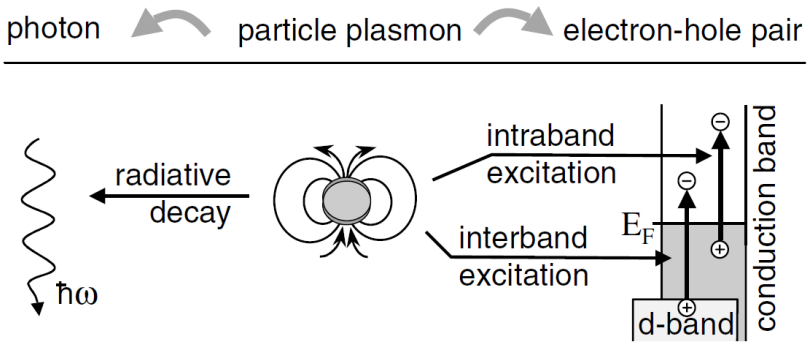

Figure 3 Schematic representation of radiative (left) and non radiative (right) decay of particle plasmons in noble-metal nanoparticles taken from (Sönnichsen et al. 2002)

1.3.4.1 Plasmon damping: gold nanorods vs nanospheres

Applications of Au NPs often require slow dephasing of the particle plasmon(Sönnichsen et al. 2002) Sönnichsen et al. have compared the dephasing rate of Au NSs and GNRs respectively with different diameters and aspect ratio . They have found that dephasing rate of GNRs decreases with increasing R (redshift), while it increases for more redshifted NSs, namely with bigger diameter. The obtained result is due to the reduced non-radiative decay in GNRs caused by the fact that interband transitions require a threshold energy of about 1.8 eV in gold. Hence, interband excitations is not possible for plasmon with resonance energy below 1.8 eV (λ=689 nm). Indeed, gold is a good low loss plasmonic metal in the infrared, but in the visible (3.1 eV-1.77eV) has large losses. This is evidenced by a deviation of the dielectric function of gold from Drude behaviour in visible region. Suppression of interband damping should also be present in nanospheres with low E_{res}. However, an increase of radiative damping is expected for bigger particles. Spheres with resonance energy low enough to avoid IB resulting in stronger decay due to their bigger volume.

Another important point of Sönnichsen et al. regards the quality factor of the resonance. As already said, increasing the life time of the plasmons (namely decrease the decay) corresponds with a decrease of the linewidths of the plasmon peak. Since the quality factor of the resonance is defined as:

$$Q = \frac{E_{RES}}{\Gamma} \qquad (8)$$

The quality factor is the enhancement of the oscillation amplitude of a driven oscillating system with respect to the driving amplitude, i.e., the local-field enhancement in the case of particle plasmons. GNRs have high quality factor thanks to suppression of IB damping. This makes GNRs superior to NSs in applications where local filed enhancements are required(Sönnichsen et al. 2002).

It is clear that GNRs are more suitable than NSs for a wide range of optical applications, furthermore NSs as shape impurity in GNSs synthesis could represents a problem.

1.3.5 GNRSs' scattering and absorption ratio

It is important to understand how scattering and absorption of GNRSs are influenced by R and the volume of the particles, this allows to choose the best nanoparticles for biomedical applications. Indeed, for imaging high scattering is preferred, while for photothermal therapy light absorption by the particles is required in order to efficiently convert it to heat for cell and tissue destruction (X. Huang, Neretina, and El-Sayed 2009).

The dependency on R and size of the relative contribution of the absorption and scattering to the total extinction have been studied by Lee and El-Sayed (K. S. Lee and El-Sayed 2005). They defined the scattering quantum yield η as the ratio of scattered efficiency to the total extinction at each resonant maximum[2].

$$\eta = \frac{Qsca}{Qext}\Big|_{\mathrm{Re}\,s} \qquad (9)$$

As regard as LSPR, differently from resonance wavelength that is linearly dependent on R and does not depend on the volume of the particle (see equation 6), η increases with the increasing of R but saturated at intermediated values that depend on $R_{eff.}$, namely on particle volume. Larger is the particle, smaller is the value of R corresponding to plateaus(Park et al. 2014). An example is reported in Figure 4.

Instead, the absorption efficiency is approximately proportional to the imaginary part of the dielectric function of the metal particles, which is negligibly small in the visible region but increases gradually moving toward longer wavelength region. Therefore, the observed decrease in η for GNRSs with high R which have LSPR at longer wavelength, could be due to the higher absorptive contribution expected at these wavelengths due to the increase in the imaginary dielectric function(K. S. Lee and El-Sayed 2005).

---

[2]Efficiencies (*Q*) of extinction, absorption, and scattering are obtained by dividing the cross sections by the geometric cross section, πR^2, where R is the radius (or effective radius for non-spherical particle). The effective radius $R_{eff}=(3V/4\prod)^{1/3}$ is the radius of a sphere having a volume, V, equal to that of the nanorod $V_{rod} = \frac{4}{3}\pi\left(\frac{d}{2}\right)^2 l = \frac{\pi}{3}d^3R$). Extinction efficiency greater than 1 means the optical species has an extinction cross section larger than its physical cross section. Finally, extinction cross section is commonly expressed experimentally as the molar extinction coefficient (L mol^{-1} cm^{-1}) (Park et al. 2014; Yang, Schatz, and Van Duyne 1995; Eustis and El-Sayed 2006a)

Regarding the dependency on the particle size it has been determined that, at fixed R, for smaller rods absorption efficiency is dominant while scattering efficiency is dominant for larger rods (X. Huang, Neretina, and El-Sayed 2009).

The total extinction increases linearly with the increasing of GNRSs volume. Considering the dependency of the total extinction on R, and having a fixed volume, Park et al. reported that R has a negligible impact on it.

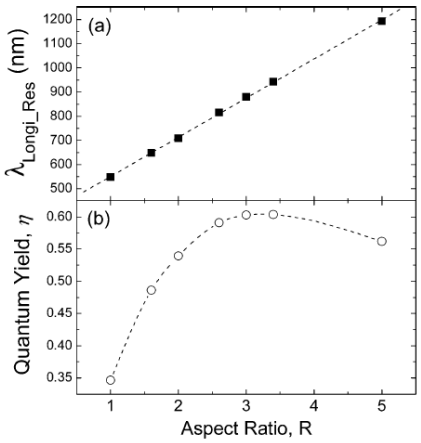

Figure 4 a and b LSPR and η as functions of R for an effective radius of 40nm c A series of calculated spectra for optical extinction, absorption, and scattering efficiencies of Au nanorods as a function of particle size at fixed R 3.4. taken from (K. S. Lee and El-Sayed 2005).

The TSPR shows different feature: the relationship between the peak position and R is not linear (it shows a blue shift by increasing R), the overall magnitude of the scattering and the absorption decreases as the aspect ratio increases (K. S. Lee and El-Sayed 2005). The relative intensity ratio of the longitudinal to the transverse mode increases with increasing aspect ratio.

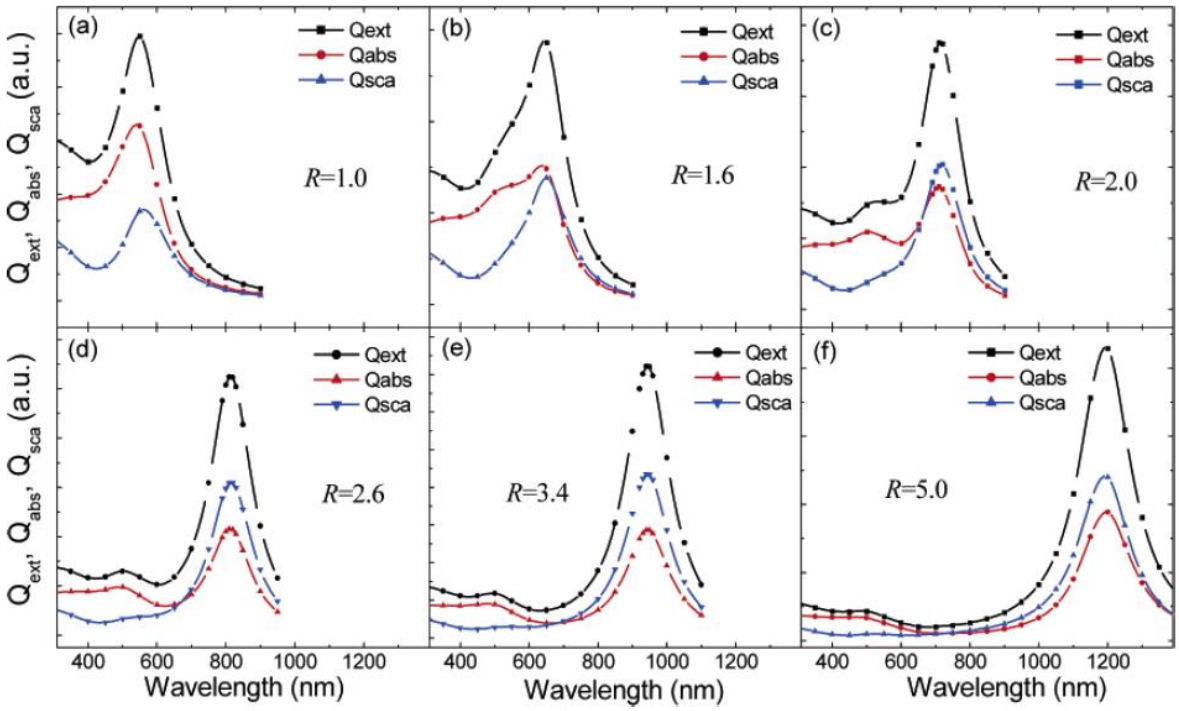

Figure 5 calculated spectra for optical extinction, absorption, and scattering efficiencies for Au nanorods with different aspect ratio taken from (K. S. Lee and El-Sayed 2005)

1.4 Synthesis

Anisotropic particles are especially interesting for their optical, electronic, magnetic and catalytic property. Nevertheless, shape-controlled synthesis of GNSs has been studied since 1980's, while Au NSs first modern synthesis is dated back in 1857 by Faraday(X. Huang, Neretina, and El-Sayed 2009).

Bottom-up top-down methods are both suitable for GNSs synthesis, but the latter is mainly used to obtain the placement of GNRs on well-defined areas of a substrate's surface. In top-down approaches, first a gold film is formed on the surface that has to be covered by GNRs, then most of the film is removed by nanoscale pattering procedures which leaves GNRSs in specific position of the surface. Examples of top-down procedures are lithographic method, catalytic method, template method.

1.4.1 Seed-mediated growth (bottom up method)

This is the most popular method for obtaining GNRs and also the method used in this work. It is widely applied since it is characterized by numerous advantages: easy procedures, flexibility for structural modification, control over particle size, high quality and yield. However, these features are mainly present in synthesis of GNRSs with LSPR between 700 and 900 (Ye et al. 2012).

This method consists in separate environments for production of seeds (small gold nuclei) and growth of the anisotropic particles. Indeed, seed particles are produced in the seed solution and they serve as a starting point for the development of GNRSs that occurs in another solution after the addition of the previous one. This is useful since the conditions required for homogeneous nucleation are opposite to those required for controlled growth (Scarabelli et al. 2015) , and this procedure of separated seed and growth solutions, avoids the formation of new nuclei during the growing step.

The first synthesis with seed mediated growth is dated back in 1989 but the current concept of seed-mediated growth is originated in 2001 by Jana(Catherine J Murphy, Jana, and Gearheart 2001) and then improved by El-Sayed et al(Nikoobakht and El-Sayed 2003).

The original idea was to use micelles formed by hexadecyltrimethylammonium bromide (CTAB) as a "soft template" to direct GNRSs growth.

1.4.2 CTAB

It is well known that surfactants molecules above the critical micelle concentration are able to self-assemble into micelles in aqueous solution. In the case of cationic surfactants, such as alkiltrimethylammonium halide and alkylpyridil halide, rod like or wormlike micelles are obtained at high concentration, while at low concentration globular/spherical micelles are obtained(Ye et al. 2012). The high concentration required is characterized by the high viscosity of the solution. Halide anions associate only moderately with the surfactants' cations, and micellar growth is slow. The required concentration could be lowered by the addition of a salt or an acid, that could also increase the rate of the micelles growth(Lin et al. 1994).

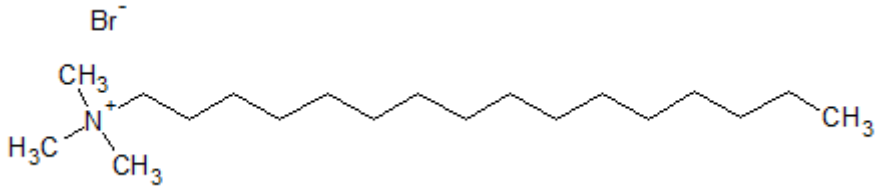

Figure 6 CTAB molecule

The micelles' shape depends upon the micellar packing parameter(p) reported in equation 10, where A the effective area of the polar headgroup, V is the effective volume of the hydrophobic chain and *l* its length.

$$p = \frac{V}{Al} \qquad (10)$$

The higher the binding energy is between the positive headgroup and the counterion, the lower would be the electrostatic repulsion between the headgroups, hence the surface area per surfactant molecule will decrease and this promote the transition between spherical to worm-like micelle(Lin et al. 1994).In the case of CTAB aqueous solution a minimum concentration of 0.27M (second critical micelle concentration) is required to obtain rod like micelles (P.S. Goyal et al. 1991). It has been proved that the high concentration of CTAB required to obtain rod like micelles(Catherine J Murphy, Jana, and Gearheart 2001) is due to the associated high concentration of counterions.

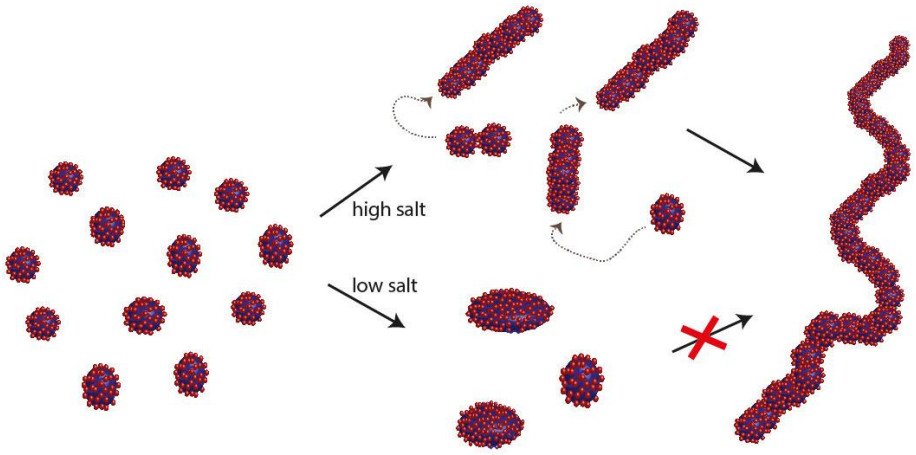

Figure 7 formation of wormlike/rodlike micelles (taken from http://www.esrf.eu/home/news/spotlight/content-news/spotlight/spotlight213.html)

It is possible to change the mean distance between headgroups or increase the volume of the micelle core by the addition of may possible counterions and cosurfactants that could be strongly adsorbed by the micellar interface(Lin et al. 1994). Aromatic compounds, such as salicylate, can influence the micellar behaviour of CTAB. Indeed, the benzene ring can penetrate between the hydrophobic alkyl chain and increase the volume V in the packing parameter.

Cosurfactants are another class of molecules that can be used for obtaining rod-like micelles, generally they are short-chain ammines or alcohols. They can be considered as surfactant molecules with small head groups, they are not able to form micelles alone, but when mixed with surfactants they can form composite micelles. They can promote the formation of rod like micelles since they

are characterized by a small head group, so the average area of the head group between surfactant and cosurfactant is decreased and the packing parameter is increased.

For obtaining rod-like shape particles, even though CTAB remains the most employed surfactants, it is possible to identify three required surfactant characteristics (Scarabelli, Grzelczak, and Liz-Marzán 2013):

1) a quaternary ammonium head group which can form a complex with the gold salt precursor and modify its redox potential;
2) bromide as counterion;
3) carbon tail short enough to achieve solubility close to room temperature but long enough to stabilize the nanorods.

1.4.3 Evolution of seed-mediate growth

Jana et al(Catherine J Murphy, Jana, and Gearheart 2001) prepared the growth solution by the reduction of $HAuCl_4$ to $HAuCl_2$ with ascorbic acid in the presence of CTAB and silver ions. Then by the addition of citrate-capped small gold nanospheres the GNRSs growth was started. Indeed, addition of seed solution is necessary since the ascorbic acid is not able to reduce the gold ions into metal without metal nanoparticles in solution, which are able to catalyse the reduction. Long nanorods (up to an aspect ratio of 25 were reached) were obtained in absence of silver ions by three step procedure. In this method GNRs obtained in the first step were used as seed in the second step, and so on. However, GNRSs with higher aspect ratio were obtained with a high percentage of shape impurities, namely Au NSs.

An improvement of this method was obtained by Nikoobakht and El-Sayed(Nikoobakht and El-Sayed 2003) in 2003. Citrate capped seed was replaced by CTAB capped seed and silver ions were implied for tuning GNRSs aspect ratio. This protocol includes two steps:

1) Seed solution: a strong reducing agent , namely ice-cold solution of sodium borohydride, was used to obtain nuclei from a solution of auric acid in the presence of CTAB(Catherine J. Murphy et al. 2010)
2) Growth solution: auric acid was added to a solution of CTAB and silver ions. A weak reducing agent, namely ascorbic acid (AA), was used to reduce Au^{3+} to Au^{1+}, then the seed solution was added to allow the reduction of Au $^{1+}$ to Au ^{0} onto the seed particles. CTAB represents a structure-directing agents that must be present in the grow solution for promoting the formation of non-spherical particles(Catherine J. Murphy et al. 2010).

the overall chemical reaction for GNRSs can be described by the following equation

$$2HAuCl_4 + 3C_6H_8O_6 \frac{CTABr \;\; Ag^+}{Au^o_{NS}} > 2Au^0_{(NR_S)} + 3C_6H_6O_6 + 8HCl$$

where $C_6H_8O_6$ is ascorbic acid, a reducing agent that is oxidized to dehydroascorbic acid (C6H6O6) after the reaction,
Aspect ratio from 1.5 to 4.5 were obtained with high yield (about 99%) and low amount of shape impurities.

In order to obtain GNRSs with higher aspect ratio a cosurfactant was used (benzyldimethylhexadecylammonium chloride) and this allows to reach aspect ratio of 10 by changing the silver concentration(Nikoobakht and El-Sayed 2003).

Comparison between CTAB and citrate capped seed mediate growth shows different kind of obtained rods. In the case of citrate capped seed in absence of silver ions pentatwinned structures are obtained, while single crystal nanorods are obtained with CTAB capped with silver ions. Moreover, the former shows larger dimension and aspect ratio (Scarabelli et al. 2015).

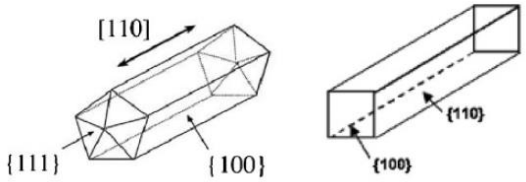

Figure 8 GNRSs from citrate capped seed in the left and CTAB capped seed in the right taken from (X. Huang, Neretina, and El-Sayed 2009)

Numerous factors influence the yield, monodispersity, size and fine shape of GNRSs. These factors include: seed concentration and crystallinity, ascorbic acid concentration, temperature, pH, auric acid concentration, surfactant concentration, presence of reagent impurities, the use of cosurfactants, additives, solvent, GNRSs aging time(Ye et al. 2012). Indeed, GNRSs synthesis require both thermodynamic and kinetic control, the former is needed to stabilize the crystallographic facets , the latter for controlling the anisotropic growth (Scarabelli, Grzelczak, and Liz-Marzán 2013). The description of GNRSs should include length, diameter, aspect ratio, reduction yield (quantities of reduced precursor), shape yield (percentage of rod-shaped particles). This requires a precise control through the whole growth process. The complexity of this control can be understood considering that nanocrystals with distinctive shapes, most of the time, correspond to the products of a set of sequential reactions instead of multiple parallel reactions as it can be seen in Figure 9(Xia, Xia, and Peng 2015).

Therefore, different synthetic approaches were explored by changing these factors in particular to improve protocols of GNRSs with LSPR beyond the interval 700-900nm.

For this purpose, various aromatic additives were studied by Ye et al. in 2012(Ye et al. 2012) in order to improve the synthesis of GNRSs and reduce the required amount of CTAB. They kept the seed mediated growth with CTAB capped seed like Nikoobakht and El-Sayed(Nikoobakht and El-Sayed 2003) but decreased the amount of CTAB in the growth solution from 0.1 to 0.05M by the addition of aromatic additives. What they found is that CTAB-5-bromosalicylic acid system allows to obtain greater dimensional control for GNRSs in the range of LSPR from 705 to 904nm, moreover they found that it is possible to increase the aspect ratio of the GNRSs ($5.9<R<8.5$) by optimizing the pH, the amount of seed and silver ions.

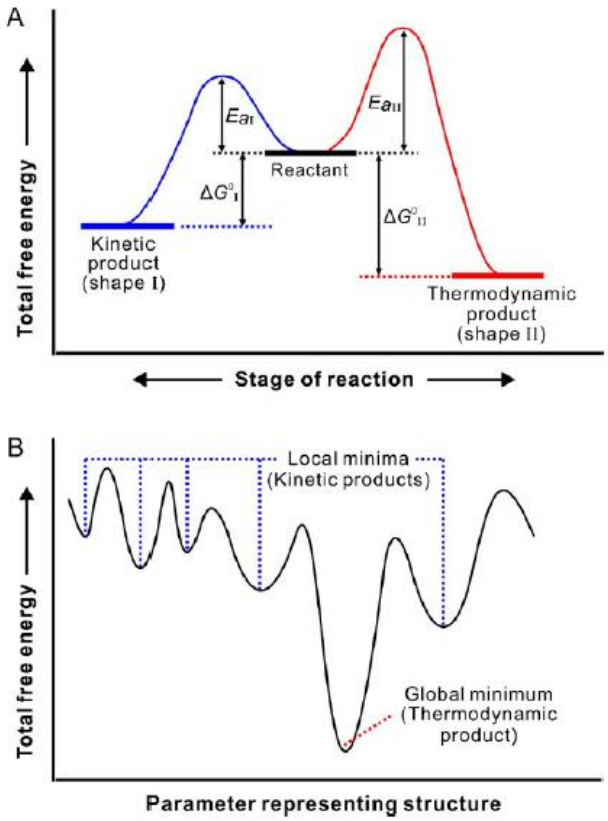

Figure 9 two different kind of thermodynamic vs kinetic control. A case of parallel reactions which, in general, is the description organic reaction. B case for a series of sequential reactions , involved the most of the time for nanocrystal growth. Taken from(Xia, Xia, and Peng 2015)

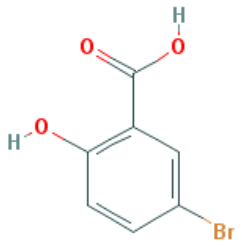

Figure 10 5-Bromosalicylic acid molecule

Additive influence has been explained as intercalation of the additive within the CTAB bilayer that could improve its stiffness but other mechanism should be take into account, like the capability of the carboxylic group of forming complex with the gold salt and hence influencing its reduction potential (Scarabelli, Grzelczak, and Liz-Marzán 2013).

Independently of the kind of protocol applied, the growth of nanorods can be arrested by centrifugation and redispersion (CR) in deionised water or by the addition of Na_2S with an optimum ratio of 4:1 sulphur to metal (followed by CR) (Zweifel and Wei 2005).

1.4.4 Proposed growth mechanisms

It is widely accepted that either versions of seed mediated growth involve the formation of CTAB bilayer instead of CTAB monolayer (Catherine J. Murphy et al. 2010) as illustrated in Figure 11. Even though the existence of the bilayer during all the growth of the GNRSs is not proved experimentally (Da Silva and Meneghetti 2018).

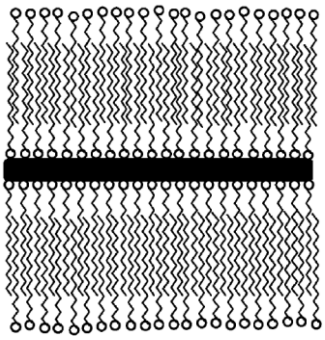

Figure 11 GNRS inside CTAB bilayer (taken from (C.J. Murphy et al. 2005)*)*

The CTAB bilayer consists of two surfactants leaflets, one presents the surfactants head groups directed toward the aqueous media while the other is associated with the gold surface via the quaternary ammonium headgroups. Three different interactions can be described for this system: the outer CTAB-bulk solution, the bilayer core and the GNR-CTAB interface. This structure is the most energetically favoured since it allows hydrophobic interaction between the surfactant tails in the bilayer core and the hydrophilic interaction at the interface nanoparticle-solvent. The bound between the surfactants and the surface is generally accepted to be due to electrostatic interaction between the cationic head group (quaternary ammonium) and anionic sites on the gold surface. The possible nature of these negative charges on gold surface was discovered to be dependent on Au-Br^- interactions. The concentration of Au-Br^- on the GNRSs surface influences the arrangement of adsorbed CTAB(S. Lee et al. 2011). Moreover, it has been demonstrated that the thickness of CTAB structure adsorbed on GNRSs is 3.2 ±0.2nm which is smaller than the double of the chain length (4.34nm). This suggests that there is a significant interdigitation of the chain(Gómez-Graña et al. 2012).

Once that behaviour of CTAB and has been understood we have to describe how this system can lead to nanorods instead of other shapes. Different mechanisms have been proposed for GNRSs' growth.

1) Electric field directed growth (Mulvaney et al. 2004)

$AuCl_4^-$ are bounded to cationic CTAB micelles by displacing bromide ions, then with the addition of ascorbic acid it is reduced to $AuCl_2$-CTAB micelles. The latter complex is negatively charged on the surface so its transport to the cationic micelle capped gold seeds is controlled by double layer interaction. The collision between seed particles and $AuCl_2$-CTAB micelles are faster at the tips than at the side, so this promote the rod shape growth. However, the mechanism does not explain how the initial tips of the seed particles are formed.

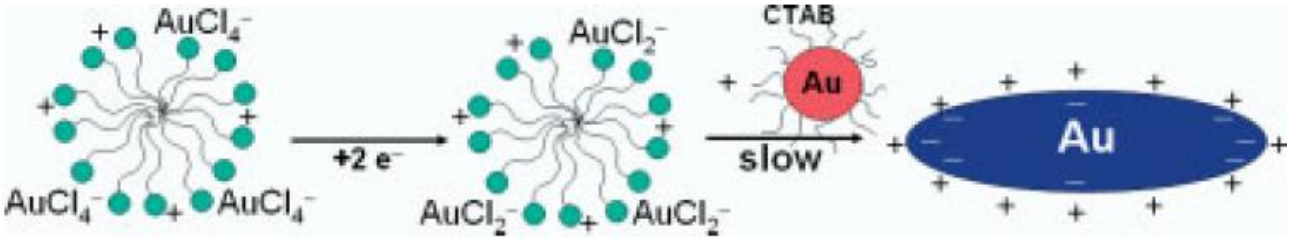

Figure 12electric field directed growth taken from(Mulvaney et al. 2004)

2) Surfactants preferential bindings directed growth (C.J. Murphy et al. 2005)

This mechanism was the first capable to explain the origin of the anisotropic growth. The growth starts with single seed particles that has facets that are differentially blocked by surfactant (or another specie that then electrostatically attracts the cationic surfactant). Indeed, they stated that CTAB preferentially adsorbed on the lateral facets of GNRSs. Hence, the CTAB bilayer forming on the later side of the growing particle permits the formation of anisotropy, since the reduction of the Au ions is possible only into the tips. In this method CTAB is not considered as a soft template, indeed this model is known as the zipping- like growth mechanism.

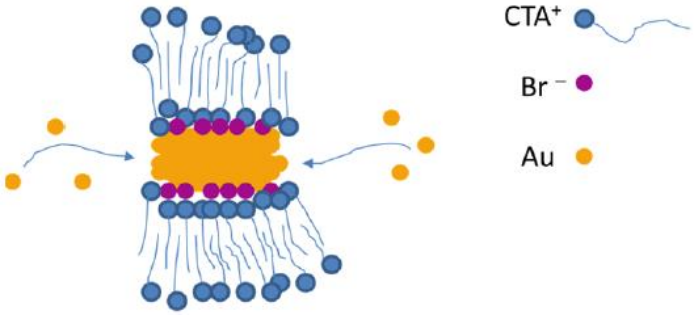

Figure 13 zipping-like growth mechanism taken from (Da Silva and Meneghetti 2018)

3) Soft template model (Jana 2005)

In this model elongated CTAB micelles in the growth solution act as template that can permit the introduction of seed particles (with diameters below 3.5nm). In this case the shape of the template is the factor that can induce anisotropy. In this scenario additives, such as salicylate aromatic additive, can be used to promote the formation of longer GNRSs due to their ability of modifying CTAB micelle structure. However, it was later found that in presence of silver ions, the symmetry breaking occurs in particles with diameters 4-6nm. Since the CTAB concentration in the growth solution is not high enough to permit the cylindrical micelles formation, only ellipsoidal micelles are present. These micelles are too small to act as a template considering the diameters at which the symmetry breaking occurs. For this reason template mechanism is not currently accepted as an explanation of anisotropic growth(Da Silva and Meneghetti 2018).

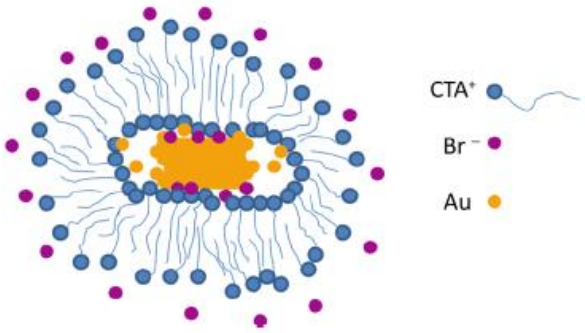

Figure 14 Soft template model taken from (Da Silva and Meneghetti 2018)

4) Recent developed model (Da Silva and Meneghetti 2018)

To investigate the growth model, recently researchers have focused on different possible kinds of CTAB structures on the surface of GNRSs. Indeed, it is proved that at the beginning of GNRSs growth, both tips and lateral facets growth, although at different rates. An explanation could be an initial formation of CTAB adjacent cylindrical micelles on the surfaces, altogether with channels (called

intermicellar channels), that allow molecular gold source to flow to the surface. The width of these channels depends on the facets on which the micelles are adsorbed, so different flows of gold are present.

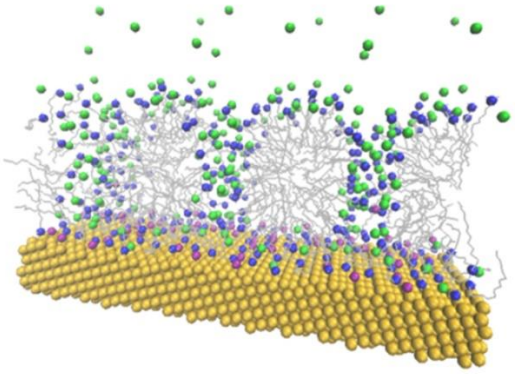

Figure 15 CTAB cylindrical micelles on gold surface. The yellow and dark blue spheres represent gold and nitrogen atoms, respectively. The grey lines are polar tails. The bromide ions are represented by magenta and green spheres. Image taken from(Da Silva and Meneghetti 2018)

Then CTAB structures evolve to a bilayer system and the growth continues with a zipping like mechanism. The driving force that separates the early and the latter stages seems to be the concentration of bromide ions on the gold surface. A relatively low concentration of bromide anions leads to the formation of the adsorbed adjacent micelles, when the concentration rises on the later stages, a bilayer structure forms. The concentration of bromide ions increases during the growth since $[AuBr]^-$ is considered to be the specie that flows on gold surface. The flux of $[AuBr]^-$ on the tips and the rate of reduction is higher so many bromide ions are released here, anyway they move to the lateral facets since their affinity is higher. The increasing bromide concentration on the lateral facets causes the change of the CTAB structure from micelles to bilayer, which sustain the anisotropic growth, as reported in Figure 16 where this mechanism is represented.

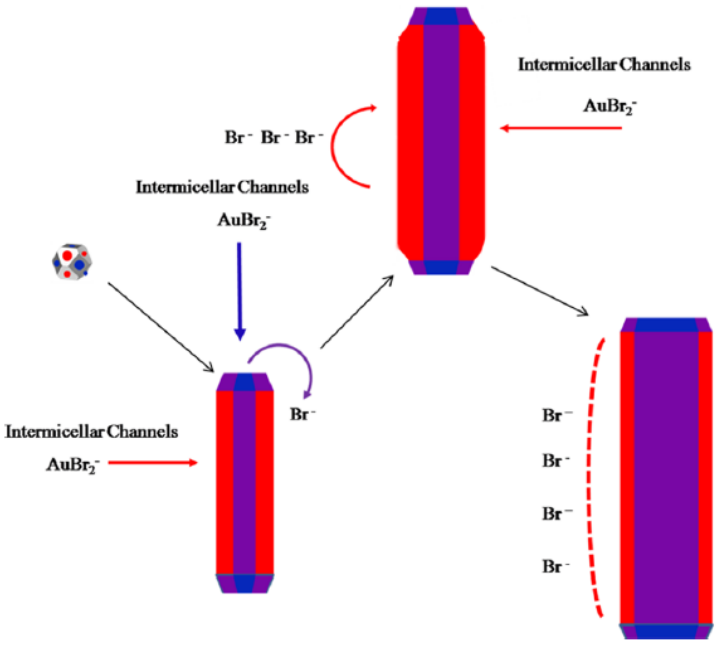

Figure 16 GNRSs growth mechanism with CTAB structure evolution taken from (Da Silva and Meneghetti 2018)

1.4.4.1 The role of AgNO3

Regarding the role of $AgNO_3$ in controlling the aspect ratios, one proposed explanation (Sau and Murphy 2004) involves the formation of AgBr in presence of CTAB (the concentrations are above the Kps) and the formation of $Ag[BrCTA]_2$ complex. Indeed, at low pH, the ascorbic acid cannot reduce silver ions to Ag^0 but could be the AgBr specie that can act as a face-specific capping agent and adsorbing differentially to the Au facets stabilizing the rod growth and directing the growth through the rod shape. Moreover, AgBr presence on the surface can decrease the charge density , and hence, repulsion between neighbouring headgroups of CTAB which allows the micelles elongation (Nikoobakht et al. 2000).

Another theory involves the under potential deposition (UPD) of silver to gold metal surface (Guyot-sionnest and Liu 2005). UPD consists in the fact that reduction potential of Ag^+ to Ag^0 is lower on a metal monolayer than bulk reduction. Orendoff and Murphy combined UPD, electric-field-directed and surfactant preferential binding models with their studies on metal quantification in GNRSs and proposed the following mechanism.

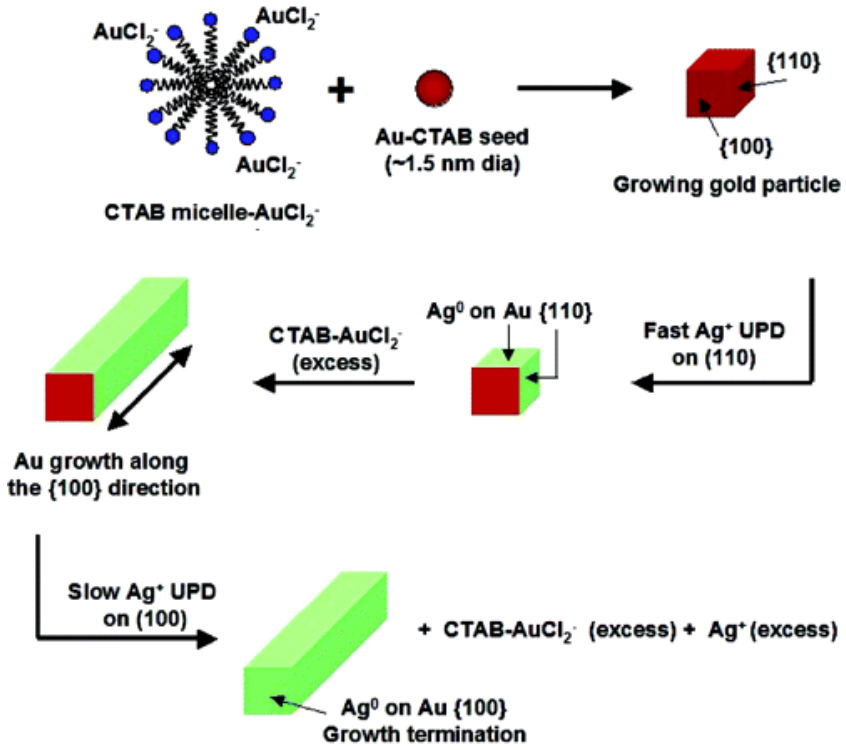

Figure 17 mechanism of nanorod growth from CTAB-protected gold seed particles in the presence of Ag+ taken from(Orendorff and Murphy 2006)

$AuCl_2$-CTAB micelles move toward seed particles by electric field interaction. Thanks to CTAB preferential binding to {110} facet (it has the higher surface energy which is lowered by CTAB binding) spherical symmetry is broken. Moreover, silver ions reduction is faster **on** {110} facet. Preferential interaction of CTAB and silver with that facet results in particle growth into rod shape along the [110] direction. When Ag deposition occurs on {100} facet it stops the particle growth (Orendorff and Murphy 2006). Indeed, this is coherent with the results that GNRSs obtained without silver anions are longer than GNRSs obtained with the silver ions (although the first ones are

accompanied by an high rate of shape impurities) and the fact that over a certain threshold of silver ions concentration, it is not possible to increase the aspect ratio(X. Huang, Neretina, and El-Sayed 2009).

1.5 GNRSs characterization

UV-VIS-NIR spectroscopy and TEM/SEM are the main techniques required for GNRSs characterization. Optical spectrum permits to obtain numerous information(Henson et al. 2017; Scarabelli et al. 2015):

- the full width at half maximum (FWHM) and the shape of the LSPR band are excellent index of size dispersion and aggregation. An example of aggregation absence is reported in Figure 18 A, while the presence of shoulder in LSPR band could be due to plasmon coupling in GNRSs aggregates. For example, Figure 18B that presents an increase in the FWHM and asymmetry in the LSPR could indicate slight aggregation or polydispersity of size and aspect ratio:

- LSPR peak position allows to estimate the average aspect ratio;

-Nanoparticles concentration could be derived from absorbance at 400nm, indeed at this wavelength for GNRSs solution the main contribution to absorbance is due to interband transitions in metallic gold and It has been found that this value of absorbance is independent of particle size and shape (until the particle volume remains below certain value otherwise scattering become a significant contribution to the total extinction); a value of absorbance equals to 1.2 corresponds to gold concentration [Au^0] =0.5mM (Scarabelli et al. 2015)

- the ratio between the maximum absorbance of the LSPR and TSPR peaks along with the presence of shoulder on the transverse band indicate the presence of by-products. Indeed, unwanted (but inevitable) nanospheres have a strong absorbance between 510-525nm, resulting in increasing the TSPR peak.

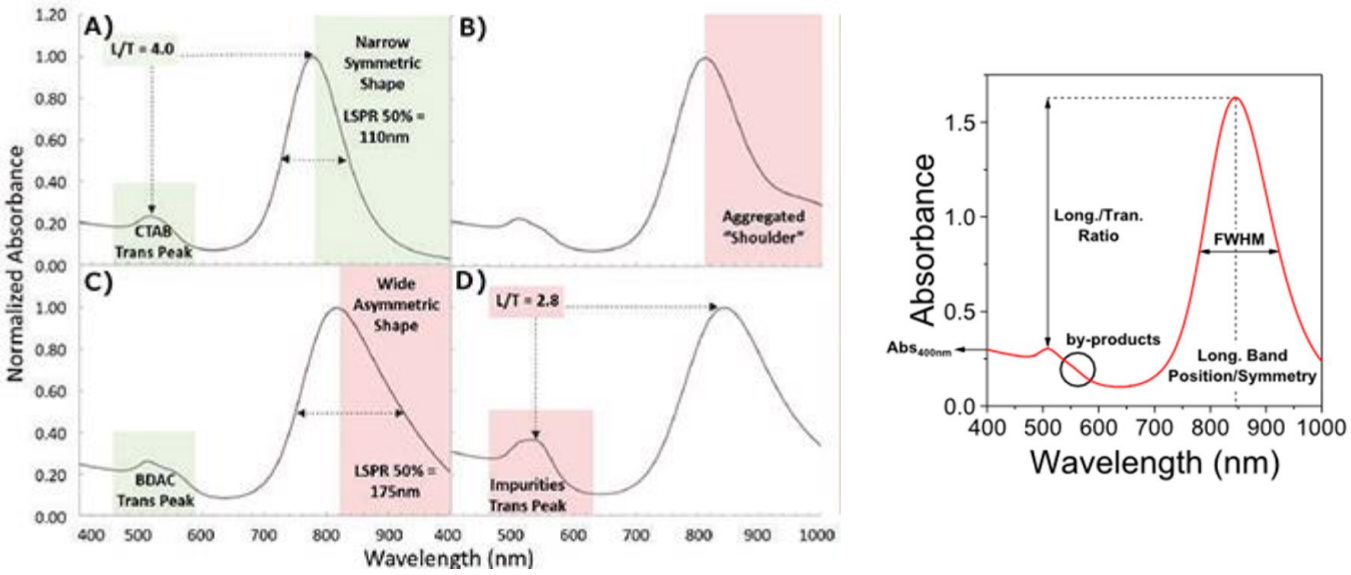

Figure 18 on the left some examples of GNRSs spectra: A) ideal GNRSs spectra B) spectra with aggregation shoulder C and D) TSPR show shoulder due to shape impurities confirmed also by the low value of TSPR and LSPR ratio. Asymmetry in the LSPR bands means wide size distribution. On the right all the interesting parameters are summarized. The images are taken from(Henson et al. 2017; Scarabelli et al. 2015)

UV-VIS-NIR spectroscopy is a useful tool to evaluate the quality of an ensemble of nanoparticles, but for determining particle dimensions TEM and SEM are the most useful tools. However, for a good use of TEM images, a sufficient number (at least some hundreds) of NPs and GNRs must be present, otherwise the figures obtained do not have a statistical meaning and the obtained average dimensions can be biased. This is a critical step and can be a source for wrong average size evaluation since GNRSs, in particular if slowly dried during TEM sample preparation, tend to present shape segregation, meaning that by-product are largely accumulate on a particular area of the grid, but also different size GNRSs tend to stay all together as it can be seen from Figure 19.

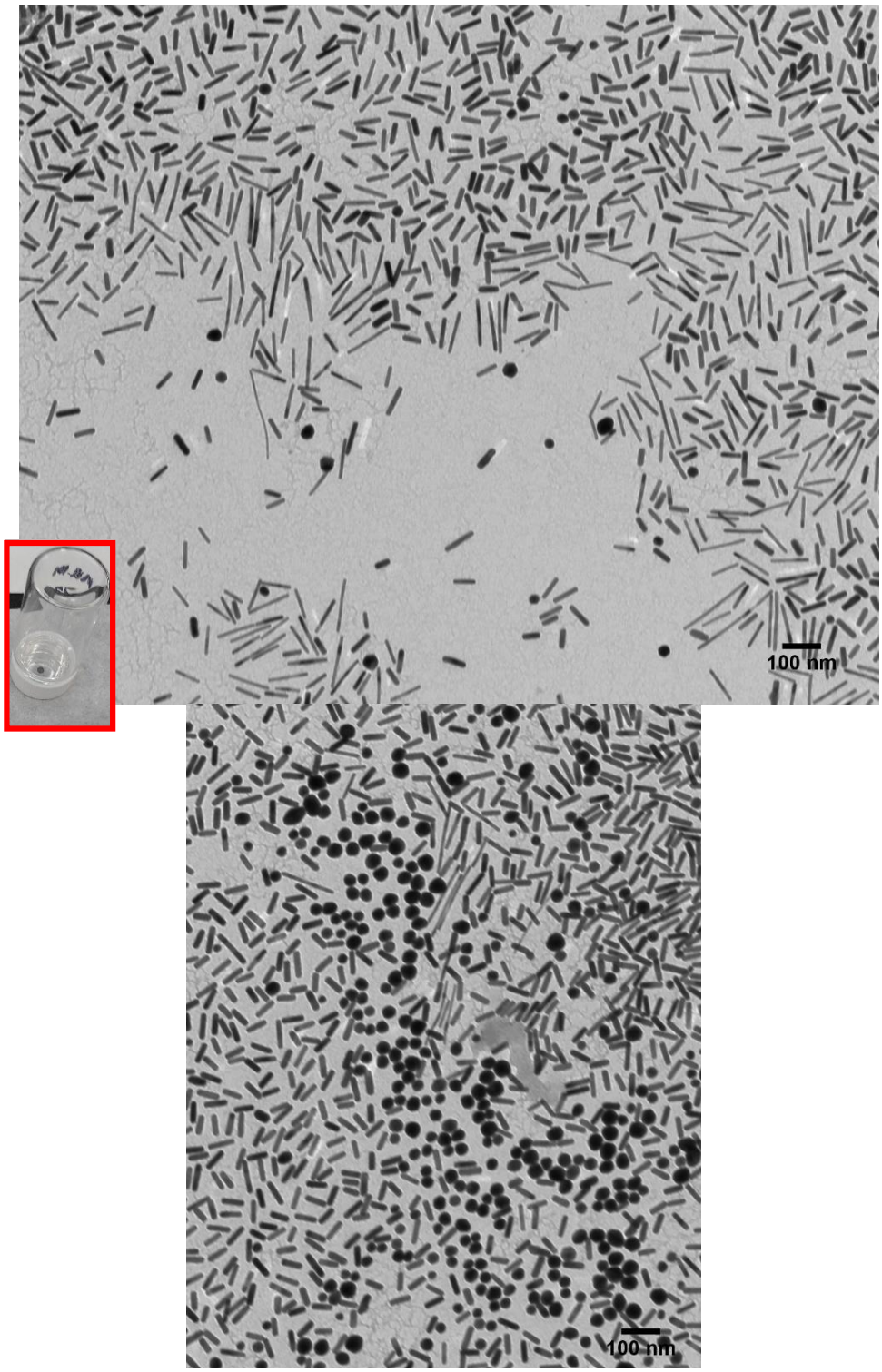

Figure 19 TEM images obtained by grid preparation as reported in the red box (this method allows for a slow drying

1.6 Application of GNRSs

Plasmonic nanoparticles (noble metal) differently from the other transition metal nanoparticles have been used far beyond the application as catalyst thanks to properties that occur at the resonance frequency. Indeed, the strongly resonant surface plasmon oscillation can be visualized as photons confined to the small nanoparticle size. The confinement of the photon oscillation with the frequency of light in resonance with SPR leads to a large decrease in its wavelength (to fit within the nanoparticle). This increases the amplitude of the electromagnetic wave by orders of magnitude, and since the intensity of the radiation is proportional to the square of wave amplitude the intensity of the light results increased dramatically. The SPR consists substantially in a focus of the resonantly coupled light that allows an amplification by orders of magnitudes of light absorption, scattering, and a considerable local-field enhancement. These properties allow numerous applications (X. Huang, Neretina, and El-Sayed 2009).

As already said gold presents numerous advantages (biocompatibility, easy functionalization etc.) and among the possible morphologies of gold nanoparticles, GNRSs are particularly interesting. Indeed, they show interesting scattering and absorption properties, high sensitivity to changes in the dielectric nature of the surrounding environment and their LSPR can be tuned from visible to NIR region which is useful in many applications. Indeed, from 800 to 1300 nm the maximum tissue penetration can be reached avoiding damage of health cell and attenuation of excitation (wavelength shorter than 800nm are adsorbed by hemoglobin and melanin, while wavelength bigger than 1300 nm are strongly attenuated by water). They also show the property to act as a transducer able to convert light (VIS or NIR) into heat which diffuses in the surrounding environment giving rise to the so called photothermal effect. Hence, the exceptional radiative and non-radiative properties of GNRSs have make them extremely interesting for applications in sensors, imaging, drug delivery, photothermal treatments(Stone, Jackson, and Wright 2011). However, for considering the impact of their application, it is necessary to evaluate their potential risks to human health and environment. Toxicities studies on GNRSs with different size, shape and surfactants showed that even if free CTAB is cytotoxic, bounded CTAB is not. Particles purified by centrifugation or dialysis membrane are supposed to be safe, nevertheless they can anyway release free CTAB (losses of bounded CTAB), so surface modification is preferred for replacing or covering CTAB molecules on the particles(Stone, Jackson, and Wright 2011).

1.6.1 Biosensing

As already said, (Frolich condition), SPR depends on the dielectric constant of the surrounding medium (or refractive index $n_m = \varepsilon_m^{\,2}$). As it can be seen from equation 5, a negative value for the real part of the dielectric constant of the metal is expected. Considering the approximate linear relationship between the real part of the dielectric constant of the gold and the wavelength, which is reported in Figure 20, a SPR red shift is obtained for an increase in the ε_m. Hence, the SPR wavelength, either by absorption and scattering, allows to monitor the surrounding environment and can be used for sensing. The sensitivity is defined as the ratio between the SPR shift and the change of the refractive index of the medium, hence considering that the geometrical factor is the proportionality constant between the dielectric constant of the medium and the real part of the dielectric constant of the metal, a high value of the geometrical factor (see equation 5) gives higher sensitivity. For this reason anisotropic particles such as GNRSs give higher sensitivity than spherical particles(X. Huang, Neretina, and El-Sayed 2009). This high sensitivity of GNRSs to the surrounding

environment has been used to monitor the bound between different kinds of IgGs (human , rabbit and mouse IgGs linked to GNRSs) and their respective anti-IgG (Yu and Irudayaraj 2007).

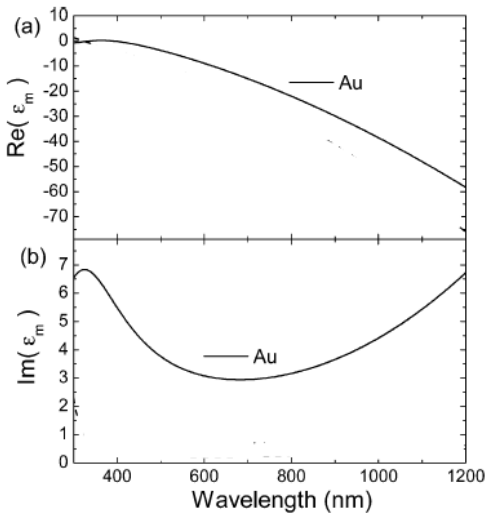

Figure 20 Wavelength-dependent dispersion of complex dielectric constant for Au taken from (K. S. Lee and El-Sayed 2005)

1.6.2 Imaging

Different imaging modalities exist but substantially they all consists in the detection of a signal (sound wave, electromagnetic wave) produced by a bioimaging probes that can be able to directly emit the signal or can emit it due to an external excitation. These bioimaging probes are defined as substances that in combination with an imaging modality provide a signal that allow the noninvasive visualization of certain process, biological structures, or conditions that would not be possible to monitor without the presence of the probe. There are two classes of bioimaging probes, conventional contrast-enhancing agents and imaging probes, the former are small chemical compounds that bear a detectable label, the latter consist in nanomaterials. The use of nanomaterials instead of conventional bioimaging probe provide several advantages(Buchwalder, Saatchi, and Häfeli 2014):

-multimodality: they allow to incorporate in the nanomaterial probes for different imaging modalities

-site specific targeting: they can be designed to become trapped in a specific area via active (attached targeting vector) or passive targeting (physical accumulation/attraction). In the case of active trapping multiple targeting vectors can be attached leading to an increase of the binding rate.

- size adaptability: they are capable to increase the circulation time since they are large enough to avoid renal clearance (filtration threshold of 7 nm). On the other hand, they are small enough to pass biological barriers and can accumulate by the enhanced permeability and retention effect (EPR)[3].

[3] In tumours and other diseased tissues an uncontrolled angiogenesis gives rise to an abnormal vasculature. Blood vessels are heavily branched, chaotically arranged and present large gaps between endothelial cells. From these holes nanomaterials can easily pass from the blood vessel to the tumour intersection. Moreover, tumour lacks lymphatic vessels and this allows nanomaterials to freely accumulate. This phenomenon of leaky vasculature and insufficient lymphatic drainage is known as EPR. Beside solid tumour, this effect occurs also in inflamed tissues such as in arthritis.

-theranostic potential: they permit to combine a diagnostic probe with a therapeutic drug. The so called " nanotheranostic" could provide the tracking of the drug and the real time assessment of the patient-specific response. Moreover, the drug administered in this way can be protected from premature degradation or it can change its biodistribution (for example it is allowed to pass blood-brain barriers).

However, nanoprobes compared to conventional small molecules have limited clinical application since they show a lower target tissue penetration and distribution and elimination of the unbounded fraction that cause an increase in the signal to background ratio(Buchwalder, Saatchi, and Häfeli 2014).

Gold nanorods, like other plasmonic nanoparticles, are suitable for optical imaging thanks to SPR. In this imaging modality, the measured signal is visible or NIR light and strong scattering from the particles increase their functionality in this imaging modality; the problem of this technique is the low penetration depth(Buchwalder, Saatchi, and Häfeli 2014).

GNRSs can also be applied for photoacoustic imaging which is based on the photoacoustic effect, namely when the sample is irradiated a certain amount of the energy is converted to heat and a thermoelastic expansion of the object is generated which causes an increase of pressure that propagate as sound waves. Detection of the pressure waves allows to localize their source and to obtain information about the studied sample. This method has the great advantage of a high penetration depth and its signal is proportional to optical absorption. In this case, the probe must have high absorption cross section, for this reason GNRSs can greatly enhance the contrast in this technique due to the high efficiency of SPR absorption in the NIR region where tissue are more transparent. It has been founded that gold nanostructures are able to enhance signal to noise ratio (Loredana Latterini 2015; X. Huang, Neretina, and El-Sayed 2009).

Photothermal imaging is another modality that can use GNRSs as a probe, it relies on the detection of heat gradients optically generated around the particles(Loredana Latterini 2015).

1.6.3 Gene delivery

Gene therapy is developing new molecular medicine whose goal is the development of new treatments for inherited and acquired life-threatening rare diseases. A genetic disease is due to a damaged gene that produce abnormal protein. By repairing the damaged gene, it is possible to cure or slow down the disease. To this purpose, the normal gene has to be insert in the patient's cells, where it can replicate and it is passed when the cells divides. The conventional vector for gene delivery is modified viruses but they can cause immunological responses and risk of cytotoxicity. GNRSs can be used for this purpose, a shape transformation of GNRSs can be obtained by exposure to NIR laser pulse and this can lead to the release of DNA (adsorbed into the GNRSs surface) due to surface atom rearrangement (Errant gene therapeutics 2019; X. Huang, Neretina, and El-Sayed 2009).

1.6.4 Photothermal treatments

The heat released by the relaxation of the excited plasmon of gold nanoparticles can be used to destroy different biological targets. GNRSs have been proved to successfully destroy cancer cells, however gold nanoshells are already applied in humans for lung and prostate cancer under the brand name of Aurolase® (https://nanospectra.com/). Photothermal treatments via heat release are

due to two different mechanism which differ in the temperature reached during the irradiation, hyperthermia and photothermal ablation. In the case of hyperthermia the tissue is heated to 45°C, this temperature causes dysfunction in the normal cell metabolism. This treatment is prolonged during time and a it is performed through the use of a continuous laser source. Photothermal ablation is due to a fast and high temperature increase that causes direct necrosis; in this case a pulsed-laser source is used(Loredana Latterini 2015).

Compared with other photothermal absorbers (e.g. carbon nanotubes), plasmonic nanoparticles allow to combine both imaging and photothermal therapy. In the case of GNRSs, they also allow to absorb light in the NIR region namely in the transparency window of biological tissue and for this reason, they are particular interesting(X. Huang, Neretina, and El-Sayed 2009).

Local heat must be selectively generated in the diseased cells, hence GNRSs has to be delivery to the cancer cells. This can be achieved by passive targeting (EPR) that in the case of GNRSs commonly involves CTAB replacement by PEG, this is due to the fact that decreases the non-specific cells absorption. Indeed, CTAB capped GNRSs tend to penetrate cells (non-specific absorption) via receptor-mediated endocytosis. Cells surface receptors are programmed to recognize proteins present in serum. The positively charged surface of CTAB molecules can interact with negatively charged serum proteins and with the new protein coating they are easily absorbed by cells. The other way can be active targeting which involves the use of conjugated compounds that specifically bind to cancer biomarkers (receptors overexpressed on the cancer cells) (X. Huang, Neretina, and El-Sayed 2009; Stone, Jackson, and Wright 2011).

1.7 Aim of the thesis

This work focuses on the study of the GNRSs growth mechanism in the innovative synthesis which utilizes an aromatic compound (5-bromosalicylic acid) along with CTAB surfactant. We focus in particular in the study of the roles of the silver nitrate ($AgNO_3$) and the aromatic compound in the different step of the growth. Silver nitrate concentration was changed for obtaining GNRSs with higher aspect ratio. The effect of the quenching step was also investigated in order to determine its efficiency. Reproducibility of the synthesis and the stability of the nanoparticles with the aging were also tested, since a precise control over the LSPR peak position is extremely important for GNRSs applications.

2 EXPERIMENTAL SECTION

2.1 Synthesis of GNRSs

Two solutions are prepared during the synthesis, the *seed solution* and the *growth solution*, both have to be maintained at 30°C and for performing the reactions the best vessels are scintillation vials.

Preparation of seed solution: 1mM (Au-stock solution) were mixed with 2.5ml of water, then 5ml of CTAB 0.2M are added. After mixing for 1 minute, 0.6 ml of ice-cold 10mM $NaBH_4$ were added and mixed vigorously (12000rpm) for 1 minute. The solution has been maintained undisturbed for 30 minutes and then added to the growth solution.

Preparation of the growth solution (Y. Huang et al. 2018): 0.36 g of CTAB along with 0.044 g of 5-bromosalicylic acid (5BrSA) were dissolved in 10 mL of water, placed in a water bath at 30°C and stirred for 1 minute. Then 0.60 mL of $AgNO_3$ 4mM were added and the solution was stirred for 30 seconds and left undisturbed for 15 minutes. Subsequently, 10 mL of Au-stock solution were added, followed by 0.084 mL HCl (37 wt%). After 15 minutes of slow stirring (400 rpm), 80 µL of ascorbic acid 64 mM were added drop by drop. The final step was the addition of 32 µL of the seed solution to the growth solution and at the same time, the stirring was stopped with the removal of magnetic rod. The growth solution was kept at 30°C avoiding any disturbance for all the time of the growth.

Table 1 concentrations of reagents for GNRSs synthesis in stock solutions and final concentration in growth and seed solution

	mM stock solution	mM growth solution	mM seed solution
$AgNO_3$	4	0.12	
$HAuCl_4 * 3H_2O$	1	0.48	0.24
Ascorbic acid	64	0.25	
CTAB	200	47.50	94.34
$NaBH_4$	10		0.57
HCl		48.40	
5BrSA		9.57	

Quenching of the growth solution: it occurs by the addition of a volume of Na_2S solution which is twice the volume of the growth solution and which enables to obtain a sulphur to metal ratio equal to 4. Then a volume of water 3.5 times the volume of the growth solution is added. After 15 minutes the solution is centrifuged at 12000 rcf for 30 minutes, then the supernatant is removed by means of a Pasteur pipette and the obtained GNRSs pellets are dispersed in a volume of water equal to the initial treated volume.

Warning:

- Every piece of glassware must be washed with aqua regia and every source of contamination has to be avoided (lab environment has to be kept clean, metallic surfaces in vials' cap have to be avoided etc).

- $HAuCl_4$ is highly hygroscopic and it attacks metal spatula, so to weight it parafilm can be used to form a plastic film on the spatula. Parafilm is also useful as weighing paper since it is possible to rinse it with water that has to be collected to Au stock solution's volumetric flask.
- $AgNO_3$ and ascorbic acid solutions must be prepared fresh every time and carefully protected from the light. If the quality of the reducing agent is adequate, after the ascorbic acid addition the solution should become colourless within about 30 seconds, even with a very low stirring (200rpm)
- $NaBH_4$ has to be weighed as fast as possible and the water used for its solution has to be previously maintain in an ice bath. The addition of $NaBH_4$ solution to the seed solution must be as fast as possible.
- CTAB and CTAB and 5BrSA solutions need to be heated for allowing organic substances dissolution (it can be done by keeping vials in hot tap water) and then it is better to maintain them under stirring. It is also important to control that at the beginning of the synthesis foam is not present, otherwise it can compromise the addition and mixing of the reagents.
- Seed solution must be aged 30 minutes before the addition to the growth solution and it has to be ready when ascorbic acid is added to the growth solution. For this reason, it is convenient to carefully schedule the timeline of the synthesis. It is useful to start the synthesis with the preparation of the seed solution until the step of $NaBH_4$ addition. At this point it is convenient to start with the preparation of growth solution. After adding $AgNO_3$, and while the growth solution has to be kept quiet, the weighting of $NaBH_4$ and the finishing of the seed solution synthesis are recommended. This schedule should assure the respect of the desired timeline.

2.2 Characterization

IR measurements were performed with Nexus FT-IR, UV-VIS-NIR spectra were obtained with Perkin Elmer Lambda 750.

2.2.1 Scanning Electron Microscopy (SEM)

Information on the sample is obtained by its interaction with an electron beam that generates signals in the form of secondary electrons, back scattered electrons and X-rays. Secondary electrons are due to inelastic interactions between the primary electron beam and the sample, these electrons are very beneficial for the inspection of the topography of the sample's surface. Backscattered-electrons (BSE) are due to elastic collisions of electrons with atoms. The higher is the atomic number of the atom the higher will be the scattering and hence a higher number of electrons are collected by the detector. When the electron beam strikes the surface of a sample it causes the emission of X-ray photons. Energy Dispersive X-ray Spectroscopy (EDS) uses this emitted X-rays to obtain a localized chemical composition through the analysis of their energy (CFAMM 2017; Phenom-World BV 2017; Joshi, Bhattacharyya, and Ali 2008).

The measures were performed with a ZEISS-Sigma VP FE-SEM

Sample preparation: the specimen is deposited on a sample holder (stub). First of all, the stub has to be properly cleaned, this can be done in an ultrasonic bath with acetone as solvent (two cycles of 15 minutes each). A double-sided conductive tape is used to mount a silicon wafer on the stub.

GNRSs aqueous solutions (after purification, see next paragraph) is then dropped onto the silicon wafer.

The purification of the GNRSs consists in the removing of part of CTAB so that a SEM measure can be performed; GNRSs solutions, have to be centrifuged two times: 1.5ml of GNRSs solution is transferred into a conic Microcentrifuge Tubes and centrifuge at 12000 rcf for 15 minutes, after that the supernatant is removed and replaced with 1.5ml of Milli-Q water. The subsequent redispersion of the pellets using a vortex mixer could sometimes be difficult and the pellet remains as a red spot at the bottom of the tube, in this case it needs to be redispersed in an ultrasonic bath. After the second step of centrifugation, supernatant is again substituted with Milli-Q water and pellet is redispersed. At the end of this process the solution can be considered purified from CTAB and be used for SEM analysis.

2.2.2 Transmission Electron Microscopy (TEM)

In this case an electron beam passes through the sample and an image is formed from the transmitted electrons that have interacted with the sample. Interactions between the atoms and the electrons allow to observe sample characteristics such as crystal structure but also its defects, for example in the High Resolution TEM (HRTEM) mode. TEM allows to perform chemical analysis of the sample by EDX(Joshi, Bhattacharyya, and Ali 2008)

The measures were performed with a JEM3010, Jeol microscope.

Sample preparation: GNRSs aqueous solutions have been dropped to TEM grids (holey carbon film on copper grid) placed above optical paper. A micropipette was used to withdraw 6 µL of the solution, then micropipette has been set to a higher volume value (about 20 µL) in order to be able to completely release the drop without the needing to touch the grid. The small volume of solution forms a small drop within the border of the grid that allows to avoid losses of GNRSs in the paper.

2.2.3 X Ray Diffraction (XRD)

ray diffraction (XRD) is a widely used technique for the study of properties of solids. A X ray beam striking the sample, it is diffracted following the Bragg law:

$$sin\theta = \frac{n\lambda}{2d_{hkl}}$$

Where n is an integer, d_{hkl} is the distance between crystalline planes with Miller indices (hkl) in the crystal, λ is the wavelength of the incident X ray beam and θ is its angle of incidence. The XRD spectra reported the intensities of the diffracted X ray beams as a function of the angle.

The equation of Debye-Scherrer allows to determine the grain dimension of crystallite

$$d = \frac{K\lambda}{b\ cos\theta}$$

Where b is the full width at half maximum of the peak, θ is the angle of incidence, λ is the wavelength of the incident X ray beam and K is about 0.9.

The measures were performed with Philips XPert diffractomer with a Cu radiation.

Sample preparation: GNRSs solutions were concentrated by centrifuge: 4ml of GNRSs solution are transferred to two conic microcentrifuge tubes and centrifuged at 12000 rpm for 15 minutes, then the supernatant was removed and about 50 µL of Milli-Q water were used for sample redispersion. The concentrated solutions were deposited to a zero-background holder by subsequent drops deposition until a good coverage of the holder was obtained.

2.2.4 Microwave Plasma Atomic Emission Spectroscopy (MPAES)

MP-AES consists of a microwave induced plasma interfaced to an atomic emission spectrophotometer (AES). Multi-analyte determination of major and minor elements can be performed simultaneously. It allows to produce plasma using nitrogen by the employ of microwave energy.

Samples are introduced into the device by means of a peristaltic pump and nebulized in a spray chamber prior interaction with the plasma. The aerosol is injected into the plasma where the solvent is removed from the sample, it is atomized and excited. The subsequent electrons return to the ground state emits light that is separated into a spectrum and the intensity of each emission line is measured at the detector.

The measures were performed with Agilent 4210 MP-AES

Sample preparation: Aqua regia has been added to the samples, obtaining a final concentration of 30% v/v as required in the sample digestion method (Coombs 2016). After 1h of digestion (Su, Yang, and Zhu 2015) solutions were diluted to obtain a final aqua regia concentration of 10%, which better fit instrument requirement. GNRSs solutions, standard gold solution and gold salt solution were treated all in the same way.

2.3 Chemicals

- Cetyltrimethylammonium bromide (CTAB, Sigma, 98%, 364.45 g/mol)
- Silver nitrate ($AgNO_3$, Sigma, 99%, 169.87 g/mol)
- Tetrachloroauric acid trihydrate ($HAuCl_4 \cdot 3H30$, Aldrich,99%, 393.83 g/mol)
- Ascorbic acid (AA, Sigma, 99%, 176.12 g/mol)
- Sodium borohydride ($NaBH_4$, Aldrich, 98%, 37.83 g/mol)
- Aqua regia (3:1 of HCl - HNO_3 solution)
- Milli-Q Water
- Sodium Sulphide (Na_2S, Sigma,78.0452 g/mol)
- 5-Bromosalicylic acid (5BrSA, Sigma,90%, 217.02 g/mol)

3 RESULTS AND DISCUSSION

3.1 UV-VIS-NIR spectroscopic study of the GNRSs synthesis

In order to describe and understand the different reactions involved in the GNRSs' protocol, UV-VIS-NIR spectroscopy has been utilized to measure solutions in the different steps of growth and nucleation process.

3.1.1. Seed solution

As reported in the experimental section, seed solution is prepared by the addition of the sodium borohydride ($NaBH_4$) in a solution of CTAB and gold precursor. The spectrum of the solution before and after the addition is reported in Figure 21, blue line spectrum (CTAB+$HAuCl_4$) corresponds to the solution prior to $NaBH_4$ addition, while the red line corresponds to the seed solution 30 minutes after the addition of the reducing agent. In the spectrum of CTAB and $HAuCl_4$ it can be seen that there is a peak at 396nm which corresponds to the formation of the complex Au(III)-CTAB (Su, Yang, and Zhu 2015).

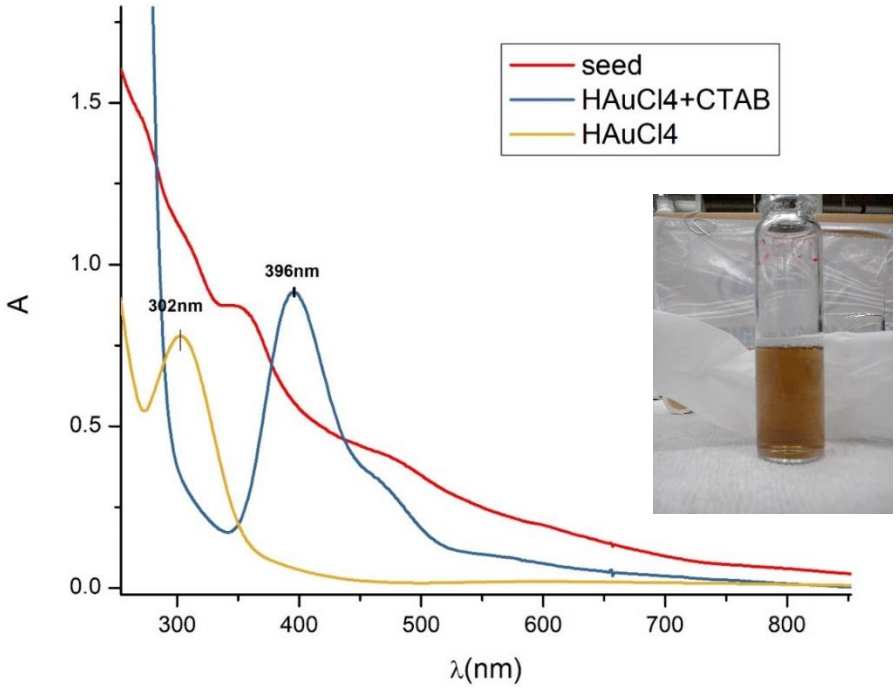

Figure 21 UV-VIS-NIR spectra of $HAuCl_4$ 0.25 mM (yellow line, seed solution before the addition of NaBH4 (blue line) and after the addition of the reducing agent (red line) at aging time of 30 minutes. On the right, the picture of the seed solution corresponding to the red line in the spectra

Even though it is commonly reported in literature the formation of the specie $AuCl_4^-CTA^+$ (Orendorff and Murphy 2006; Mulvaney et al. 2004) considering the chemistry of Au(III) the following reaction should be taken into account (Scarabelli et al. 2015):

$$[AuCl_4]^- \rightleftharpoons [AuCl_3Br]^- \rightleftharpoons [AuCl_2Br_2]^- \rightleftharpoons [AuClBr_3]^- \rightleftharpoons [AuBr_4]^-$$

Indeed, Au (III) is a d^8 soft metal center, forming square-planar complex. The complexation strength between Au(III) and halide anions follows the series $I^- > Br^- > Cl^-$. Thus $AuCl_4^-$, in the presence of bromide ions deriving from CTAB, can exchange chloride with bromide anions. Then $AuBr_4^-$ ions will

form an ion pair with the quaternary ammonium surfactant monomers ($AuBr_4^-$-CTA^+). This is proved by the difference between the spectra of $HAuCl_4$ and $HAuCl_4$+CTAB solutions, respectively yellow and blue line in Figure 21. Indeed, the former presents a peak at 302nm and appears pale yellow, while the latter shows the already mentioned absorption maximum at 396nm, which is attributed to $AuBr_4^-$ (Usher, McPhail, and Brugger 2009) and appears dark-yellow/orange.

After the addition of $NaBH_4$ the solution turns light brown due to the formation of small nuclei. Since the solution does not present red-pink shade, and more importantly, the absorption spectrum does not present band corresponding to surface plasmon resonance in the region between 500 and 600nm, the obtained particles have an average diameter equal or below 2nm (Link, Mohamed, and El-Sayed 1999; Scarabelli et al. 2015). However, absorption at about 350nm and just before 500nm are due to absorption peaks associate with interband and intraband transitions for Au clusters (Park et al. 2013)

3.1.2. Growth solution

Figure 22 reports the spectra, respectively in pink and yellow line, of the growth solution prior to the addition of seed solution and of a solution of CTAB, 5BrSA and $HauCl_4$ in the same concentrations as the growth solution. The peak at 396nm is not present in the pink line spectrum due to the reduction of Au (III) to Au (I), that occurs after the addition of ascorbic acid and causes the color of the solution turning from yellow to colorless (the ligand to metal charge transfer disappears for a d^{10}metal center as Au(I)).

In the spectrum of the growth solution after the addition of the weak reducing agent, the peak at 310 nm is the only peak present, since it is attributable to 5BrSA. The fact that this peak is due to 5BrSA is clear looking at Figure 23 where the spectra of CTAB and 5BrSA, CTAB and $HAuCl_4$, CTAB,5BrSA and $HAuCl_4$ solutions are compared. Indeed, it can be seen that solutions containing the gold precursor show the absorption of $AuBr_4^-$, but only solutions containing 5BrSA show the peak at 310 nm.

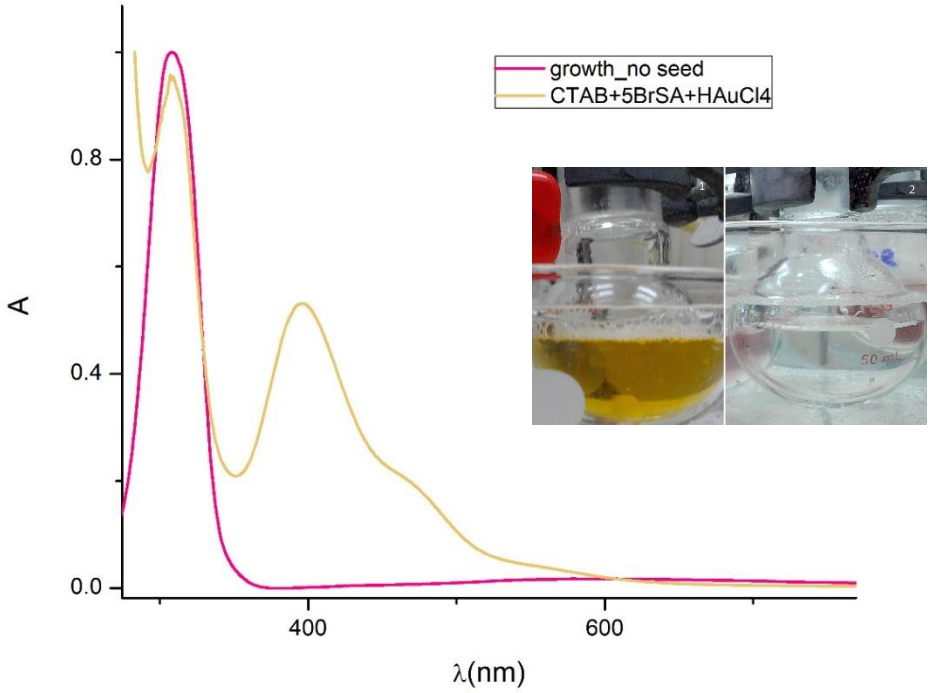

Figure 22 the pink line is the absorption spectra of growth solution before the addition of seed solution. The yellow line is the spectrum of a solution of CTAB, 5BrSA and HauCl4 in the same concentrations as the growth solution. The spectra are normalized. In the pictures it can be seen the growth solution before (1) and after the addition of ascorbic acid (2)

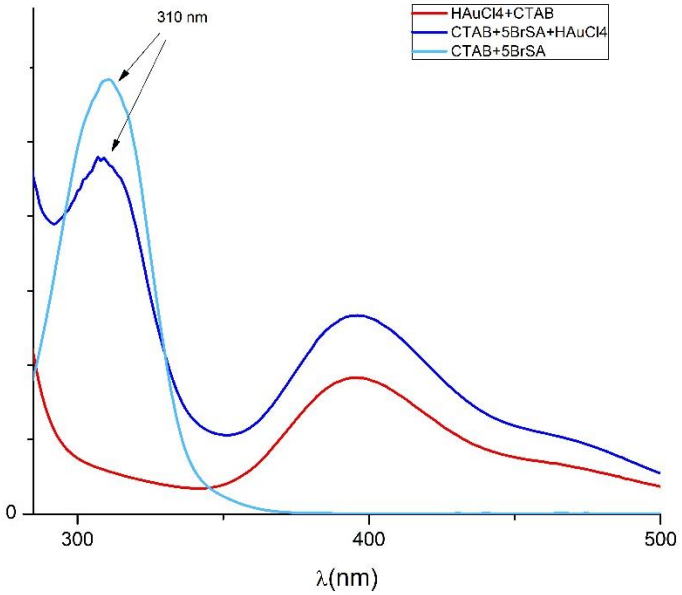

Figure 23 spectra of solutions of CTAB and 5BrSA (light blue line), CTAB and HAuCl4 (red line) CTAB,5BrSA and HAuCl4 (blue line). The spectra were shifted for distinguishing them better.

3.1.3 Reducing agents in the growth solution

The aromatic additive employed in the synthesis is a phenol derivative which is known to be a mild reducing agent. For this reason, 5BrSA capability to reduce Au (III) to Au (I) has been studied. A solution of CTAB,5BrSA and $HAuCl_4$ in the same concentrations as the growth solution, has been monitored during the time by UV-VIS-NIR spectroscopy. The same was done to CTAB, ascorbic acid and $HAuCl_4$ solution, for comparing the two results and hence the two reducing powers. The addition of the ascorbic acid in the growth solution changes the colour of the solution in about 30 seconds (30°C, under mixing), so in order to better compare the two reducing agents both the studies were carried out at room temperature and without mixing.

In both systems the peak at 396nm was monitored during the time, and it was found to gradually decrease as reported in Figure 24. Therefore, the reduction of Au (III) occurs in both systems, even though at different rate, so 5BrSA is proved to be capable of reducing Au (III) but it takes longer time than the ascorbic acid. Indeed, during GNRSs synthesis the growth solution remains coloured until the addition of ascorbic acid.

In the case of 5BrSA solution the peak at 310nm, previously attributed to the aromatic additive, decreases during the time due to its action as reducing agent.

In the spectrum of the ascorbic acid solution, it can be seen that during the time also the peak at 258 nm disappears, so it is attributable to $AuBr_4^-$ too (ascorbic acid shows a peak at 246nm).

In order to understand the influence of the reducing power of the additive, a growth solution was prepared without the addition of the ascorbic acid. Even though it was kept in the same conditions as the normal growth solution, after an initial disappearance of the solution color (it occurred in about 30 minutes) that proved the reduction of the gold precursor, the solution remained colorless, hence GNRSs did not form. This means that, even if the aromatic additive is capable of Au (III) reduction, the presence of the ascorbic acid is anyway fundamental for obtaining Au^0.

The three oxidation states of gold involved in the GNRSs' synthesis are related by the following equilibrium:

$$3Au^{+} \leftrightarrows Au^{3+} + 2Au^{0}$$

Depending on the relative stability of each specie in the mixture, the equilibrium can be pushed toward comproportionation or disproportionation. Indeed, Au (I) which is present in the growth solution as complex $[AuBr_2]^-$, tend to strongly disproportionate in water, however elevate halide excess can stabilize it (Cotton and Wilkinson 1988). Indeed, in the growth solution Au(I) is the most stable specie, it means that GNRSs (Au^0) are oxidized in presence of Au(III). The role of the weak reducing agent in the seed mediated growth is to avoid the presence of Au(III) in solution without permitting secondary nucleation (reduction of Au(I) to Au^0 have to occur only on the seed surface)(Scarabelli et al. 2015).

As regard as the mechanism of gold reduction into the seed surface two mechanisms have been proposed:

1) The disproportionation reaction, catalysed by the seeds, produces Au(0) and Au(III), the latter one immediately being reduced again into Au(I) by the remaining reductant(Kumar, Gandhi, and Kumar 2007) ,
2) The Au(0) surface drains electrons from the reductant and catalyses the in situ reduction of Au(I) (Rodríguez-Fernández et al. 2006).

All these equilibriums and mechanisms could be influenced by the presence of additives with reducing properties, even if weak. This demonstrates that 5BrSA could influence the growing system beyond the effect on the CTAB structure.

In this scenario, the ligand exchange and the $AuBr_4^-$-CTA^+ complex formation must be considered since they shift the redox potentials (toward lower values) (Scarabelli et al. 2015). These variations will influence the kinetic of the growth, so after the step of gold precursor addition in the growth solution, it is important to ensure that the ligand exchange has been completed before continuing the synthesis.

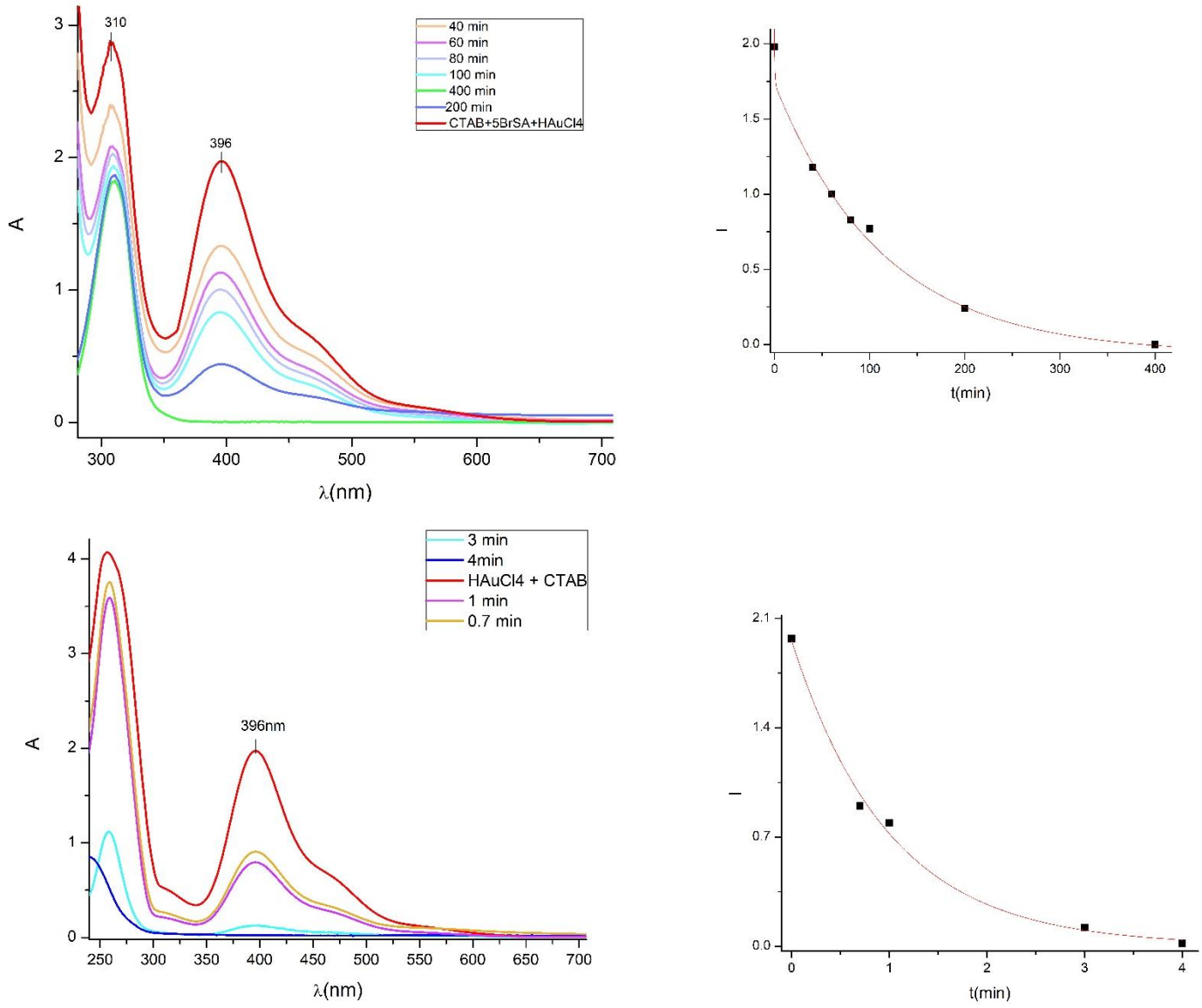

Figure 24 time evolution of UV-VIS spectra of CTAB+$HAuCl_4$ and 5BrSA solution on the top, CTAB+$HAuCl_4$ and ascorbic acid solution on the bottom. On the left is reported the time evolution of intensity of the peak at 396 nm

3.2 Organic layer on GNRSs surfaces: the role of 5BrSA

It is reported in literature that 5BrSA is likely to be involved in the interactions between CTAB and the GNRSs, and this would influence the size and the shape of the obtained particles. To verify the existence of this interaction, FTIR spectrum of the synthesized GNRSs was obtained in order to determine if the aromatic additive is part of the organic layer around the particles or if only CTAB is present.

To determine the composition of the organic layer on the surfaces of the particles, it is important to remove the residues of these substances that remain in the solution after the quenching. For this reason, the sample has been purified as reported by Su, Yang, and Zhu 2015: GNRSs aqueous solution (6ml), obtained after the quenching of the growth solution (Na_2S addition and centrifugation process), was centrifuged for 15 minutes at 12000 rcf, then the pellet was redispersed in Milli-Q and centrifuged again in the same way. Hence, considering the quenching process, the sample was washed by centrifugation process three times in total.

The obtained GNRSs pellets at the end of the washing procedure were dried at 50°C for 1h and then mixed with KBr and pressed to a pellet. The obtained FTIR spectrum is reported in Figure 25 altogether with CTAB and 5BrSA spectra obtained from a KBr pellet too.

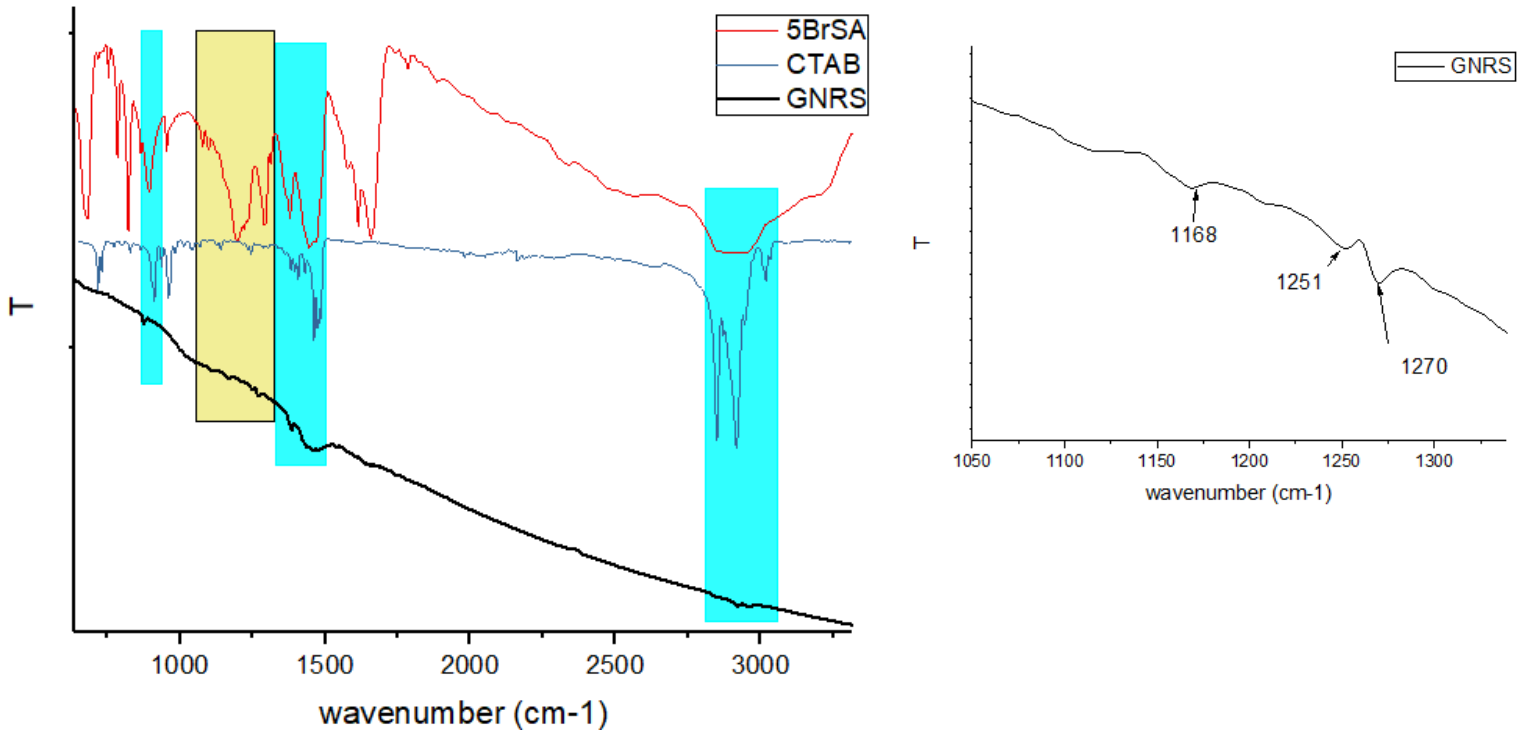

Figure 25 FTIR spectra of purified GNRSs (black line), pure 5BrSA (red line), pure CTAB (blue line). Spectrum of GNRSs in the fingerprint region is enlarged on the right

Peaks identified with the blue area can be attributed both to CTAB and 5BrSA,however in the region between 1050 and 1350 cm^{-1}, which is identified with the yellow area and enlarged in the picture on the right in Figure 25, CTAB spectrum does not present any absorptions so the bands in the GNRSs

spectrum are due to 5BrSA. Indeed, this is the so called “fingerprint region” that contains contributions from in-plane C-H bending, C-O stretching of the hydroxyl group and vibrations of the benzene ring.

Since a mix of vibrational modes is present in this region, for aromatic compounds a clear interpretation of these FTIR peaks remains challenging. However, the presence of the peaks in the yellow area in the spectrum of GNRSs suggests that aromatic additive is present in the organic layer on the surface of the particles.

Further evidences of 5BrSA presence on the GNRSs surfaces come from UV-VIS-NIR spectra.

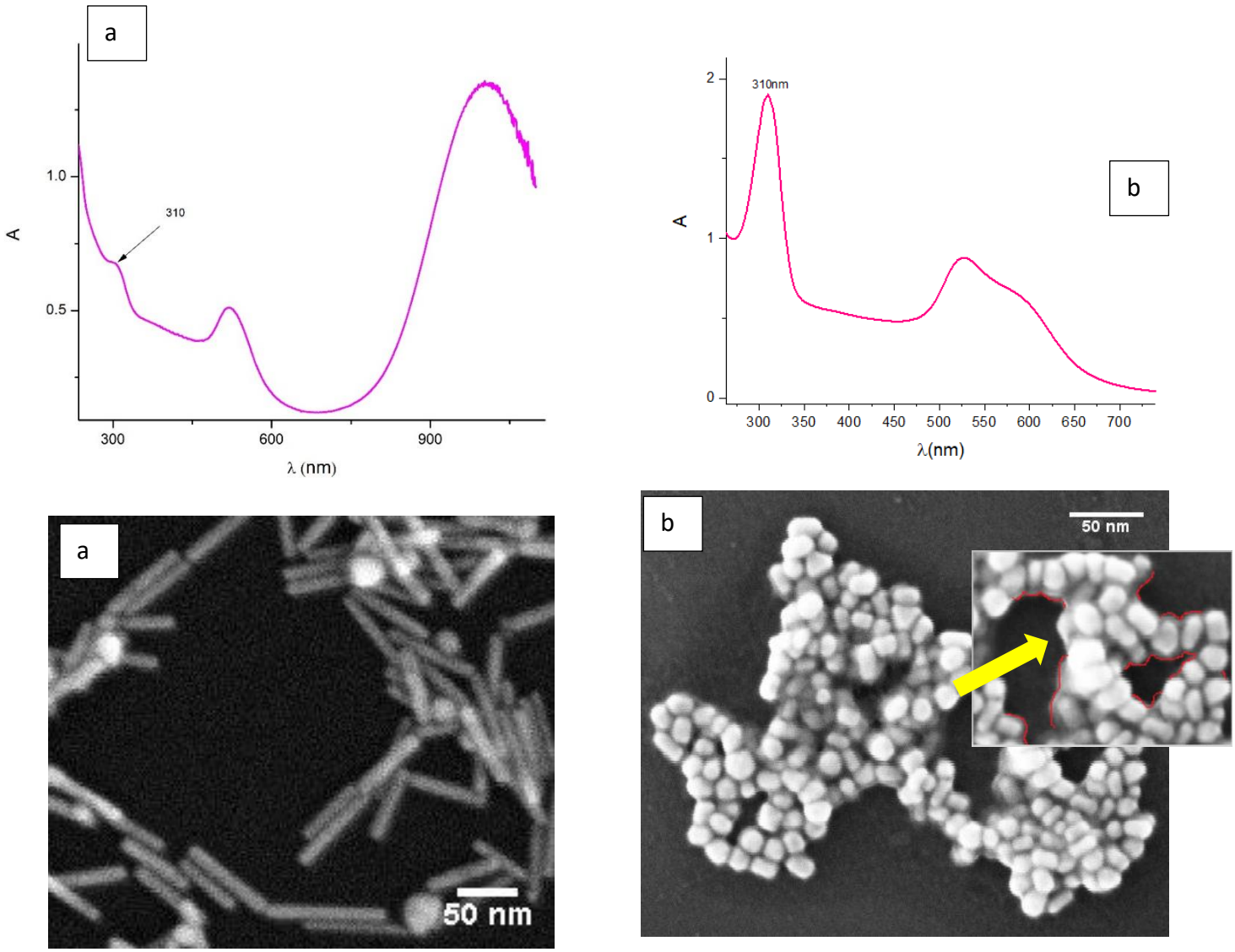

Figure 26 UV-VIS-NIR spectra and SEM images of (a)carefully purified GNRSs sample (like the sample used for FTIR measure), (b) sample washed in total only two times. In the enlargement of the SEM image of the sample b the layer around the particles is highlighted

In

Figure 26 UV-VIS-NIR spectra and SEM images are reported for two samples that have been differently purified. Indeed, sample b has been subjected to two washing cycles, instead of three. Both the spectra present the peak at 310 nm which is attributed to 5BrSA, but it shows different intensities. Sample b, differently from sample a, in SEM image shows a visible organic layer around the particles and from UV-VIS-NIR spectrum it can be determined that the layer contains a relatively high amount of 5BrSA. However, even if sample a does not present a visible organic layer around the particles in SEM image, it anyway shows the peak of 5BrSA, even if less intense.

Hence, from FTIR, UV-VIS-NIR and SEM results, it is possible to confirm the presence of the aromatic additive in the surface of GNRSs which decreases with the increasing of the particle purification. However also for particles with a high degree of purification 5BrSA is present, indeed suggesting that it may be strongly embedded within the CTAB capping layer of GNRSs; for this reason, even the highly purified samples continue to maintain 5BrSA onto the particle surface. This result suggests that some kinds of interactions take place between the additive and the surfactant, this is in line with the proposed model that suggest the penetration of the additive aromatic ring into CTAB hydrophobic alkyl chain (Ye et al. 2012).

3.3 Influence of the quenching step in the obtained GNRs

Quenching of the growth solution can occur by simple centrifugation and redispersion (CR) or by the addition of sodium sulphide (Na_2S) with an optimized sulphur to metal ratio of 4:1 followed by CR (Zweifel and Wei 2005). In this work, to evaluate different aspects of GNRSs growth, aliquots were sampled from growth solutions and treated in the same way as the whole volume of growth solution. In order to understand the sensitivity of GNRSs to centrifugation process and addition of sodium sulphide and also the reproducibility of sampling, the reported following steps were carried on.

3.3.1 Studies on sampling step

Reproducibility of the aliquots was investigated by UV-VIS-NIR spectroscopy. The whole quenching process, as already said, consists of:

1) Na_2S addition with ratio S/M=4 (Q);

2) centrifugation for 30 minutes at 12,000 rcf and redispersion in a volume of Milli-Q water equal to the volume of the sampled aliquot.

Three aliquots (identified as 1,2,3) of 1 ml each were taken from the same solution at the same time (sample 3_R_2d, see paragraph 3.8), they were all equally Q and CR. In Figure 27 the spectra of the three samples are reported, while in Table 2 are reported the evaluated parameters. Even though some differences are present among the samples, RSD% for each parameter remains acceptable. As regards to A_{400}, this absorption value increases with increasing the number of Au° atoms in the solution, namely with increasing GNRSs concentration.

Since the three aliquots were centrifuged in the same way, the difference in the evaluated parameters among the aliquots, could be due to the subsequent step of pellet purification. Indeed, after the centrifuge, GNRSs separation from the supernatant may be responsible of A_{400} values dispersion since GNRSs pellets tend easily to return in the supernatant, so it is necessary to carefully remove the liquid using a Pasteur pipette, but during this process an undeterminable fraction of GNRSs could be lost.

Table 2, maximum peak positions of LSPR and TRSP, intensity of absorption of the LSPR at λmax, ratio L/T, half width at half and maximum, absorption at 400 nm (A_{400}) values and their standard deviations, confidence intervals and relative standard deviations for the three aliquots of the sample 3_R_2d.

sample n°	LSPR(nm)	TSPR(nm)	A 400 nm	I LSPR	I TSPR	L/T	HWHM low
1	1019	515	0.40	1.16	0.40	2.90	117
2	1020	515	0.38	1.13	0.37	3.08	118
3	1016	514	0.37	1.09	0.36	3.02	116

	σ	RSD%	δ (95%)
LSPR	32	0.2	5
TSPR	0.6	0.1	1
A 400 nm	0.02	4.6	0.04
I LSPR	0.03	3.0	0.09
I TSPR	0.02	1.9	0.05
L/T	0.09	3.0	0.2
HMHM low	1.00	0.9	2

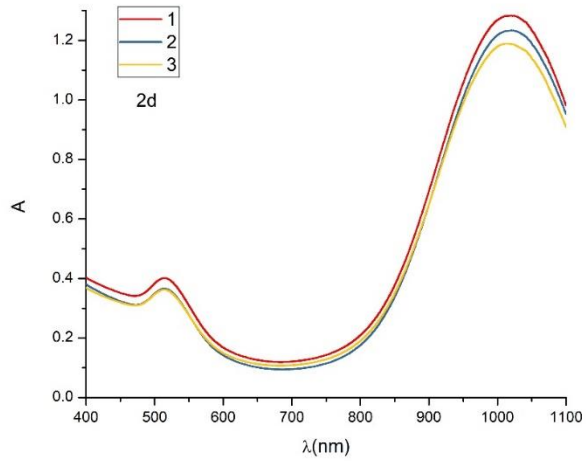

Figure 27 UV-VIS-NIR spectra of three aliquots Q and CR taken from 5.5mM2_1809_2d growth solution

In order to establish if the Q and CR process are the main source of errors, three aliquots have been sampled at the same moment from the same growth solution and measured without any treatments (except for dilution 1:2 that was necessary for the measure). As it can be seen from Table 3,it is proved that Q and CR process is the main source of value dispersion.

Table 3 maximum peak positions of LSPR and TRSP values and their standard deviations, confidence intervals and relative standard deviations

n°	LSPR(nm)	TSPR(nm)
1	834	515
2	833	514
3	834	514

	σ	δ (95%)	RSD%
TSPR	0.6	1	0.2
LSPR	0.6	1	0.2

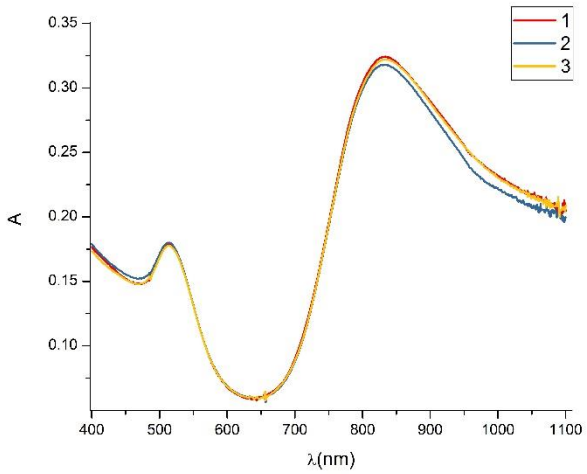

Figure 28 UV-VIS-NIR spectra of three aliquots taken from 4_W_7d growth solution, aliquots were diluted 1:2

3.3.2 Effects of Q and CR process

In order to determine Q and CR effects on GNRSs, during the growth of 4_W sample (see paragraph 3.4), aliquots were taken at different growing time (t=0 corresponds to the moment of seed addition in the growth solution). Two aliquots were sampled simultaneously 4,5,6,7 days after seed addition, and every time one aliquot was quenched by the addition of Na_2S and centrifuged as already reported (Q/CR), while the other was directly measured by UV-VIS-NIR spectroscopy without being subjected to any treatments (sample). In this study we focus on the differences between peak positions of SPR of the two set of aliquots.

Table 4 positions of λ_{max} of both LSPR and TSPR for aliquots Q/CR and untreated (called sample)

4_W	Q&CR		sample	
t (day)	LSPR(nm)	TSPR(nm)	LSPR(nm)	TSPR(nm)
7	844	515	834	515
6	853	514	843	514
5	865	514	851	514
4	878	515	870	512

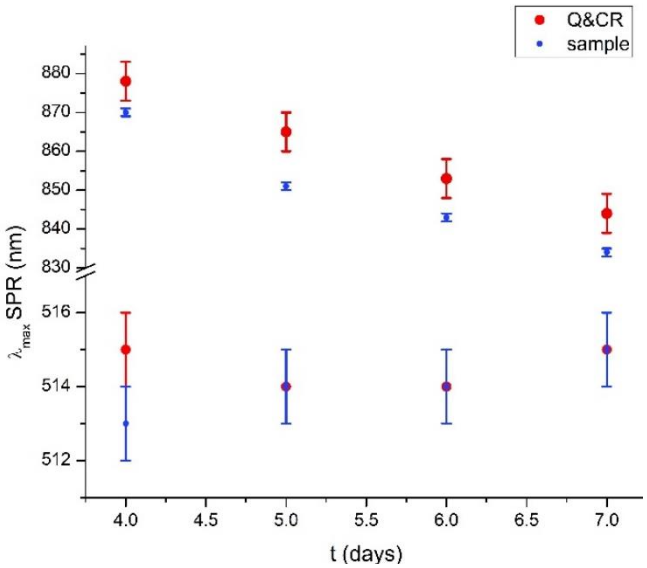

Figure 29 time evolution of TSPR and LSPR for both untreated aliquots (sample) and Q/ CR aliquots, the errors bars are taken from the previous studies on reproducibility

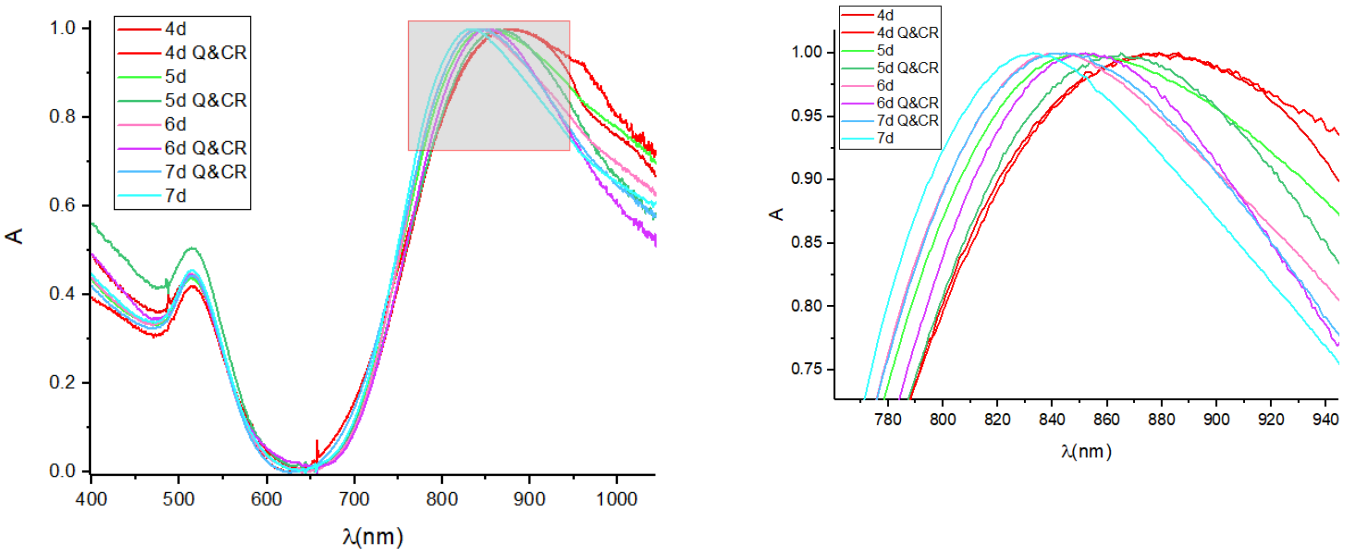

Figure 30: normalized spectra of aliquots taken from 4_W during the time and diluted 1:2. More bright lines refer to untreated aliquots. Enlargement of the grey area in the spectra is reported on the right

As it can be seen from the above results, Q/CR process determine a red shift of LSPR peak (about 10 nm) that seems not to be dependent on the aging time considered, while TSPR peak does not show a significative change. In order to determine which step of the Q/CR process is responsible of the shift, two growth solutions (4_B and 5_B see paragraph 3.7) were used for further studies. The aliquots were sampled at the same aging time, namely 2d after seed addition, and they were treated as follows:

- Sample: untreated aliquots, they were taken and measured;
- CR: aliquots were taken, centrifuged, redispersed, and then measured;
- Q/CR: aliquots were taken, quenched with Na_2S (S/M=4), centrifuged, redispersed, and then measured;
- Q: aliquots were taken, quenched with Na_2S (S/M=4) and measured.

Peaks positions (both LSPR and TSPR) are reported in Table 5, while spectra and peak positions trends are reported in Figure 31.

Table 5 positions of λmax of both LSPR and TSPR for aliquots only quenched(Q), quenched and centrifuged-redispersed (Q/CR), untreated (sample) and only centrifuged-redispersed (CR), ΔLSPR refers to the difference between the value of λ_{max} of Q aliquots- and λ_{max} of other aliquots.

	5_B			4_B		
aliquot	LSPR (nm)	TSPR (nm)	Δ LSPR	LSPR (nm)	TSPR (nm)	Δ LSPR
Q	947	512	-	899	514	-
Q /CR	943	517	4	896	519	3
sample	934	516	13	883	514	16
CR	932	516	15	880	519	19

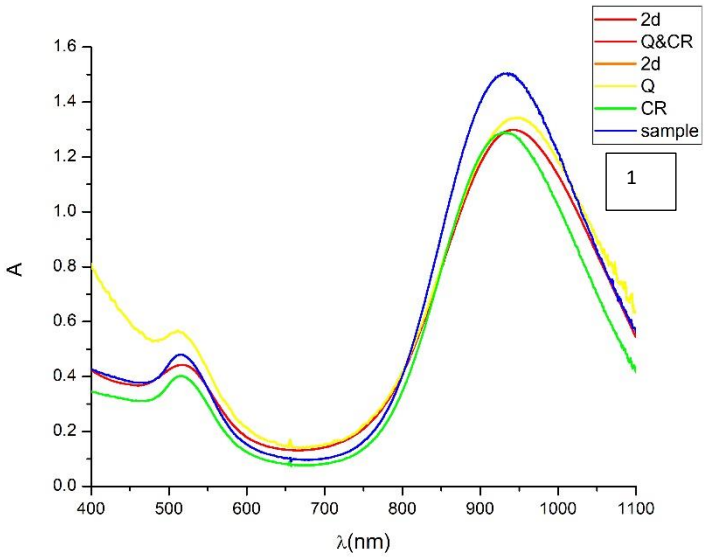

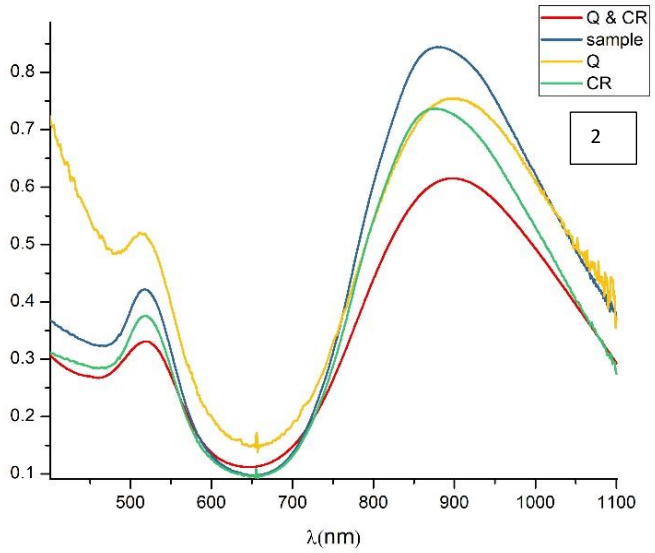

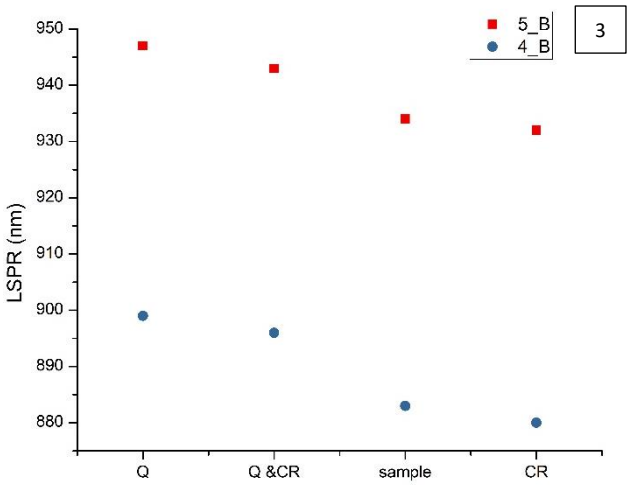

Figure 31 1) spectra of aliquots taken from 4_B 2) spectra of aliquots taken from 5_B 3) λ_{max} of LSPR of different aliquots

From the above data it can be seen that the value of LSPR peak position for Q aliquots is the highest, hence Na_2S addition is the responsible for the red shift. Na_2S, which serves as a scavenger for metal ions (gold and silver), causes a red shift probably due to its absorption into GNRSs surfaces. Indeed anisotropic nanoparticles, such as nanorods, are really sensitive to the changes in their local environment (plasmon resonance is strongly related to the dielectric constant of the medium) (Zweifel and Wei 2005). CR aliquots have the lowest value of λ_{max} LSPR, even lower than the untreated aliquots (sample) that are likewise Na_2S free, so the centrifugation process may be responsible of a weak blue shift of the LSPR maximum. Moreover, between Q and Q/CR aliquots, the latter shows a slightly smaller value of λ_{max} LSPR that can be also in this case due to centrifugation too.

Considering that 4_B and 5_B have different R mean values, respectively R=4.7±0.3 and R=5.6±0.2, comparing the previously reported results for these two samples, they do not show significative differences, moreover the differences in the LSPR maximum position between Q/CR aliquots and the untreated aliquots are comparable to what has been determined before for the sample 4_W,

namely the shift is around 10 nm. These results suggest that Q and CR process do not differently affect GNRSs with different aspect ratio.

In order to determine if slightly different S/M ratios can cause a significant change in the position of LSPR, different ratios S/M were used for the quenching of sample 3_R (see paragraph 3.8).

Three aliquots of 1ml each ([Ag+Au]=0.65mM) were quenched with 2ml of Na_2S 0.65mM, 0.97mM, 1.30mM, 2.05mM so respectively corresponding to a ratio S/M equal to 2,3,4 and 6.

Table 6 positions of λmax of both LSPR and TSPR for aliquots quenched with Na_2S solutions corresponding to S/M ratios of 2,4 and 6.

M/S	TSPR (nm)	LSPR (nm)
2	512	1015
3	513	1017
4	514	1018
6	516	1023

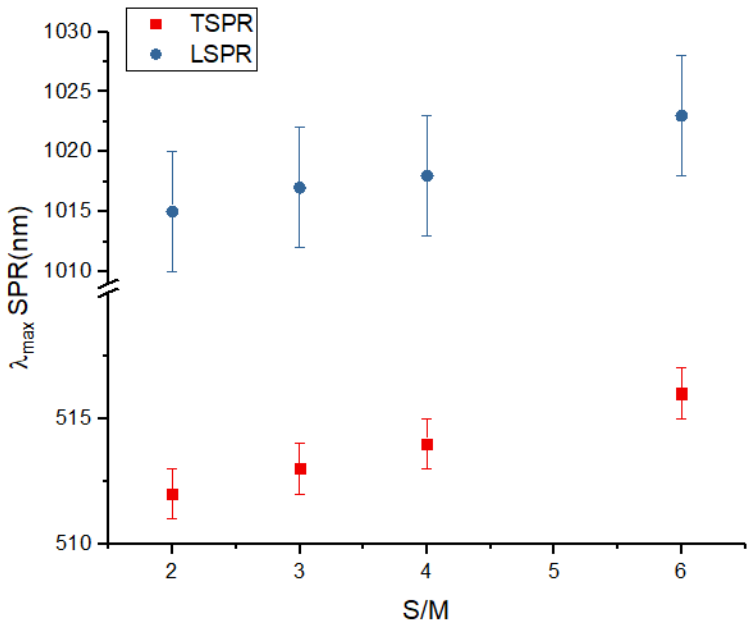

Figure 32 positions of λ_{max} of both LSPR and TSPR for S/M ratios of 2,3,4 and 6. The errors bars are taken from the previous studies on reproducibility

As it can be seen from the above data, Na_2S induces a concentration dependent shift of plasmon resonance toward longer wavelengths. In this case, where only the S/M ratio is changed, also the TSPR shows a trend in line with the one of LSPR, hence different ratio S/M shifts both the resonance peaks. For the values of LSPR a linear fit (R^2 =0.989) gives an intercept value of 1010nm, corresponding to a difference of 9 nm between S/M=4 and S/M=0 and this is in line with the previous results.

Considering the uncertainty for the LSPR peak position values, a difference of 2.5 in the M/S ratio is required to determine a significative difference in the LSPR maximum peak position (5nm). This means that sligth differences in the S/M ratio (derived from the use of a common Na_2S solution for

the quenching of growth solutions with different $AgNO_3$ concentrations) must not be considered the cause of LSPR shift.

3.4 Studies on GNRSs growth

For obtaining GNRSs with LSPR peaks in the NIR region, namely with high values of R, as already said, 5BrSA can be used in addition to CTAB and this allows to reduce CTAB concentration in the growth solution from 0.1M to 0.05M and to prevent the use of a binary micelle-forming surfactants such as CTAB/BDAC (Benzyldimethylammoniumchloride). For the synthesis with CTAB/BDAC as surfactant system, the growth was studied during the time and it was determined that two growth phases are present. The first one finishes about one hour after the seed addition, while the second one ends about after one week and both of them determine a red shift of the LSPR of the obtained GNRSs (Nikoobakht and El-Sayed 2003). It is reported in literature that 5BrSA/CTAB system should show the same behavior as CTAB/BDAC, so for obtaining GNRSs with higher R values, the time of the growth has to be extended to one week (Ye et al. 2012). However, for this surfactant system the effect of this prolonged growth is not reported.

For studying GNRSs growth evolution during one-week, GNRSs synthesis were performed as reported in the experimental section and growth solutions were kept at 30°C for 8 days after the seed addition. Aliquots (of 1ml each) were sampled at different time during the growth, then quenched and centrifuged as reported in the experimental section, the obtained solutions were measured by UV-VIS-NIR spectroscopy and TEM.

The appearance of the color in the growth solutions occurs about 1.5/2 hours after the seed addition, in some cases it was possible to distinguish a pale red/pink shadows about after 1/1.5h. However, aliquots sampled in these early moments appear pale and in the majority of the cases, after the centrifugation an insignificant number of pellets is obtained. For this reason, for most of the samples, data are available from 1day after seed addition.

Each sample obtained at different time during the growth consists of a single aliquot, indeed multiple aliquots were not sampled in order to keep the growth solution undisturbed as much as possible and in order to determine a smaller variation in the growth solution volume. For this reason, the uncertainties of the reported data are taken from what has been determined in the studies on sampling step.

Four samples were studied during 8 days of growth (4_W,4_W1,4.18_W2, 4.18_W3), as it can be seen from UV-VIS-NIR spectra reported in Figure 33. During the growth the LSPR gradually shift to shorter wavelength. TSPR is around 520nm but it does not show a clear shift trend during the growth, anyway any further discussion will be focused on LSPR since this peak is the most sensitive to the shape of GNRSs, so it is the most suitable parameter to evaluate the occurrence of modifications in the particles. Looking at Figure 34, where λ_{max} of LSPR is reported as a function of the time, it can be said that, even if small shifts occur within about 3 days after the seed addition, they are negligible, while after that period λ_{max} of LSPR decreases faster. Sample 4.18_W2 and 4.18_W3 were synthetized with a slightly higher concentration of $AgNO_3$, indeed stock solution concentration was 4.18mM instead of 4mM. Considering the high sensitivity of the aspect ratio of the obtained GNRSs to $AgNO_3$ concentration in the growth solution (see following paragraph) this little increase of silver ions can be responsible of the higher value of λ_{max} of LSPR. The slightly higher silver ions concentration could be also responsible for the difference in the value of ΔLSPR calculated

between 1d and 8d values of λ_{max} of LSPR (obtained from the fitted curves), which is about 55 nm for 4_W and 4_W1 (respectively 58 and 52) and about 80nm for 4.18_W2 and 4.18_W3 (respectively 84 and 76nm).

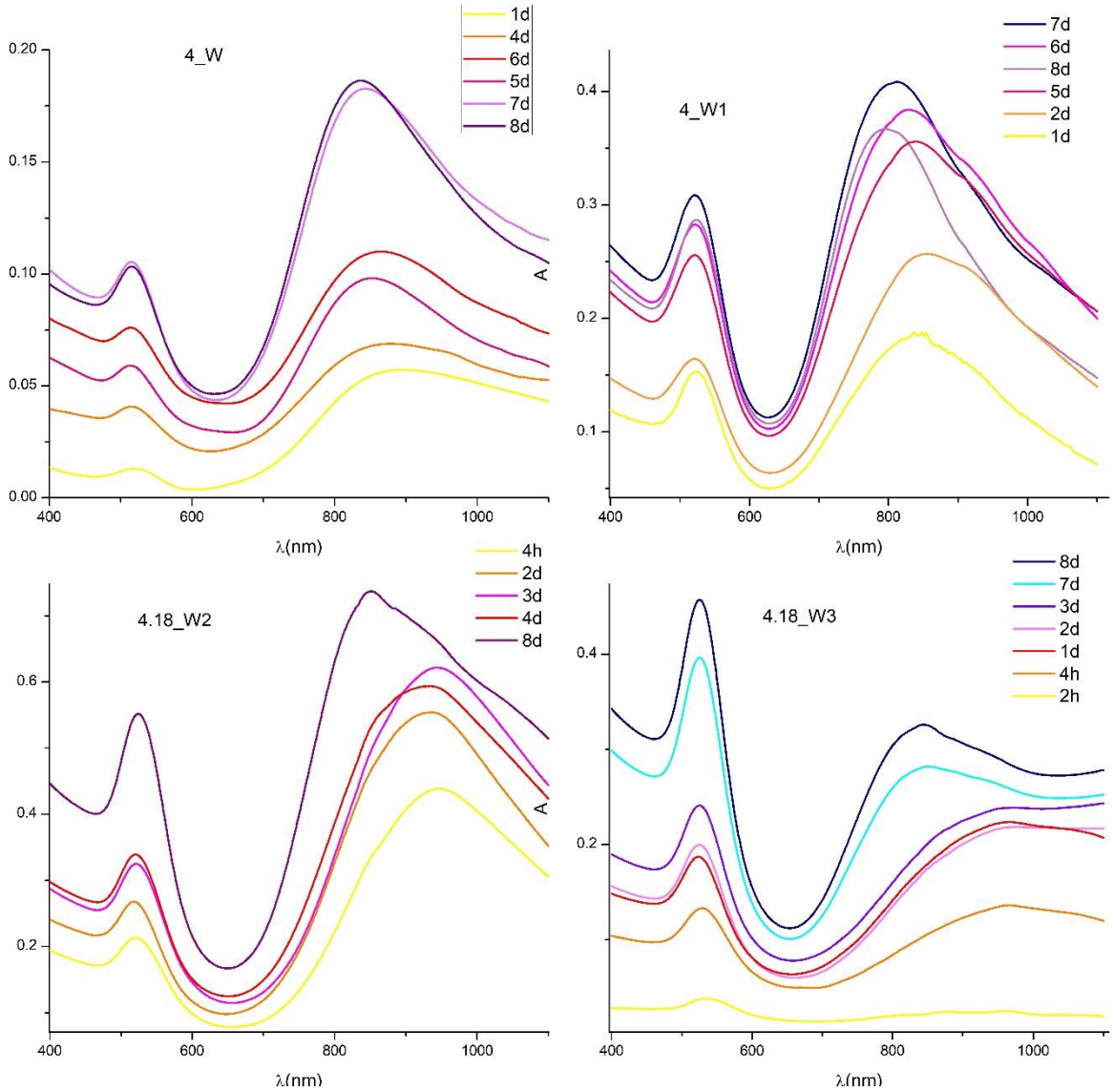

Figure 33 UV-VIS-NIR spectra of aliquots taken at different time during growth. 4_W aliquots are diluted 1:2

In the case of silver assisted growth of GNRSs, it is reported that two different and opposite phases could characterize LSPR shift during the growth. The first one consists in a fast red shift that create an anisotropic structure, the second one consists in a slow blue shift due to isotropic growth or reshaping of GNRSs (Su, Yang, and Zhu 2015; Scarabelli, Grzelczak, and Liz-Marzán 2013). This means that seed particles initially achieve their largest aspect ratio, and as growth continues, the aspect ratio decreases (Park et al. 2014). In the case of 4.18mM_2905 the 2h aliquot was obtained (it was possible to separate the pellets from the supernatant after the centrifugation) and its spectrum shows only the TSPR peak, while at higher wavelengths not even a peak tail is visible, so the presence of LSPR peak may be excluded. Considering that 4h aliquots for both 4.18_W2 and 4.18_W3 present the LSPR peak, a red shift phase could occur between 2h and 4h since in this range time an anisotropic structure is formed. The timing of the appearance of the color and the possible red shift

phase suggest a low grow rate that is a positive factor in GNRSs synthesis even if it is time consuming (Su, Yang, and Zhu 2015).

During the reaction the absorption peak intensities constantly increase, this means that the growth of the GNRSs continues for the whole time. This is confirmed also by the increasing in the absorption at 400nm that is shown in Figure 34, which is determined by the increase in metallic gold concentration in the growth solution. Probably early aliquots have particles too small to obtain a significant number of pellets in the centrifuge (as it can be seen from A_{400} values correspondent to 2h and 4h aliquots), for this reason it was not possible to obtain them. Indeed, the same problem has been highlighted by Park et al., they sustain that in the early stage of the growth it is hard to properly stop the reaction and to separate the particles from the growth medium due to their small dimensions (Park et al. 2013) (they used strongly binding polymeric ligands to stop the growth and allow a phase transfer of the particles in toluene, namely a nongrowth medium). As it can be seen in Figure 34, a linear trend can be attributed to the increasing of A_{400} during the time if we excluded the value corresponding to 2h aliquot in 4.18_W3 growth. In that early stage the rate of gold reduction may be faster since the anisotropic structure of GNRS is forming, indeed as reported in section 1.4.4, at the beginning of the growth both tips and lateral facets directions are allowed to grow even if with different rate, while in a second phase the growth rate of lateral facets decreases importantly.

All the A_{400} data reported correspond to aliquots, indeed GNRSs solutions obtained from the Q/CR process of the total growth solution (8^{th} day), present lower A_{400} value than the one of same sample aliquots. This is probably due to a lower centrifugation efficiency caused by the higher volume of sample treated. For this reason, in the case of 4.18_W2 and 4.18_W3, an aliquot was sampled the 8th day just before the quenching of the entire solution.

Table 7 values of absorbance at 400nm for the aliquots sampled from the growth solutions at different growth time

	A_{400}			
t(day)	4_W1	4.18_W2	4.18_W3	4_W
2h			0.028	
4h		0.194	0.104	
1d	0.119		0.149	0.027
2d	0.148	0.240	0.156	
3d		0.287	0.190	
4d		0.298		0.086
5d	0.223			0.132
6d	0.242			0.165
7d	0.264		0.299	0.214
8d		0.446	0.342	0.201

Table 8 values of λ_{max} of LSPR for the aliquots taken from the growth solutions at different growth time

	λ_{max} LSPR			
t (day)	4_W1	4.18_W2	4.18_W3	4_W
4h		946	958	
1d	848		952	897
2d	856	938	955	
3d		943	953	
4d		932		881
5d	840			865
6d	828			853
7d	812		887	844
8d	800	856	882	837

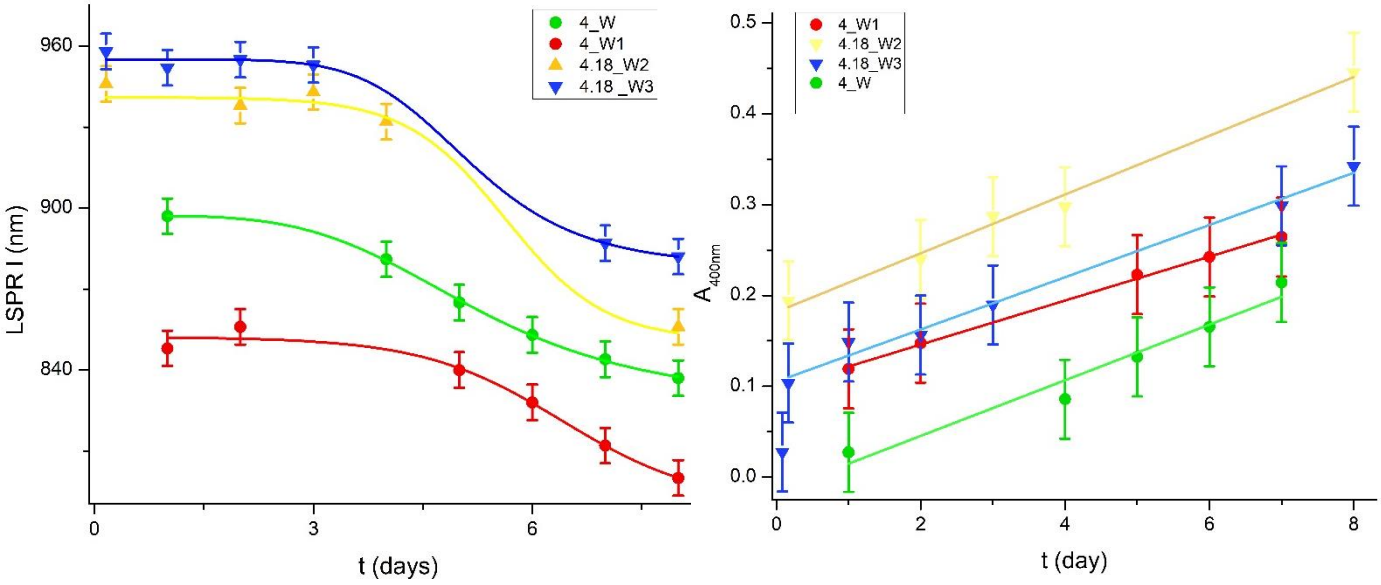

Figure 34 value of λ_{max} of LSPR at different growth time for all the four measured samples on the right, value of absorption at 400nm during the growth time for all the samples studied on the left

As reported in section 1.5, the ratio L/T can be used to estimate the amount of shape impurities, however, as reported in section 1.3.5, it is known that the relative intensity ratio of the longitudinal to the transverse mode increases with increasing aspect ratio, namely with red shifted LSPR peaks. L/T ratio was determined for the aliquots corresponding at different growth times for the sample 4_W, 4_W1 and 4.18_W2 (the case of 4.18_W3 will be discussed later), the data are reported in Table 9 and Figure 35. Different samples show comparable values of L/T ratio, which is around 1.5. During the growth, a significative variation in the L/T values are not present for the considered samples, it means that the fraction of shape impurities does not increase during the time for sure, or rather, since the ratio should decrease due to the LSPR blue shift, it is possible that some isotropic particles may evolve to anisotropic structures during the time.

Table 9 values of L/T for the aliquots taken from the growth solutions at different time

	L/T		
t (day)	4_W	4_W1	4.18_W2
0.16			2.0
1	1.7	1.2	
2		1.5	2.0
3			1.9
4	1.7		1.8
5	1.6	1.3	
6	1.4	1.3	
7	1.7	1.3	
8	1.8	1.2	1.6

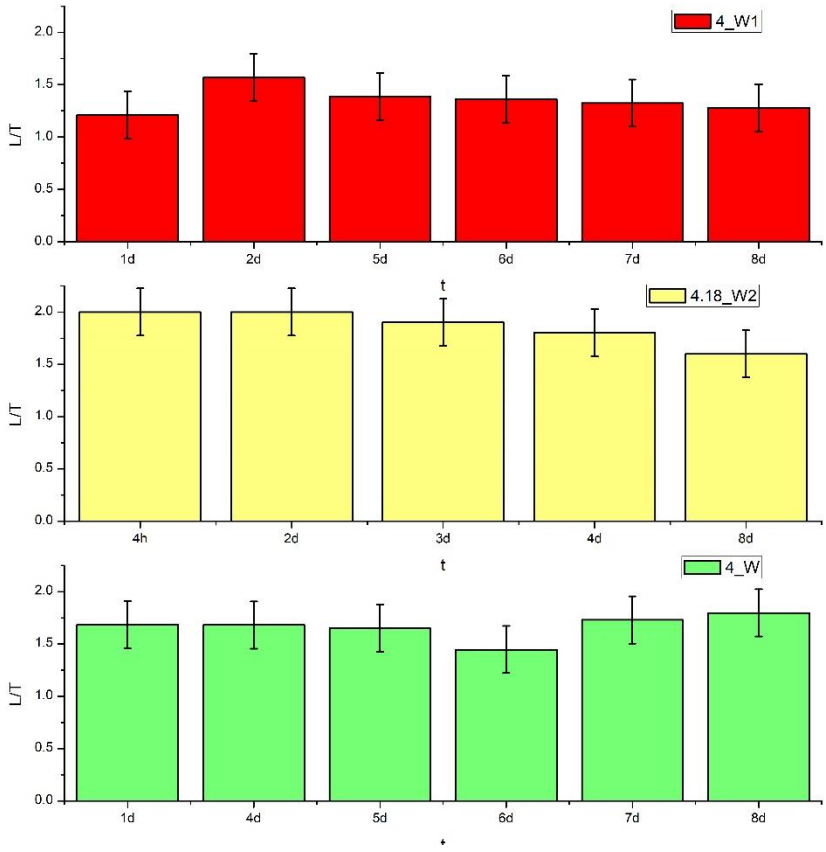

Figure 35 values of L/T for the aliquots taken from the growth solutions at different time

The full width at half maximum (FWHM) and the shape of the LSPR band, as already said, are excellent index of size dispersion and aggregation. As it can be seen from the spectra, LSPR peaks are asymmetric, for this reason half width at half maximum for each side of the peaks (HWHM low and HWHM high) have been determined separately as reported in Figure 36. Unfortunately, only for the sample 4_W1 was possible to measure the both the widths at half maximum. As it can be seen from Figure 36 HWHM low shows a common general trend for all the samples, until the 3rd day it seems to slightly increase, then it rapidly decreases. As regards as HWHM high and FWHM of 4_W1, an initial rapid increase within the 3th day is followed by a rapid decrease.

Since all the aliquots were treated in the same way, even if in absence of zeta potential data that can be a good marker for GNRSs stability(Henson et al. 2017), it can be assumed that the variation of the width of the LSPR peaks is due to changes in the GNRSs size distribution instead of aggregation.

The observed trend is in line with what has been determined based on LSPR λ_{max} *f* (t), namely the presence of two phases in the growth of GNRSs with the 3th day as a border between them. Both the decreases of HWHMs and FWHM suggest that the size distribution becomes narrower after the 3rd day, indeed considering a single particle the blue shift of LSPR (due to a decrease of R) should increase the FWHM (Eustis and El-Sayed 2006a), given that in our case the blue shift is accompanied by the reduction of FWHM values (after the 3rd day), it means that the monodispersity increases for sure. However, HWHM high remains bigger than HWHM low and this means that GNRSs tend to remain more dispersed toward bigger values of R during the whole time of the growth. Moreover, after the 3rd day the decrease of HWHM high allows to return substantially to the value corresponding to the 1st day, while the decrease of HWHM low generates a significative decrement respect to the value of 1st day. This means that the population of GNRSs with values of R smaller than the mean value is the one that has significantly decreased from the beginning of the growth.

Table 10 value of HWHM and FWHM for the aliquots of the considered samples.

	HWHM low			HWHM high	FWHM
t (day)	4_W	4.18_W2	4_W1	4_W1	
0.16		130			
1	130		110	140	140
2		136	110	204	340
3		141			
4	123	133			
5	108		114	220	141
6	95		106	210	133
7	94		96	172	220
8		99	81	146	210

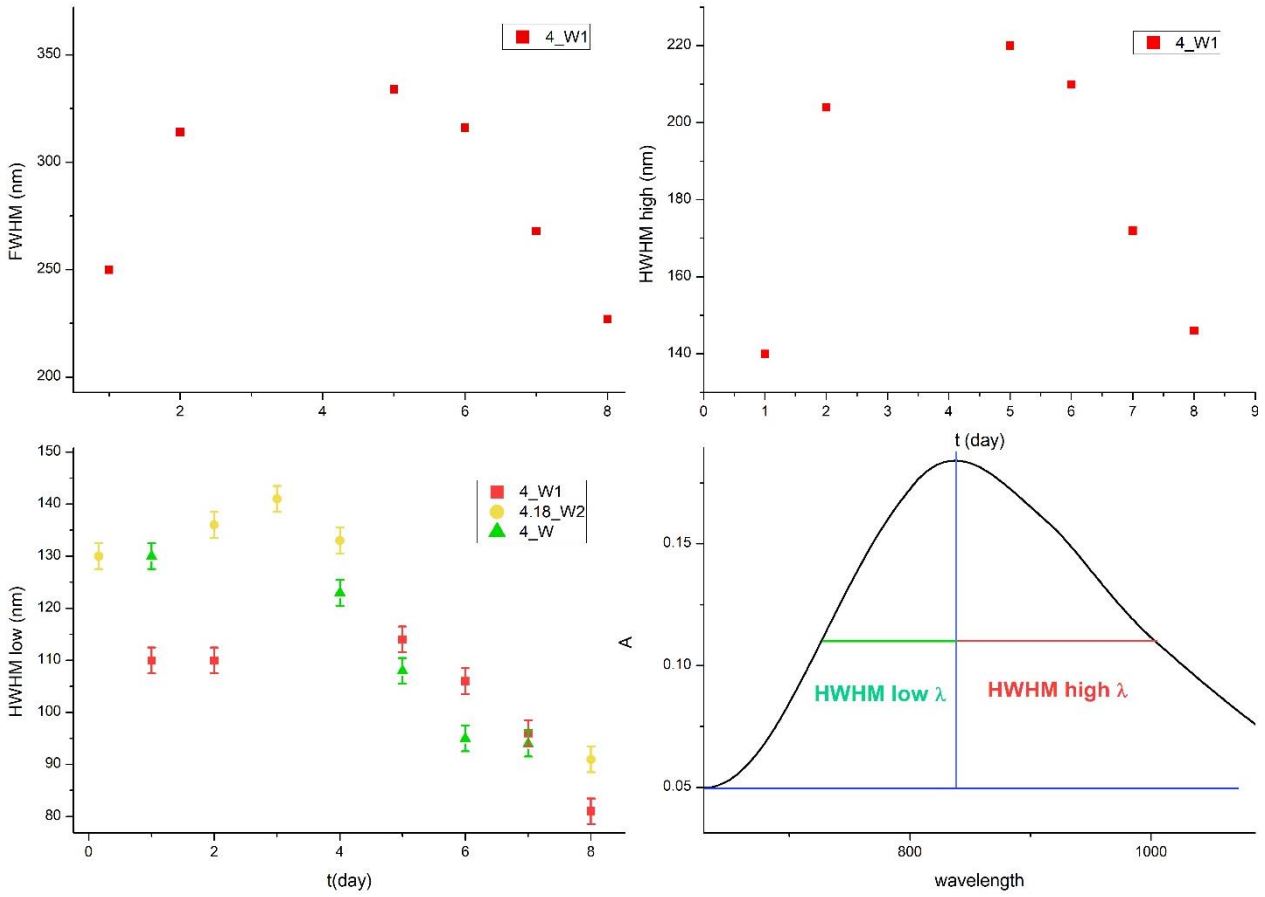

Figure 36 in the upper side 4mM_0905 aliquots values of FWHM on the left and HWHM high on the right. In the bottom HWHM low during the time for aliquots of 4.18_W2, 4_W1, 4_W samples on the left (in this case was possible to consider the error from paragraph 3.3.1), on the right is reported an example of values determination.

These results are confirmed by TEM measurement; distributions of length, diameter and R for some aliquots of 4_W1 and 4.18_W2 are reported in Figure 40 and Figure 41. It can be seen that in both samples, R distributions have longer tails toward higher values and during the time the tails toward shorter values tend to reduce, likewise HWHM low.

A clear shift in the R distribution toward smaller values is not present, however the blue shift could be due to surface reconstruction. Indeed, atomic defects on surfaces of GNRSs determine facets instability, for this reason gold atoms on the surfaces of GNRSs tend to reconstruct the unstable facets, and consequently the size of the particles changes slightly, which causes a LSPR blue shift (Su, Yang, and Zhu 2015).

From TEM distributions it can be seen that the volume of the particles change during the growth since both d and l increase. Considering the continuous increase in the A_{400} value and in the peak intensities, the reduction of gold ions continues and, since no additional nucleation is possible in the seed-mediated growth, it determines an increase in the size of GNRSs. For this reason, it is more reasonable to consider that small GNRSs grow and become bigger particles instead of considering their dissolution and inclusion in the already formed bigger GNRSs. It should be considered that for non-spherical particle surface area along different growth directions is different, so even if the

growth rates on various surfaces is comparable, a non-spherical evolution will occur anyway (Park et al. 2013).

From the mean values of length and diameter the mean value of volume was calculated as reported by Eustis and El-Sayed 2006:

$$V_{rod} = \frac{4}{3}\pi\left(\frac{d}{2}\right)^2 l$$

Table 11 mean value of volume

	4_W1		4.18_W2	
t (day)	V(nm^3)	δV	V(nm^3)	δV
0.16			2351	864
1	4515	510		
2	4515	510	4264	411
4			4236	235
8	7169	1068	5119	549

Table 12 mean value of length and diameter

	4_W1					4.18_W2				
t (day)	counts	l (nm)	δl (nm)	d (nm)	δd (nm)	counts	l (nm)	δl (nm)	d (nm)	δd (nm)
0.16						123	30	2	8.6	0.3
1	65	43	3	10.0	0.5					
2	181	38	3	10.0	0.3	176	45	2	9.5	0.4
4						296	47	2	9.3	0.2
8	77	51	3	11.6	0.8	114	48	2	10.1	0.5

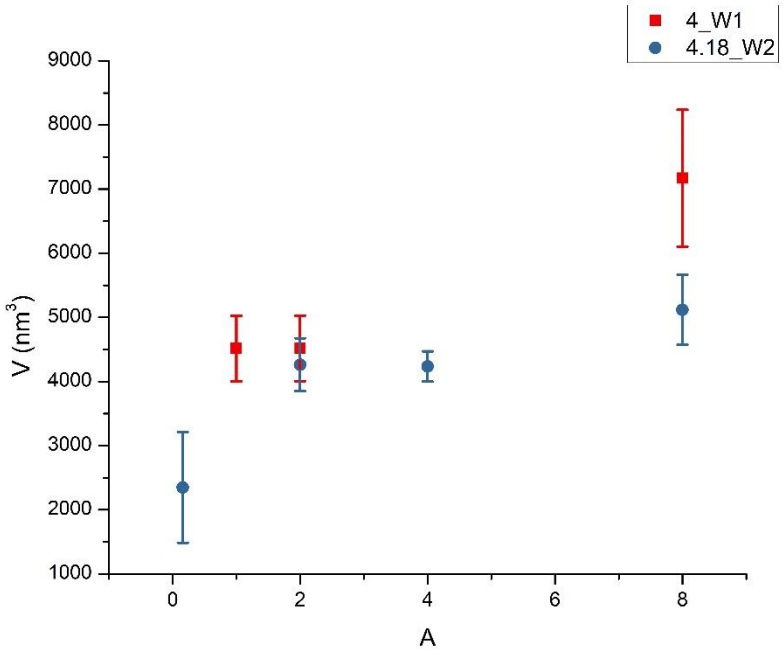

Figure 37 mean value of volume as a function of the aging time

As it can be seen in Figure 38 and Figure 39, the longer are the GNRSs the thinner they are, this is due to the mechanism of seeding synthesis. Indeed, in this synthesis due to its kinetic process GNRSs tend to maintain similar volume even if they show different aspect ratios. Hence, considering the reduction of a certain amount of gold, this amount is quite equally distributed among the particles in the solution, so longer nanorods show narrower diameters (Eustis and El-Sayed 2006a).

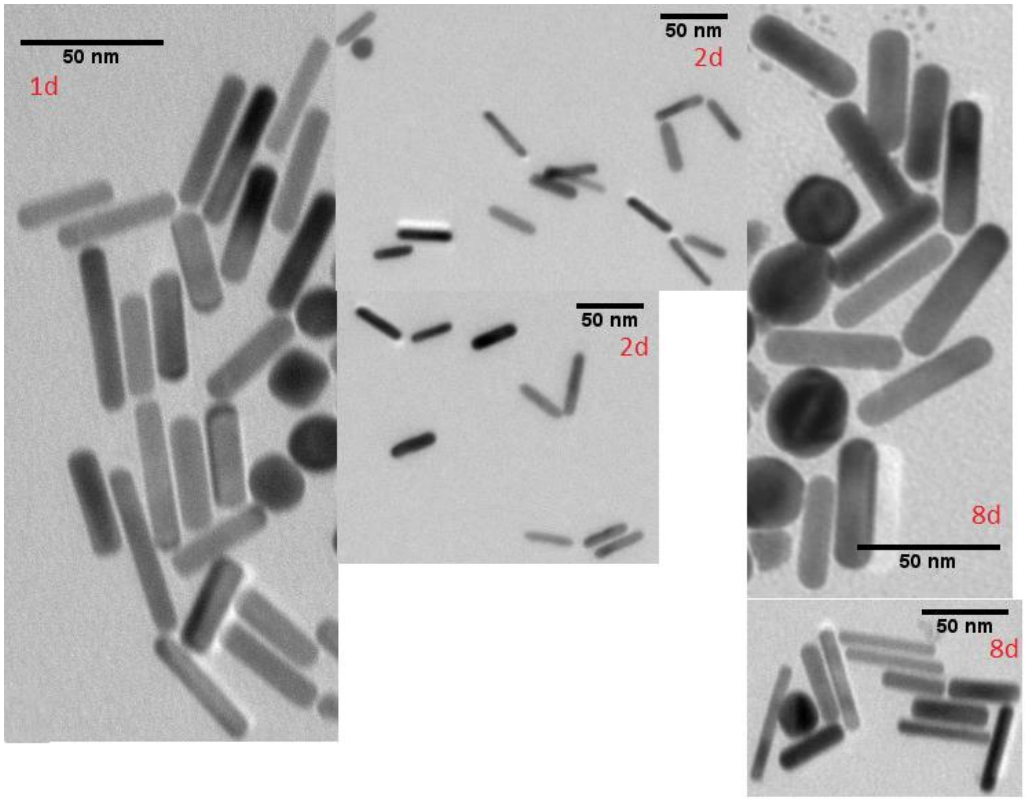

Figure 38 TEM images of 1d, 2d, 8d aliquots of 4_W2 sample

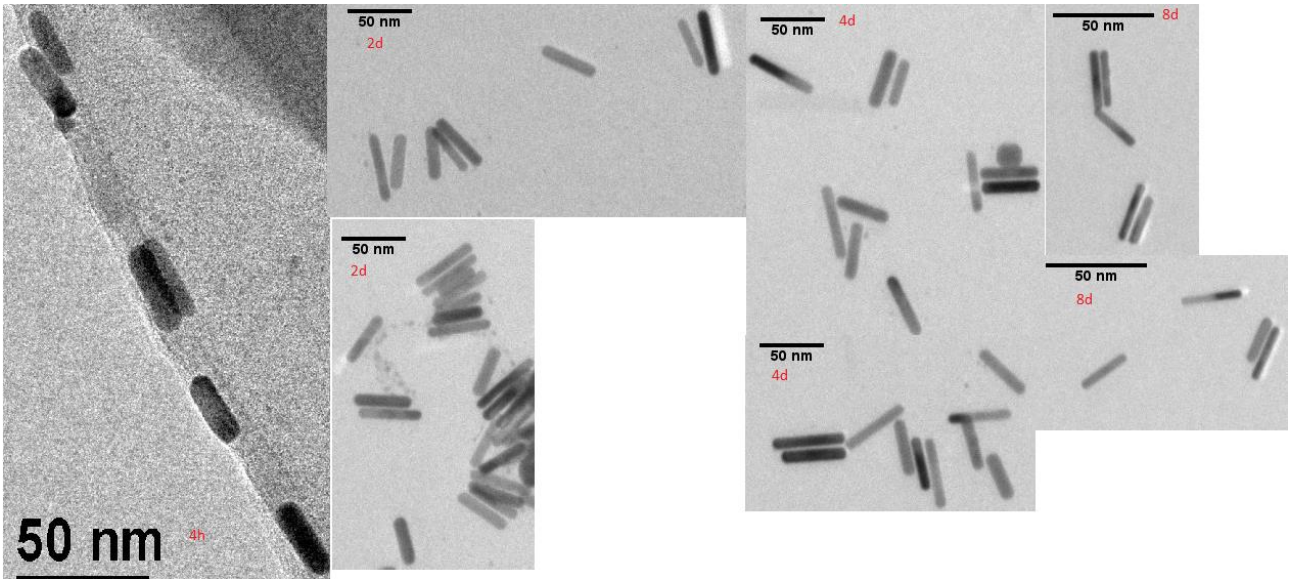

Figure 39 TEM images of 4h,2d, 4d, 8d aliquots of 4.18_W2 sample

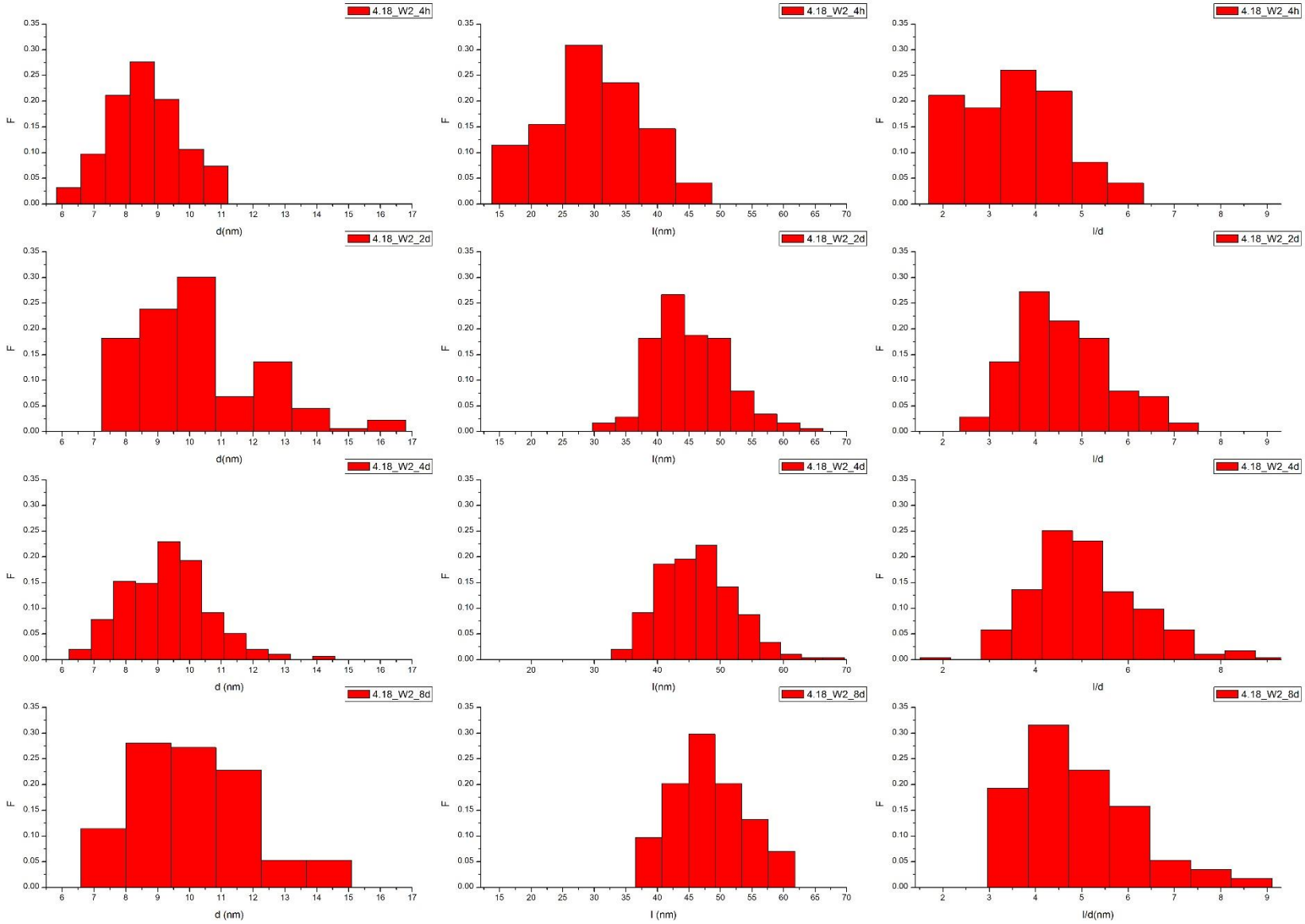

Figure 40 length, diameter and R distributions of 4h,2d, 4d, 8d aliquots of 4.18_W sample

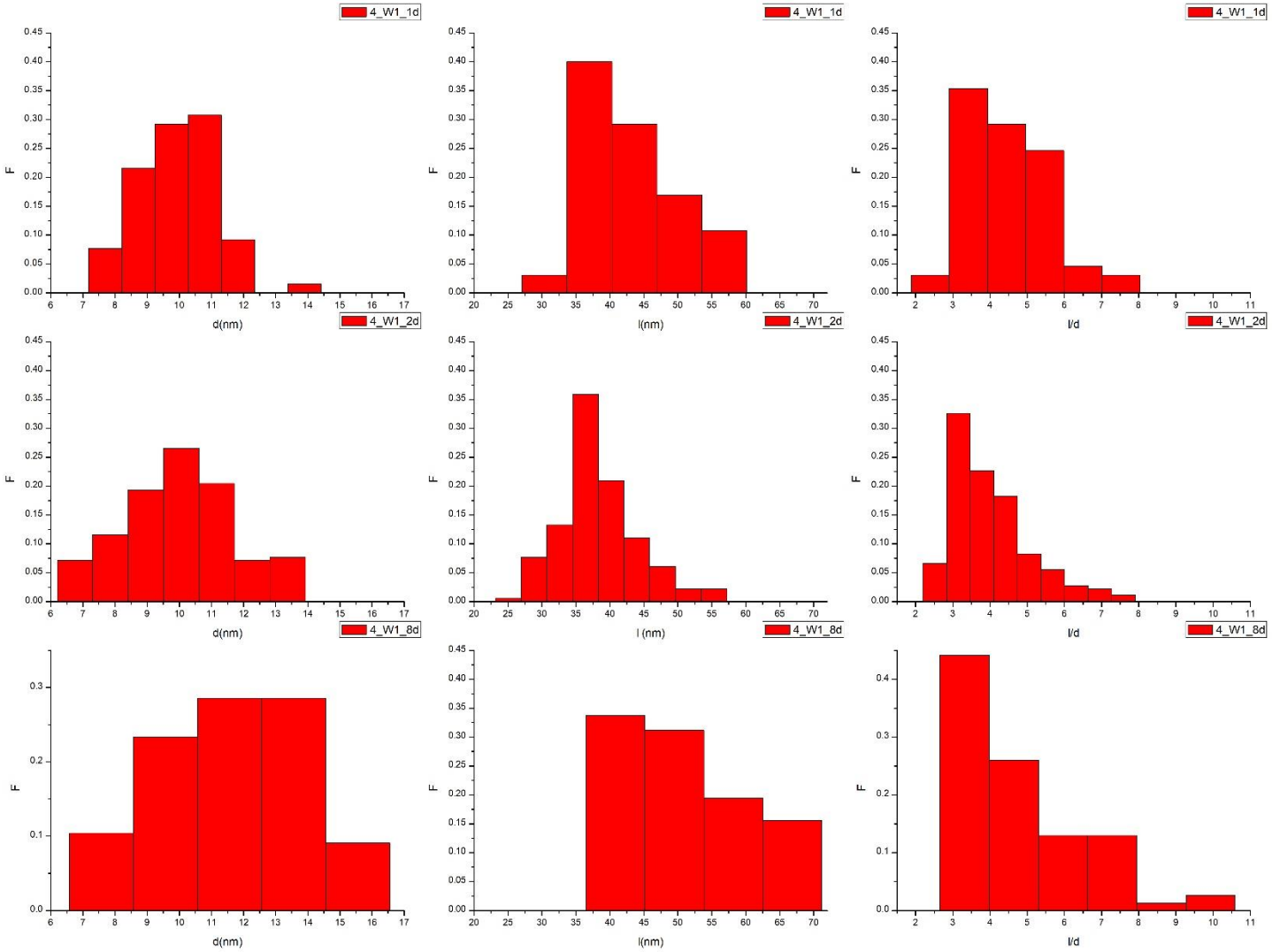

Figure 41 length, diameter and r distributions of 1d, 2d, 8d aliquots of 4mM_0509 sample

These results can be in line with the model of GNRSs growth presented by Park et al. They studied the growth of GNRSs for the well-defined protocol proposed by Nikoobakht and El-Sayed in 2003, it is analogous to the one used in this work but some differences are present. The growth solution differs for the concentrations of the reagents (reported in Table 13)and for the surfactant system that consists of only CTAB. The seed solution is prepared in the same way, but the aging time before its addition to the growth solution is different (5 minutes instead of 30 minutes). The obtained GNRSs are characterized by smaller aspect ratios and the LSPR peaks lie between 800-700nm (Park et al. 2013)

Table 13 seed solution and growth solution used by Park et al. in the GNRSs synthesis, the volume refers to the volume (V) of stock solution added, the concentration ([C]) refers to the final obtained concentration of the chemical in the seed solution and in the growth solution.

seed	V (ml)	[C] mM
NaBH4	0.6	0.6
HAuCl4	0.025	0.2
CTAB	10	94.1

growth	V (ml)	[C] mM
HAuCl4	0.5	0.5
AgNO3	0.08	0.1
CTAB	100	98.8
AA	0.55	0.5
seed	0.1	

Park et al. dived the GNRSs growth in five different steps as reported in Table 14

Table 14 steps involved in the growth of GNRSs determined by Park et al.

N°	**Kind of process**	**Time (after seed addition)**	**description**
I	Rapid isotropic growth	0-2min	Isotropic growth of the seed particles until a final diameter of about 6nm (they remain spherical nanoparticles)
II	Rapid anisotropic growth	2-5 min	Growth in one direction, retaining the diameter of the spherical particle. Large distribution of GNRSs length
III	Non uniform rod growth	5-20 min	the length growth decreases, while the diameter growth increases. At the rod ends the growth is faster and dumbbell shaped particles are obtained. 10 minutes after the seed addition LSPR reaches the maximum red shift, the length distribution becomes narrow, while the dispersion of the diameter increases.
IV	Facets reconstruction	20-45 min	Side facets reconstruction occurs along with a decrease in the overall growth
V	relaxation	45min-1week	Evolution toward a thermodynamically stable shape, minuscule decrease in the length and a progressive increase in the diameter, the growth rate is insignificant.

Considering that a spherical particle of 6nm shows SPR, the growth is colored when it contains these particles, so in our solution this size is reached later (about 2h instead of 2 minutes!). This means

that in our growth system the kinetic of the process is definitely slower, hence it is reasonable to consider that all of these steps can occur later, and the first step could continue until about 2h after the seed addition, namely in concomitance with the color appearance. Considering the high difficulty to obtain particles in the first step (as already discussed), and the graph of LSPR as a function of the time reported in Figure 42, it is reasonable to consider that in the time range among 1d-3d after the seed addition, our system could be between phase II and phase III. Indeed, even if dumbbell shaped particles were not observed (neither in the case of the 4h aliquot of the sample 4.18mM_0528), the following evidences determined in our system seem to be in accordance with Park et al.'s model:

- The FWHM until the 3rd day increases and then it decreases, moreover from Figure 40 and Figure 41 it can be seen that the diameter distributions seem to become wider while the length distributions to become narrower. This is in line with the model that describes an initial increase in the length distribution (phase II) followed by its decrease along with an increase in the diameter distributions (phase III).
- The diameter and the length increase along with the absorption values at 400nm, which is in line with the model that considers that the growth continues until the last phase.
- In Figure 42 the maximum wavelength value of LSPR is reached after 10 minutes, so considering the slower kinetic determined in our system, it is reasonable to consider that the maximum could consist with the value obtained at 1d. Moreover, the following time range in which LSPR seems to be constant in Figure 42, in our system can correspond to the stability of LSPR determined in the first 3 days after seed addition.

It is reasonable to consider that in our system the phase IV occurs after the third day, and probably we never have reached the phase V since the absorbance at 400 nm continues to increase during all the growth time considered.

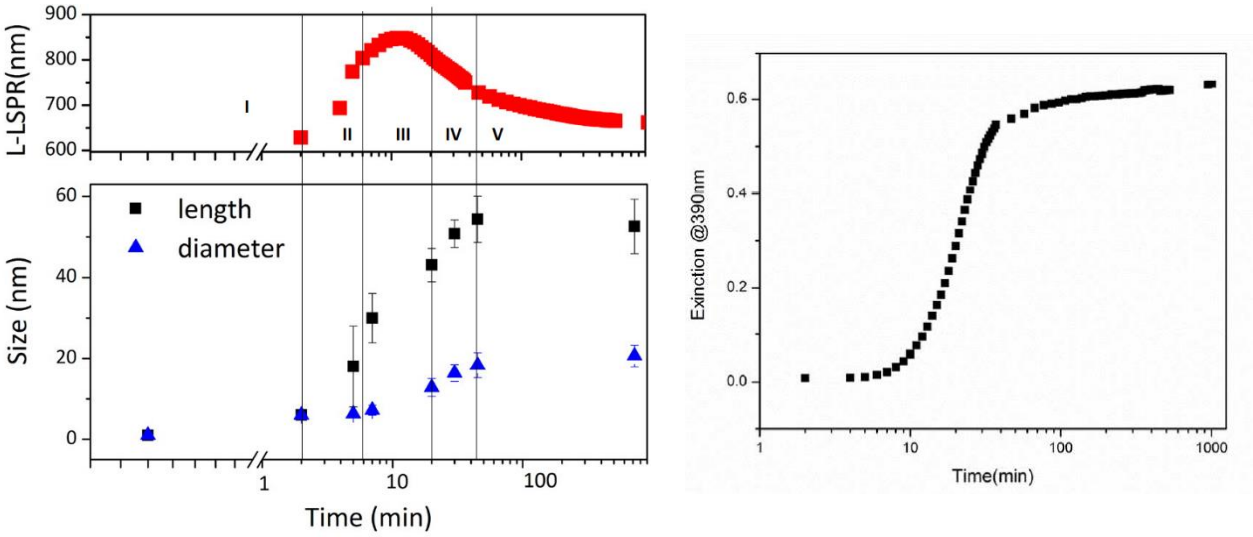

Figure 42 LSPR f(t) and extinction value at 390nm during the time for the synthesis of GNRSs of Park et al. (taken from (Park et al. 2013)).

The delay in the first phase can be due to the dependence of the initial growth rate to the size and crystallographic facets of the added seed particles, and to the kinetic of mineralization and surfactants absorption on the various facets (Park et al. 2013). Indeed, it is reported that CTAB below its critical first micelle concentration (0.008M) takes 11h to reach the equilibrium absorption on gold

surface, while above critical micelle concentration the equilibrium is faster since it is given by micelle absorption instead of molecule absorption. In our case, even if CTAB concentration is above the first micelle concentration it is half as the one used by Park et al. in their synthesis, moreover 5BrSA is proved to insert into the CTAB structures on GNRSs surfaces (see section 3.2). Thus, it is reasonable to consider that CTAB absorption equilibrium on the growing Au surfaces could require longer time in our system. Park et al. determined that the morphological evolution of GNRSs during the growth is closely related to the time scale of the formation of a dense CTAB bilayer on the Au surfaces due to the coalescence of absorbed CTAB micelles. Hence the different kinetic of CTAB absorption taken into account for our system could be responsible of the absence of the dumbbell shaped particles. Moreover, it can explain also the continuing growth of particles that occurs in our system, since the formation of a dense CTAB bilayer is the cause of the slowdown in the rate of the gold ion reduction on GNRSs surfaces.

Even though the mechanism of Park et al. explains the whole growth process without considering any influence of $AgNO_3$, which is indeed involved, it seems to be anyway in line with what has been determined in our system. Moreover, the slower kinetic that has to be considered for our system, on the basis of the assumptions of Park et al., can explain the differences determined between the model and our system. For this reason, even if other factors could be the causes of the slow growth, e.g. lower ascorbic acid concentration, it is reasonable to consider as main cause the different kinetic of CTAB bilayer formation since it allows to explain also the other differences.

3.5 The importance of the quality of the reducing agent in the seed preparation

It is widely reported in literature that GNRSs synthesis strongly depends on the quality of the reagents, e.g. the change of the CTAB supplier can lead to a completely different product (X. Huang, Neretina, and El-Sayed 2009; S. Lee et al. 2011; Zweifel and Wei 2005; Scarabelli et al. 2015). In this work the freshness of sodium borohydride was found to be a determinant factor for the quality and the growth of the GNRSs.

A high quality seed solution (seed particles should be monodisperse and show the same crystallographic habit) is necessary for obtaining high quality GNRSs. A fast addition of an excess of a strong reducing agent under vigorous stirring is required to obtain a good quality seed particles (Scarabelli et al. 2015). Sodium borohydride is used in the seed solution preparation, it is soluble in water, but it reacts with water and hydrogen gas is formed as a reaction by-product:

$$NaBH_{4(s)} + 4H_2O_{(l)} \rightarrow NaB(OH)_{4\,(aq)} + 4H_{2\,(g)}$$

Sodium borohydride has to be prepared with ice cold water in order to slow down this reaction (that occurs fast at room temperature) and allow the reduction of the gold ions instead of water.

Moreover, $NaBH_4$ is hygroscopic and can react also with the water contained in the air, therefore it is important to weight it fast and stored it in a proper way.

When the quality of the reagent is compromised, it has been found that the time spent on $NaBH_4$ addition become a crucial factor for the success of the GNRSs synthesis. This has been proved by the simultaneous preparation of two seed and two growth solutions. The two syntheses differ only in the timing of $NaBH_4$ addition (same $NaBH_4$ stock solution for both the samples), indeed it occurred with a difference of 30 seconds. The growth solution which received the reducing agent later, was not able to develop GNRSs in the growth solution, that remained colorless. This is known as loss of

seed catalytic activity, that can be due to abnormal size and structure of the obtained Au seed nanoclusters (Park et al. 2013).

Moreover, even if the growth occurs a large fraction of shape impurities is obtained along with GNRSs widely polydisperse. This is the case of the sample 4.18_W3 whose $NaBH_4$ solution quality was compromised, and even if GNRSs were obtained, it showed a low L/T ratio (high amount of shape impurities) and a wide size dispersion that can be seen from a comparison of distributions reported in Figure 44 and the shape of the UV-VIS-NIR spectra. This is probably caused by low-quality seed particles obtained due to $NaBH_4$ degradation.

If the reagent is not replaced, at some point if the growth takes place, only gold NSs are obtained as the case of the sample whose UV-VIS-NIR spectra are reported in Figure 43. Beside the importance of the fast $NaBH_4$ stock solution preparation and addition, also the color of the seed solution is a clear evidence of $NaBH_4$ quality. Indeed, seed solution color appears paler and more yellowish if the $NaBH_4$ is compromised.

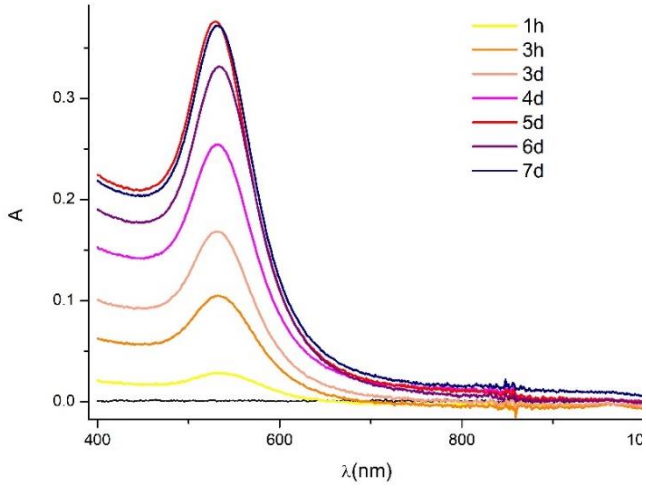

Figure 43 UV-VIS-NIR spectra of aliquots of NSs growth obtained due to a low quality NaBH4 stock solution

All these facts prove the importance of the quality of the seed solution for obtaining GNRSs, and how much reagents quality is crucial in this synthesis. Indeed, it is reported that to obtain anisotropic structures seed particles have to be single crystal structures, otherwise only NSs or other isotropic structure can be obtained (see paragraph 3.6). For gold particles in the size<10nm the minimum free energy structure is multiple twinned. This kind of structure is expected to generate twinned particles as end-products if used as nucleation points in a seed mediated growth. CTAB presence in the seed solution should avoid the formation of twin structures (Walsh, Barrow, and Tong 2015). However, if the gold reduction is not efficient, probably a proper evolution of the seed particles is not possible, and this may lead in the growth solution to the development of isotropic structure or loss of catalytic activity.

.

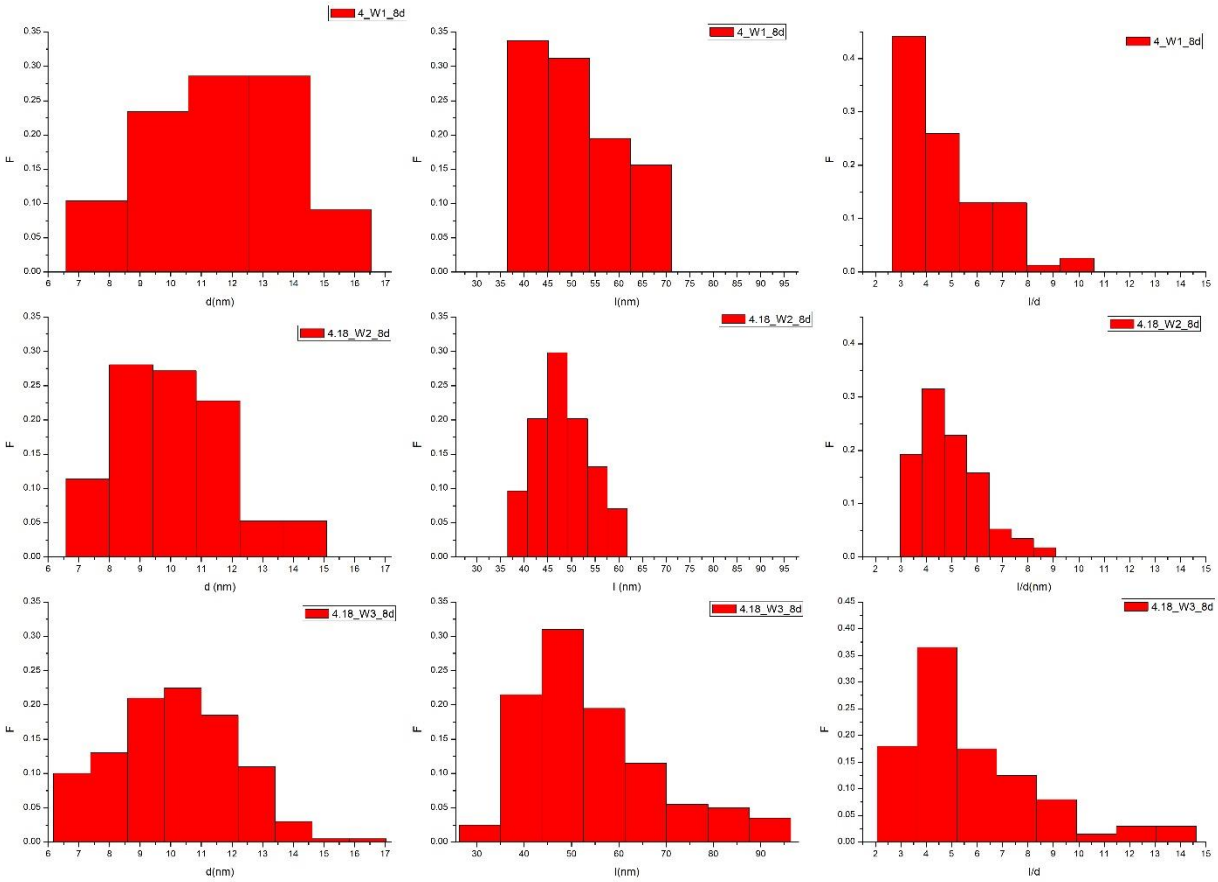

Figure 44 length, diameter and R distributions of the 8d aliquots of the sample 4_W1, 4.18_W2, 4.18_W3

3.6 The role of $AgNO_3$

In order to better understand the role of silver ions in the GNRSs growth, three different solutions were prepared. One growth solution was silver free while the two other samples were prepared with silver concentration as reported in Table 15.

As it can be seen from Figure 45, the spectrum of no_Ag does not show LSPR, but it shows only a band at 526nm which matches with SPR of Au NSs. The absence of GNRSs in the sample no_Ag is confirmed by the TEM images reported in Figure 46 where it can be seen that the sample contains spherical and multiple twinned morphologies. The obtained solution shows a characteristic pink color and, as it can be seen from Figure 45, in the centrifugation process not all the particles were collected, since the SPR band is also present in the spectra of the supernatant (in GNRSs synthesis is a good rule to keep and control the supernatant solution after the centrifugation, in order to evaluate the efficiency of the particles' collection that can be different for particles with different shapes and sizes). This means that the applied purification protocol helps to reduce shape impurities.

Table 15 $AgNO_3$ concentrations in the stock solutions used for the synthesis of the samples reported on the left, respective effective concentration in the growth solutions and ratio of gold to silver concentration

	[$AgNO_3$] Mm		
sample name	stock sol.	growth sol.	Au:Ag
noAg	0	0.000	-
0.4_L	0.4	0.012	41.67
0.55_L	0.55	0.016	30.30

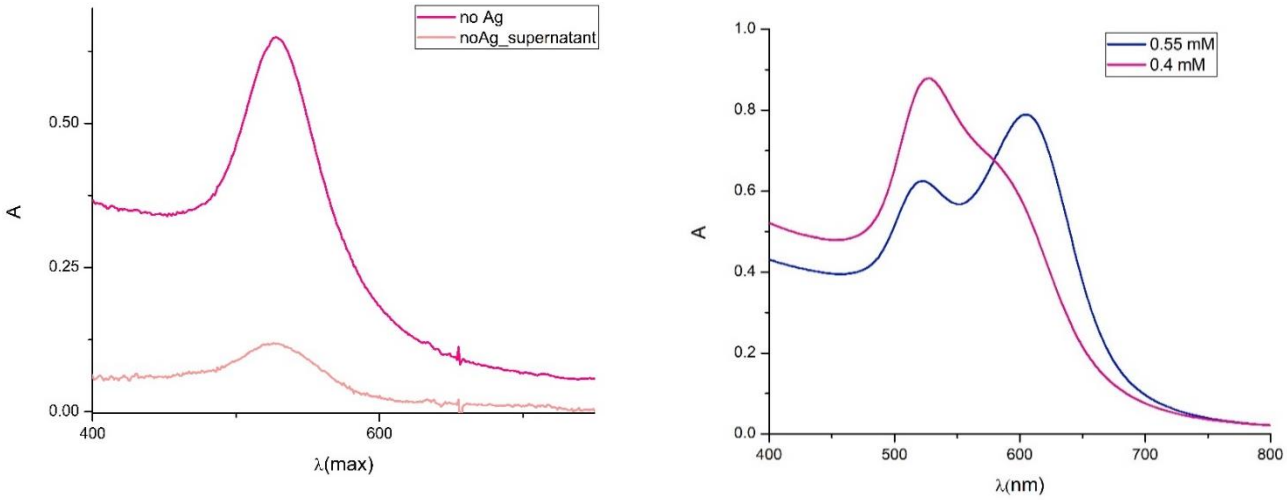

Figure 45 UV-VIS-NIR spectra of the sample no_Ag and its supernatant solution on the upper left and of the samples 0.55_L, 0.40_L on the upper right. In the picture are reported 0.4_L and 0.55_L samples, respectively the violet and the blue one, the two red solutions on the left are reported to compare these solution with the others obtained in this work. The two red solutions are GNRSs solutions synthetized with $AgNO_3$ stock solutions 4 and 5.5mM, their colour is only due to the TLSPRs, since LSPRs lie in the NIR region.

0.4_L and 0.55_L were synthesized with a silver concentration in the growth solution an order of magnitude smaller than the other samples considered in this work. As it can be seen from Figure 45 a silver concentration in the growth solution equal to 12 µM (sample0.4_L) was able to determine the presence of LSPR, even if it is present like a weak shoulder in the TSPR band. In the case of 0.55_L an increase of 4 µM has determined the formation of a clear LSPR band in the UV-VIS-NIR spectra.

As it can be seen from Figure 46, the higher concentration of silver in the growth solution seems to guarantee a better control in the diameter growth and to promote the formation of longer nanorods in accordance with what will be described in the following sections.

Looking at the R distribution of the sample 0.44_L in Figure 46, it can be seen that the most of GNRSs have R<2, while the sample 0.55_L shows an R distribution centered at R=2.

Hence, we can conclude that in the absence of $AgNO_3$ it is not possible to obtain anisotropic structures from the growth of the seed particles. Instead, Ag^+ ions in the growth solution, even if in a low concentration, determines the presence of the LSPR band in the spectrum of the obtained particles, and when R reaches a mean value equal to 2, LSPR band appears clearly separated from TSPR band.

Table 16 mean value of diameter, length and R for the sample 0.55_L and 0.44_L

	counts	d (nm)	δd (nm)	l(nm)	δl (nm)	R (nm)	δR(nm)
0.4_L	148	15.3	0.7	55.6	0.9	1.8	0.1
0.55_L	160	14.1	0.5	73.7	0.6	2.0	0.1

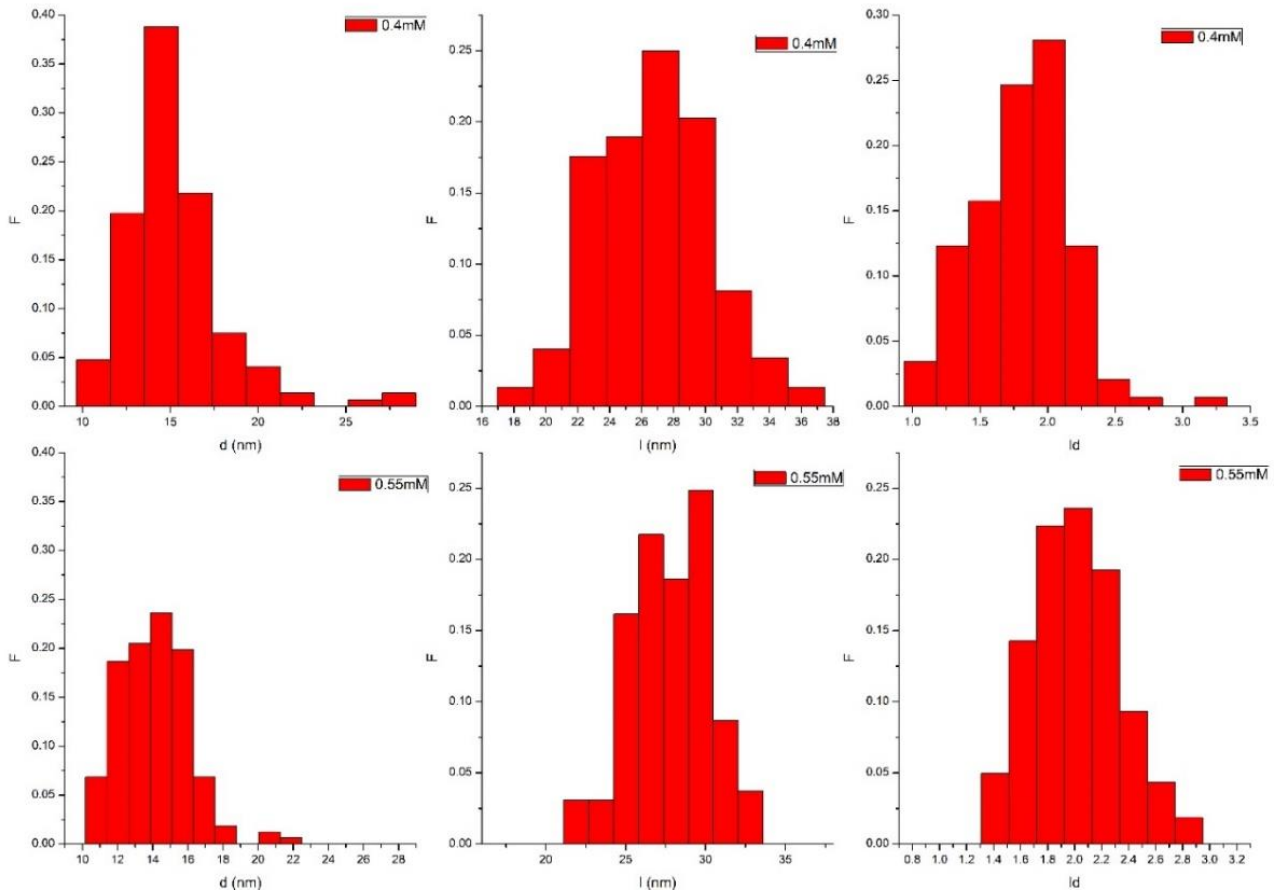

Figure 46 distributions of diameter, length and R for the sample 0.55_L and 0.44_L

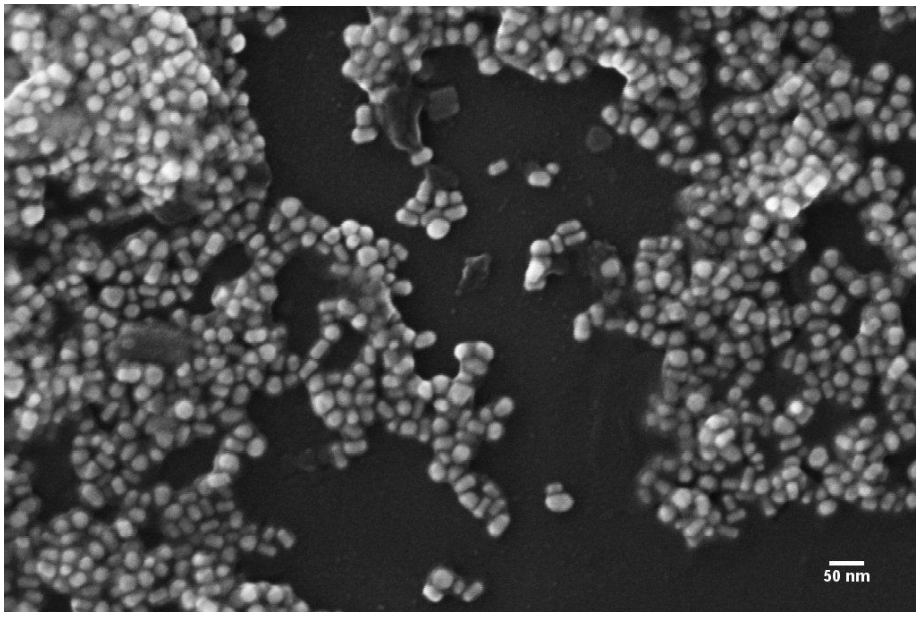

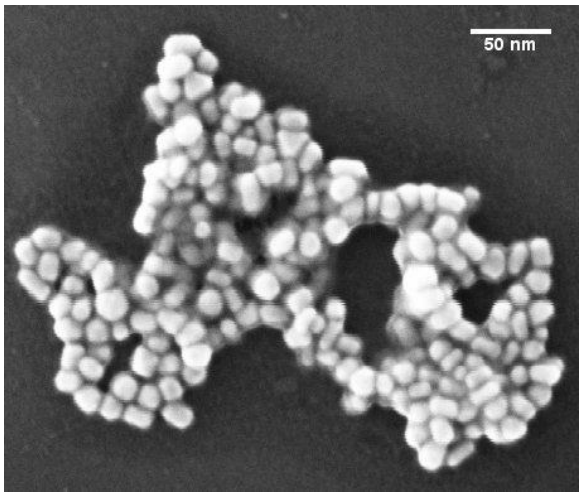

Figure 47 SEM images of 0.44_L

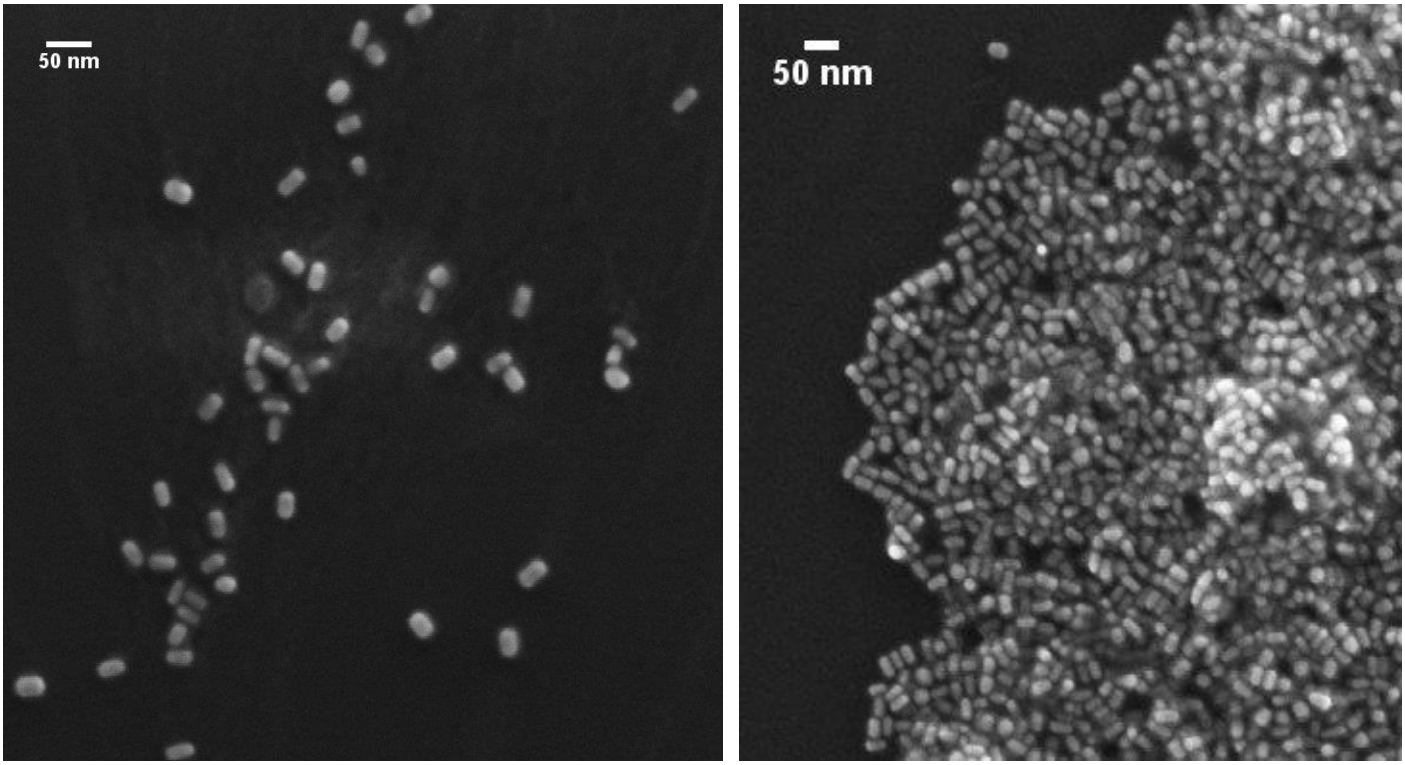

Figure 48 SEM images of 0.55_L

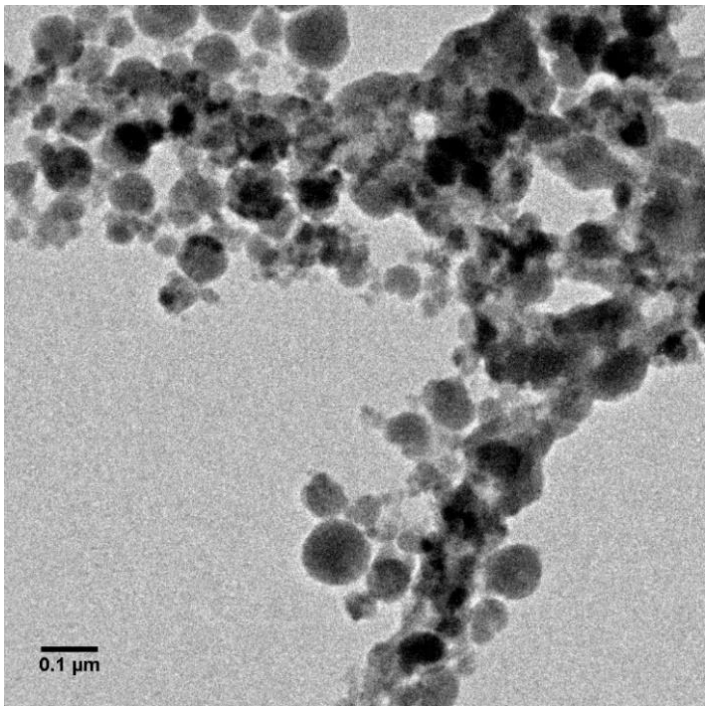

Figure 49 TEM image of the sample NoAg

These results are in line with what has been determined in the studies of Walsh et al., namely that Ag^+ must be present in the growth solution to obtain anisotropic particles. This is different from the opinion of Park at al., which considered CTAB interaction with the growing seed particle facets, the responsible for the growth of anisotropic structures (Walsh, Barrow, and Tong 2015; Park et al. 2013). As already said, at the beginning of the growth the seeds grow is isotropic, then a symmetry breaking must occur to allow the further anisotropic growth. Walsh et al., determined that the symmetry breaking occurs at particle diameter between 4-6 nm, but only single crystal structures can undergo symmetry breaking, while any twinned or multiply twinned particles remain approximately spherical. As already discussed, under optimized conditions, seed particles are single crystal structures when added to the growth solution, but in the absence of Ag^+, during the initial isotropic growth, seeds begin to incorporate an increasing number of twins and other defects. Instead, if silver ions are present, symmetry breaking of single crystal structure can occur when the growing particles have reached the critical size. Indeed, Ag^+ can passivate higher index surfaces, and by this stabilization it is possible to maintain a single crystal structure in the seed particles. At the critical size, particles show asymmetric truncating surfaces with an open atomic structure, at the intersection of {111} facets on the small seeds. These more open atomic structures can be potentially preferred sites for Ag underpotential deposition. Stabilization of the higher index truncations prevents Au deposition, hence growth proceeds on the lower-index surfaces, leading to the truncation becoming side facets in the growing embryonic GNRS structure (Walsh, Barrow, and Tong 2015).

This mechanism also explains why the amount of shape impurities does not vary during the growth, since shape impurities are formed in the first step of the growth process.

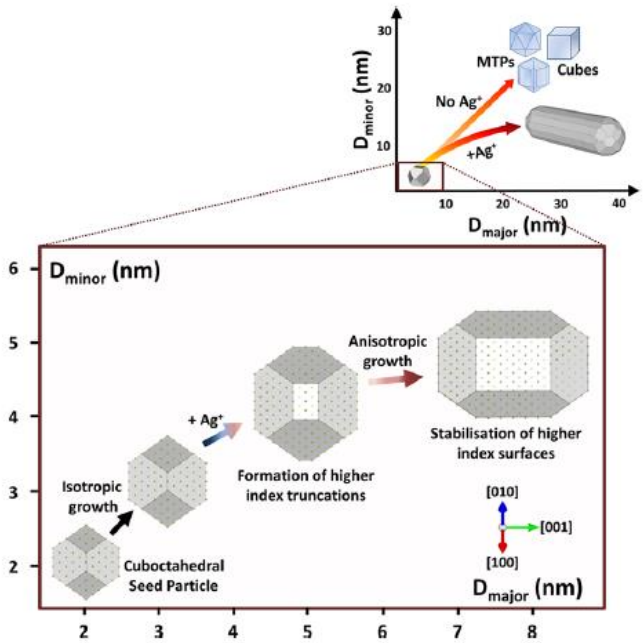

Figure 50 scheme of the seed particles evolution to an anisotropy structure taken from (Walsh, Barrow, and Tong 2015)

3.7 Effect of $AgNO_3$ concentration

The growth of GNRSs, as already said, is affected by different parameters such as concentration of ascorbic acid, silver ions, pH and the amount of seed particles. It is reported in literature that more silver ions or fewer seed particles are added to the growth solution, the longer will be the obtained GNRSs. However, when the number of seed particles is reduced, it causes the extension of both diameter and length, hence the aspect ratio decreases and LSPR blue shifts. If the amount of ascorbic acid is increased, it tends to selectively deposit onto GNRSs end facets and dog boned shaped GNRSs are obtained. By lowering the pH of the growth solution, it is possible to obtain higher aspect ratio GNRSs but this increases the obtained fraction of shape impurities. $AgNO_3$ concentration is hence the best parameter that can be changed for obtaining higher aspect ratio GNRSs (Ye et al. 2012).

In order to obtain higher aspect ratio GNRSs and to evaluate the effect of $AgNO_3$ on the growing particles, $AgNO_3$ concentration was increased in the samples studied in this section.

In these studies, the growths were carried on for 3 days instead of one week, this determines a less time-consuming synthesis and permits to avoid significative LSPR blue shift, while permitting an increase in the reduction yield.

Six different samples (A set) have been prepared with different $AgNO_3$ concentrations as reported in Table 17.

These samples were prepared in couples (4.3_A/8.36_A, 5.53_A/6.83_A, 12.36_A) and for each couple only one seed solution was prepared and used for both.

In all the reaction conditions considered in this work, silver (Ag^+) and bromide (Br^-) concentration (derived from CTAB molecules) is above the maximum value determined by their K_{ps}, hence AgBr precipitation should occur. However, AgBr precipitation in our samples has not been observed on the macro scale until the $AgNO_3$ concentration in the growth solution has reached the value of 242µM (8_A). Indeed, in the case of the samples 12_A, 15_A the solutions turned milky in colour right after the addition of $AgNO_3$, while in the case of 8_A the colour changed 20 minutes after the seed addition. Moreover, during the growth (3days), no solid precipitate was found at the bottom of the flask, it seems like that AgBr remained as a dispersion in the solutions

Table 17 $AgNO_3$ stock solutions concentrations used in the syntheses of the samples reported on the left, and respective concentrations and ratios $HAuCl_4$: $AgNO_3$ in the growth solutions

	[$AgNO_3$] Mm		
sample name	stock sol.	growth sol.	Au:Ag
4_A	4.30	0.125	3.88
5_A	5.53	0.160	3.01
7_A	6.83	0.198	2.44
8_A	8.36	0.242	1.99
12_A	12.36	0.358	1.35
15_A	15.78	0.457	1.06

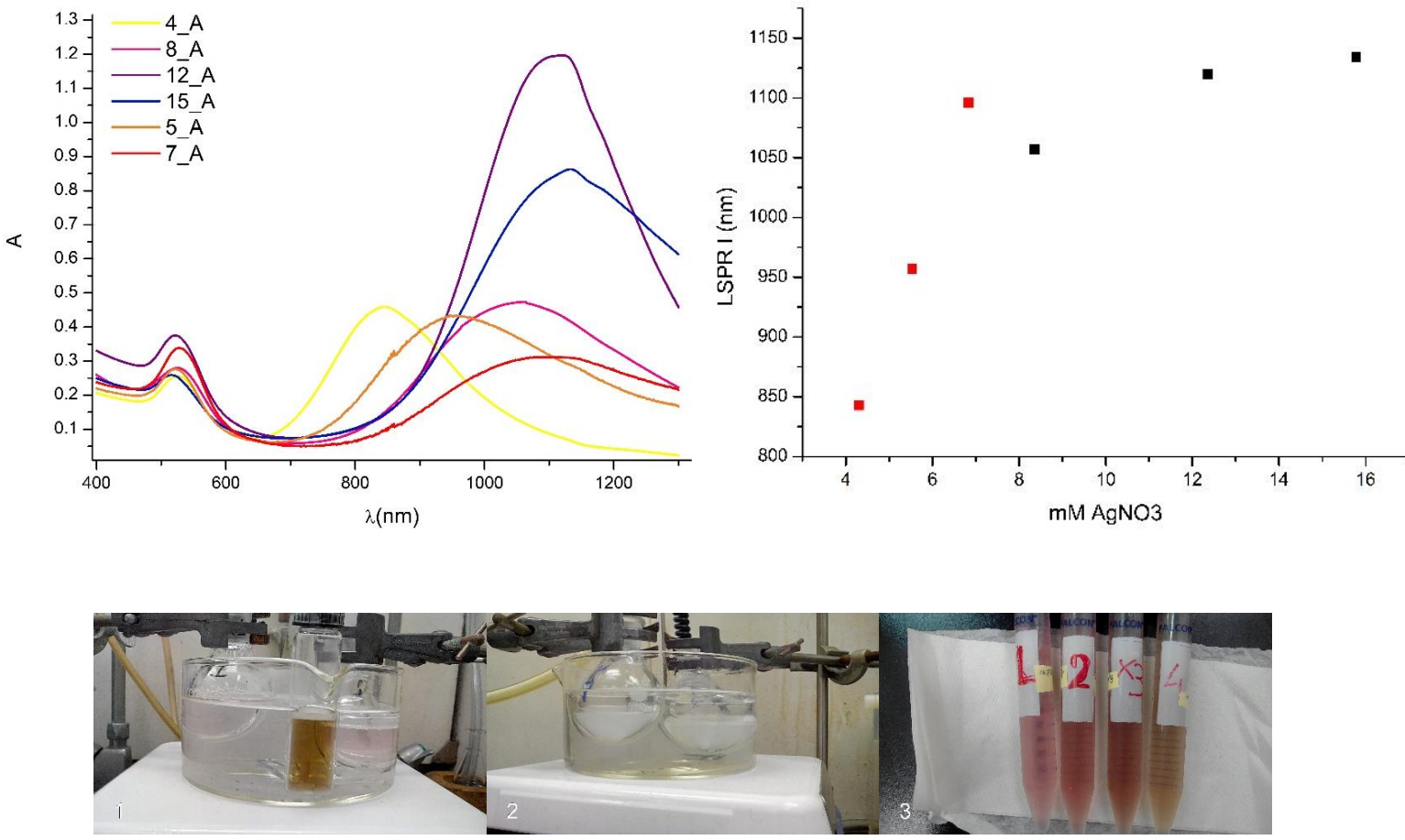

Figure 51 on the top left the UV-VIS-NIR spectra of the samples reported in Table 17, on the top right the λ_{max} of the LSPR reported as a function of the $AgNO_3$ stock solutions concentration. At the bottom, pictures show the differences between solution with and without AgBr precipitation (1 and 2), and the how the colour of the GNRSs solutions tend to change from pink to red to brown when R increases (3).

As it can be seen from

Figure 51, in the graph where λ_{max} LSPR is reported as a function of $AgNO_3$ stock solution's concentration, samples that have not showed AgBr precipitation on the macro scale, seem to show a linear trend (red spot) while the others seem to follow a curve trend.

EDX reveals Ag presence only for 8_A,12_A and 15_A. Considering that, Ag has proven to be always present in the GNRSs 'surface(Jackson et al. 2014), probably its concentration in the samples that did not show AgBr formation, is too low to be revealed by EDX used with the SEM microscope.

In Figure 52 (top part), XRD patterns of all the samples are reported, as it can be expected, gold has face centred cubic structure (fcc). In the case of the samples that have showed AgBr precipitation, mainly thanks to the presence of the peaks at about 2Θ equal to 11, 13, 32, 34 the presence of Ag_3AuS_2 can be determined. The AgBr presence was also investigated but no matches were found, this may be due to its conversion to the detected specie by Na_2S during the quenching process. Indeed, surface science literature suggests that AgBr chemisorb on Au crystal facets (C.J. Murphy et al. 2005), moreover the Na_2S concentration dependence increases in the LSPR of GNRSs previously determined proving the capability of sulphide to reach and be adsorbed by Au surface, so it is

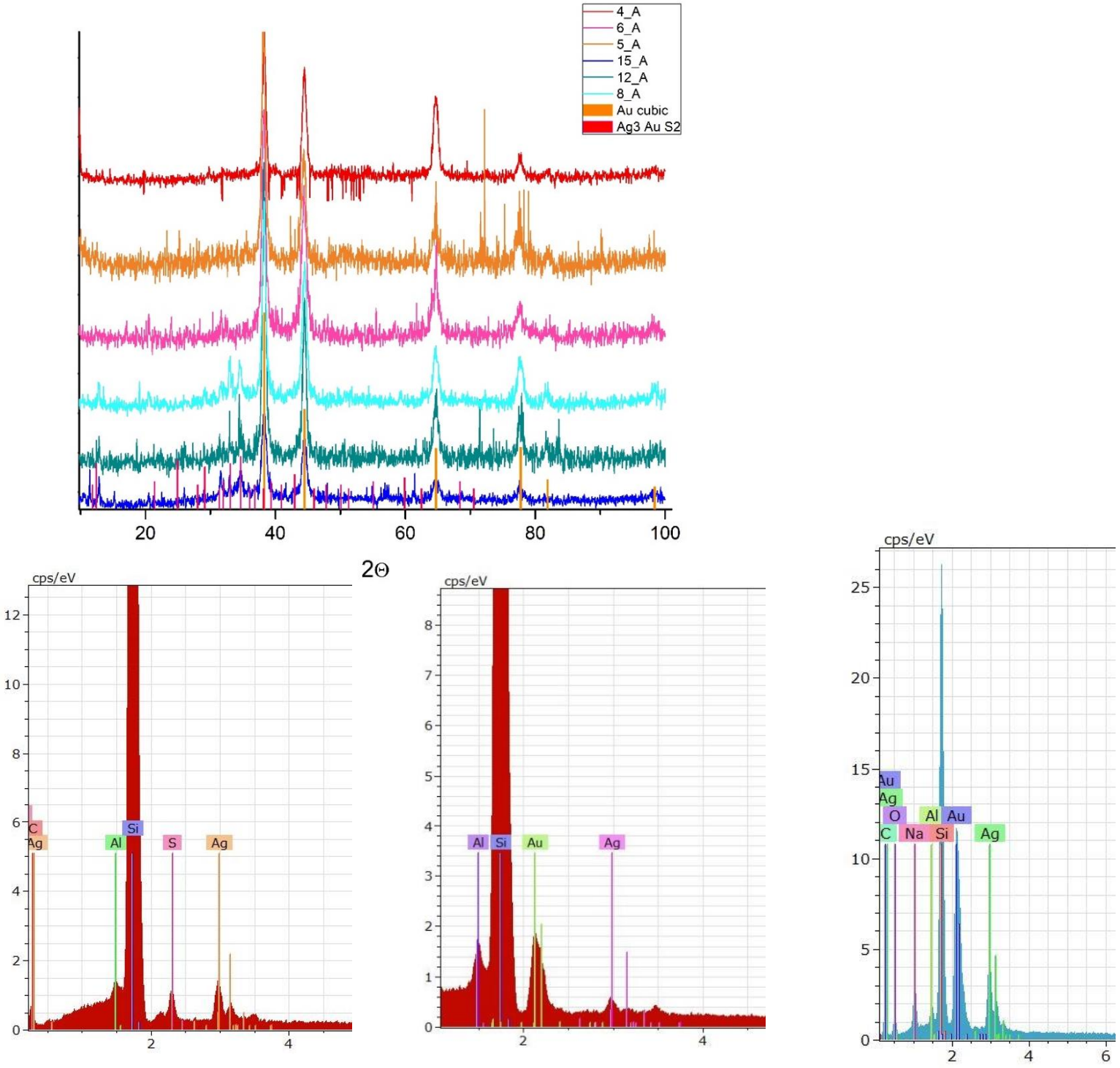

reasonable to consider its activities on AgBr on the GNRSs surfaces. It was not possible to evaluate the presence of Ag on the GNRSs due to the overlapping of the Ag and Au X-ray peaks.

Table 18 λmax of LSPR, diameter, length, R values for the samples reported on the left

sample	λ_{max} LSPR	d (nm)	δd (nm)	l (nm)	δl (nm)	R	δR
4_A	843	13.5	0.3	59	2	4.6	0.2
5_A	957	11.8	0.3	60	2	5.2	0.3
7_A	1096	10.3	0.2	68	2	6.7	0.2

Figure 52 on the top XRD patterns of the samples reported in Table 17, Au fcc and Ag3AuS2 patterns reported as a comparison. On the bottom EDX of GNRSs sample that showed AgBr precipitation

8_A	1057	12.5	1.0	70	5	5.9	0.5
12_A	1108	12.6	0.3	82	2	6.6	0.2
15_A	1133	9.6	0.3	67	2	7.2	0.4

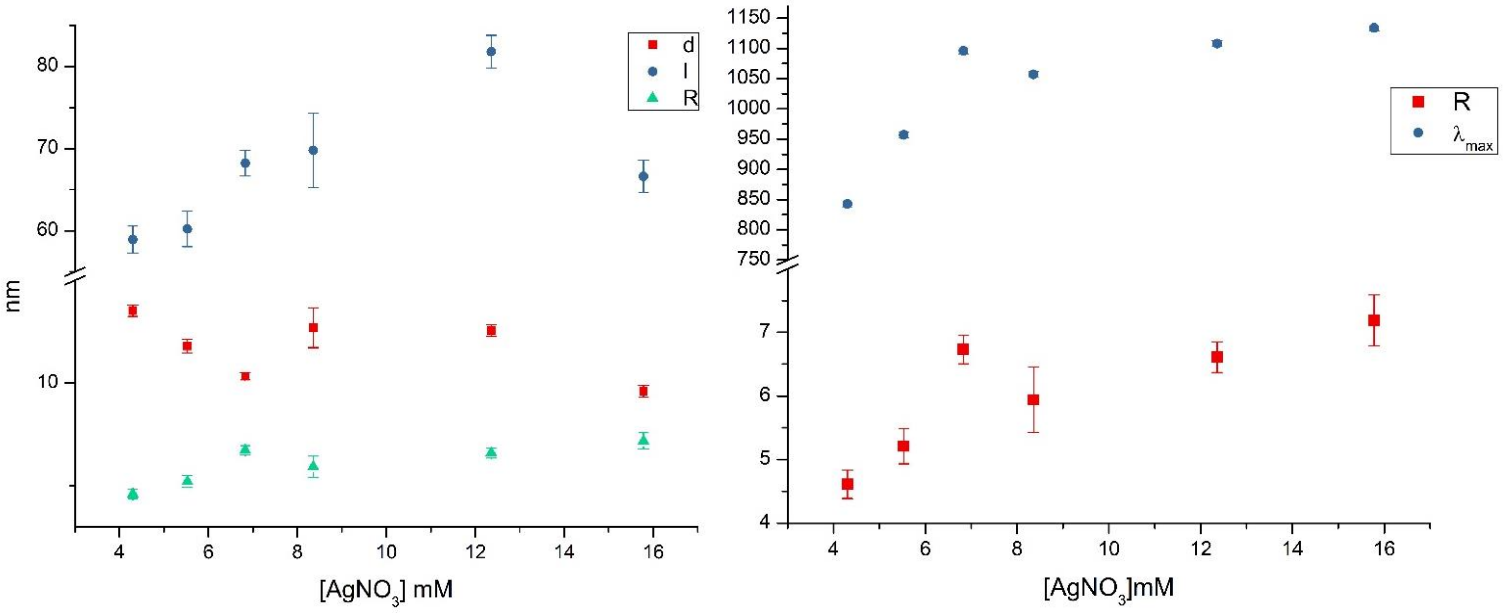

Figure 53 mean values of diameter, length and R as function of the AgNO3 concentration in the stock solution on the left, mean value of R and peak maximum positions as function of AgNO3 concentration in the stock solution on the right

As it can be seen from Figure 53 (right), when silver concentration in the growth solution increases λ_{max} LSPR and R show the same trend. Hence, it is reasonable to consider the variation of R values in the obtained GNRSs, as the main cause of λ_{max} LSPR shift, instead of considering other factors such as significative differences in the size of GNRSs, the end-cape shape or the index of the surrounding medium (K. S. Lee and El-Sayed 2005). However, considering that Ag_3AuS_2 has been determined on the surfaces of GNRSs that have shown AgBr precipitation, it is not possible to exclude that ε_m can be influenced, but it is reasonable to assume that it does not influence the λ_{max} LSPR as much as R.

Considering the samples with $AgNO_3$ concentrations below 8mM, as the silver concentration increases the diameter decreases along with an increase in the length, hence R increases. This is in line with what has been reported in literature as regard to the influence of the silver. Indeed, as already said, after the initial isotropic growth of the seed particles, a symmetry breaking occurs in the size range of 4-6nm. The absolute size at which the symmetry breaking takes place is determined by the $[HauCl_4]$:$[AgNO_3]$ ratio in the growth solution. The increase in the Ag:Au ratio determines that symmetry breaking occurs at smaller particle diameters (considering CTAB and ascorbic acid constant). The final width of the GNRS depends on the size at which the symmetry breaking occurs and on the following growth, they can be both reduced by higher silver concentration. Hence, a higher $AgNO_3$ concentration substantially determines a final smaller diameter (Walsh, Barrow, and Tong 2015). Even though the size range of symmetry breaking (4-6nm) has been determined for the reaction conditions reported in Table 13, since the obtained diameters are comparable (from 9-14nm) it can be reasonable to consider that the symmetry breaking lies within the same upper and lower size limits also in our system. The upper size limit seems to be determined by the loss of single

crystal structures that occurs when this size is exceeded. The lower size limit seems to be determined by the unfavourable energy condition for obtaining the truncations (that are the basis for the anisotropic growth) when the particles diameter is below 4 nm (Walsh, Barrow, and Tong 2015). Hence, even in a different system it is reasonable that the limits are the same. UPD of silver seems to be responsible of the relationship between the Ag amount and the size of the symmetry breaking since higher $AgNO_3$ concentrations will result in the onset of the silver deposition at smaller particle size (Walsh, Barrow, and Tong 2015).Also in the mechanism of Orendorff and Murphy, UPD was considered (along with CTAB interaction with the lateral facets) the responsible of the anisotropic growth. They considered that Ag deposition continues during the growth and with a higher rate on the side on the rods, reducing the growth in the diameter direction.

In Figure 53, it can be seen that, after AgBr precipitation (sample 8_A), the mean d value increases, but a further increase in the $AgNO_3$ concentration causes another decrease of its value. The formation of AgBr corresponds to a decrease in the Ag reduction potential (standard reduction potential is equal to 0.7994 V for Ag+ and 0.0713 V for AgBr), hence the increase in the d value is expected considering AgBr responsible of the UPD. However, the following decrease in d value seems to suggest that an increase in the silver concentration is anyway capable of better control the d growth.

As regards to the length of the GNRSs, as it can be seen from Figure 53,it increases at increasing $AgNO_3$ concentration, with the exception of the value corresponding to the higher $AgNO_3$ concentration. Walsh et al. proposed that the length is determined by the amount of the remaining available gold in the growth solution. The width of the nanorod is determined when the symmetry breaking occurs and after that only a slight increase occurs during the growth. Considering the reduction yield, the remaining reducible gold can be incorporated and increase the length. Hence narrower nanorod are longer since less gold is used to increase the nanorod in the diameter direction and can be incorporated in the length direction (Tong et al. 2017). Orendoff et al. determined that the low yield obtained in presence of Ag^+ ions (about 15% in the standard protocol like the one reported in Table 13), is caused by the termination of the growth of the nanorod due to the complete surface passivation by silver UPD. Indeed, even if the deposition of silver is faster on the side of the rods it occurs also at the tips, so when the passivation of the entire nanorod surface is reached the growth is stopped (Orendorff and Murphy 2006). However, also CTAB-Au surface interactions have to be considered, indeed Murphy et al. determined that CTAB contributes to the inhibition of the growth in the diameter direction by its preferential binding to some facets mediated by AgBr absorption on the nanorod surface. Moreover, it has been found that the higher the CTAB bilayer stability is, the narrower and the longer the nanorods will be. Indeed, higher interaction CTAB-Au in the lateral facets better inhibits the diameter growth and the formation of CTAB bilayer around the nanorod is easier, which is required for GNRS elongation in the zipping like mechanism (C.J. Murphy et al. 2005). These observations could suggest that at low $AgNO_3$ concentration (until sample 8_A) the length increases due to the reduction in the diameter that allows to incorporate more Au ions in the length direction. Then, length of GNRS from sample 7_A to sample 12_A may continue to increase, even if the diameters are bigger, thanks to the higher AgBr absorption in the gold surface that help to form CTAB bilayer around the particles. The easier interaction CTAB-Au is not able to reduce the diameter growth as efficiently as before the AgBr precipitation since UPD has decreased, but it could be the reason of the decrease in the diameter

that follows AgBr precipitation. The increase in the length from sample 7_A can be also attributed to the decrease in the UPD that, beside increasing the diameter, permits to increase the total amount of reducible gold (indeed sample 7_A and 12_A show higher value of absorbance at 400nm).

For the higher $AgNO_3$ concentration it can be said that, whatever mechanism is behind the decrease in the diameter (an increase in the interaction CTAB-Au due to AgBr absorption or an increase in the UPD of AgBr), considering that sample 12_A shows the lower value of diameter, it seems that the intensity of the growth inhibition is high enough to take place also on the lateral facets. This is in line with what has been determined for other reaction systems, namely it can be found a silver concentration high enough to promote relevant inhibition of the growth also in the length direction that determine a maximum value of R, which cannot be exceeded by further $AgNO_3$ addition(Walsh, Barrow, and Tong 2015; Orendorff and Murphy 2006). This is reasonable to be considered also due to the trend of the points in the graph LSPR*f*($AgNO_3$) reported in Figure 53 that seems to reach a maximum.

As regard to the color appearance, a common trend can be identified among the different samples synthetized in this work, namely the higher was the $AgNO_3$ concentration the slower the growth solution became colored. This delay in the color appearance is particularly precise in the case of growth solutions prepared with the same seed solutions, in Figure 55 a picture shows this. Considering that, seed particles have an average diameter below 2nm and that 2h aliquot of 4.18_W3 shows only TSPR, the appearance of the color occurs when the initial isotropic growth produce diameters big enough to show SPR (AuNSs with average diameter of 3 nm shows SPR). In the case of the growth of only NSs, the growth solution became pink 10 minutes after the seed addition, so definitely earlier than GNRSs. It has been determined that the initial growth of the seed particle, is slower in presence of $AgNO_3$ (Tong et al. 2017). Hence both silver ions concentration and seed particle characteristics can influence this initial growth step. All of these evidences confirmed that the more anisotropic are the obtained particles, the slower is the growth of the seed particles and the slower is the color appearance.

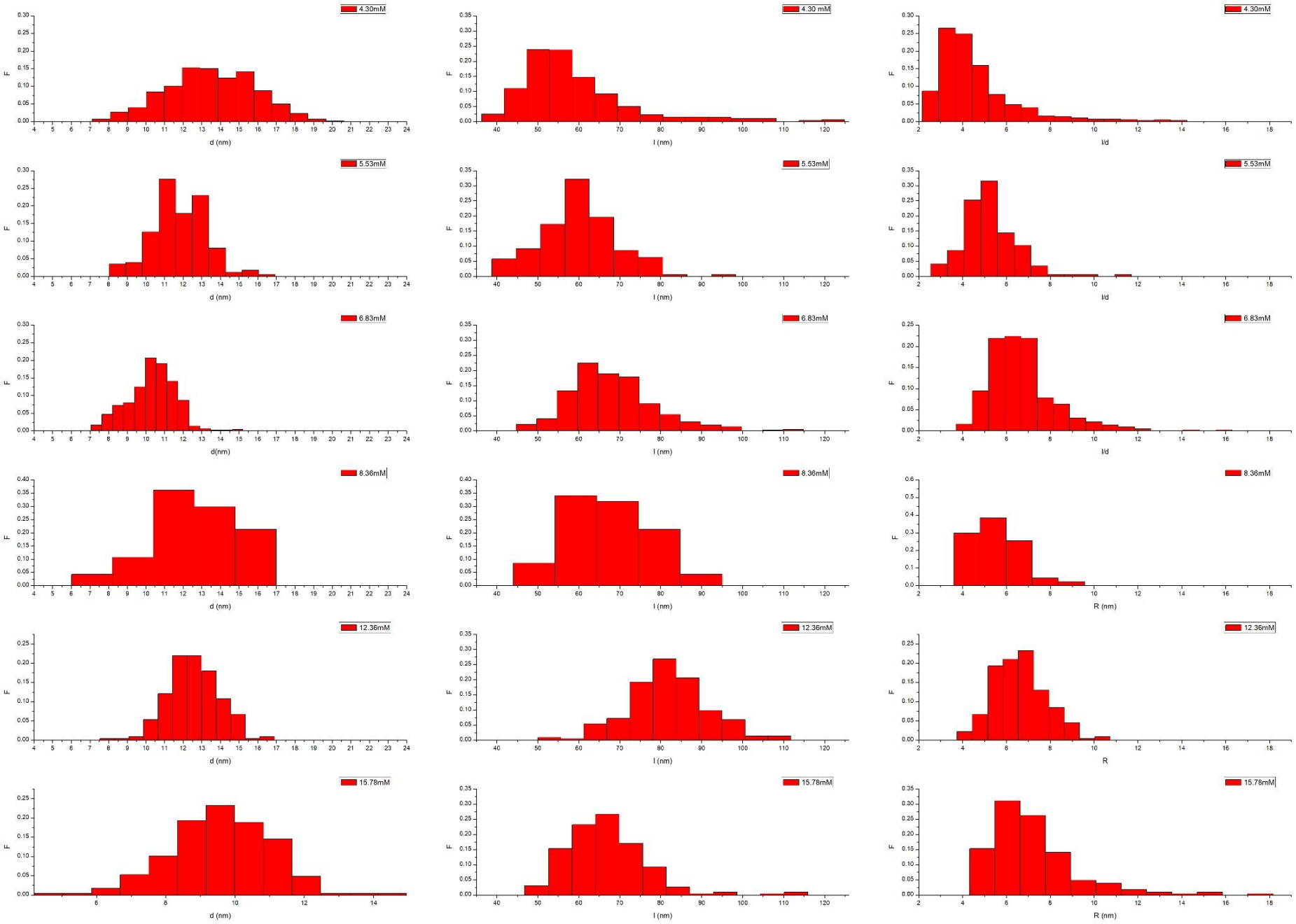

Figure 54 diameter, length and aspect ratio distributions of the samples reported in Table 17

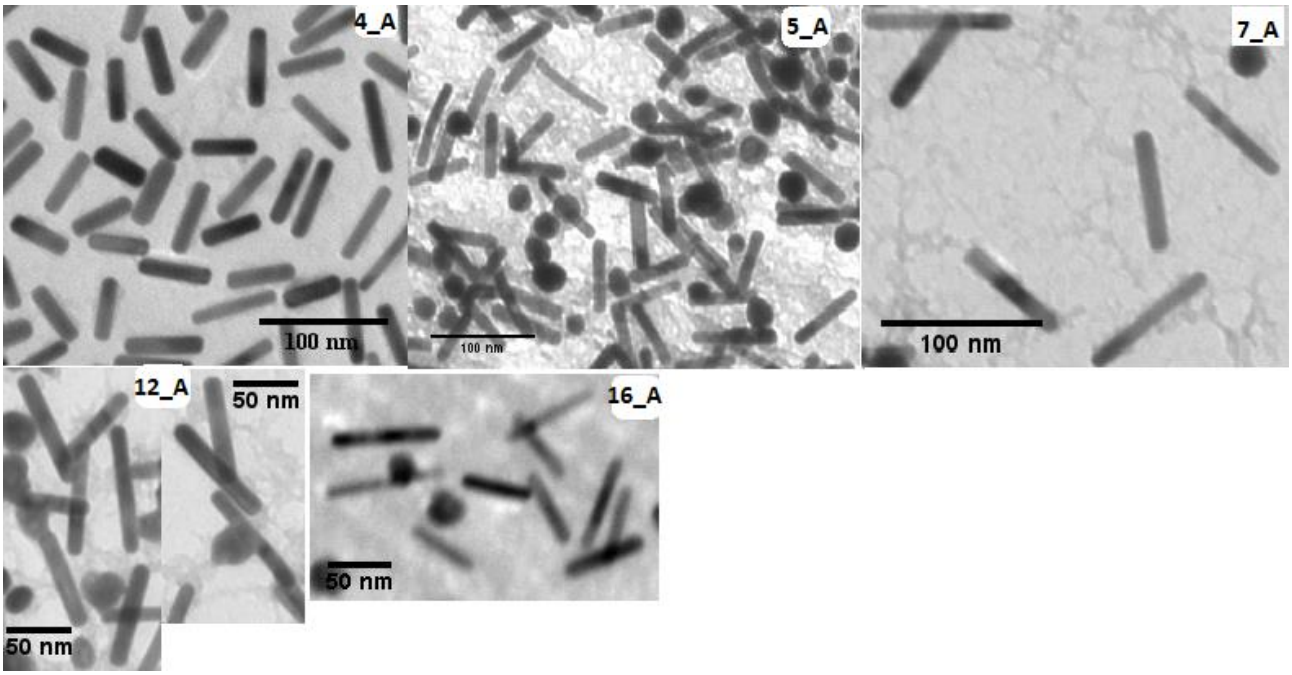

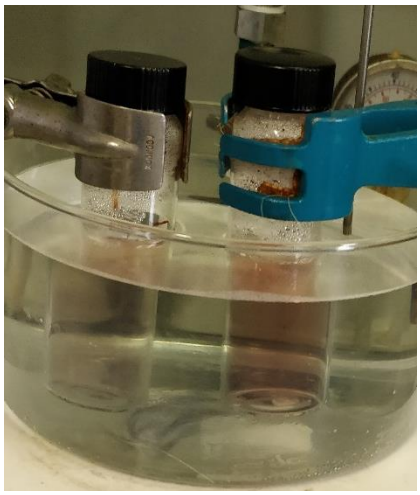

Figure 55 images of the samples specified in the white box on the top, picture of two growth solutions in the moment of the colour appearance, prepared simultaneously with the same seed solution, the more pale colour of the solution on the left is due to its higher AgNO3 concentration(5.5mM stock solution while the solution on the right used 4mM AgNO3 stock solution) on the bottom

3.7.1 Working in the linear range

Four more solutions were prepared with silver ions concentration below the precipitation concentration, in order to confirm the linear trend of λ_{max} LSPR at increasing Au:Ag ratio. Moreover, the initial step of CTAB and 5BrSA dissolution was fixed. Indeed, the aromatic additive is sparingly soluble in water but in pair with CTAB can form homogenous aqueous solution due to its inclusion in the micelles' structures. An homogenous initial solution is crucial for the following steps of the reaction, CTAB must be heated to be dissolved in water and it is important to avoid any foam formation. When the initial dissolution is performed by keeping the vial in hot tap water, 5BrSA can be found not to properly dissolve and foam can easily forms. To improve and standardize this step, the initial solutions of CTAB and 5BrSA were stirred for 5 minutes at 50°C in the water bath used for the growth reaction. After that, solutions were stirred and allowed to reach the temperature required for the synthesis (30°C) by decreasing the temperature of the water bath.

Table 19 AgNO3 concentrations in the stock solutions used for the synthesis of the samples reported on the left, and respective effective concentration in the growth solutions and ratios HAuCl4 : AgNO3.

	[$AgNO_3$] Mm		
sample name	stock sol.	growth sol.	Au:Ag
4_B	4.00	0.116	4.17
5_B	5.00	0.145	3.33
6.6_B	6.60	0.191	2.53
6.8_B	6.83	0.198	2.44

Table 20 value of mean aspect ratio and peak position for both LSPR and TSPR of the samples reported on the left

sample	R	δR	λ_{max}LSPR (nm)	λ_{max}TSPR (nm)
4_B	4.6	0.2	886	519
5_B	5.2	0.3	941	516
6.6_B	6.7	0.2	1062	511
6.8_B	5.9	0.5	1073	511

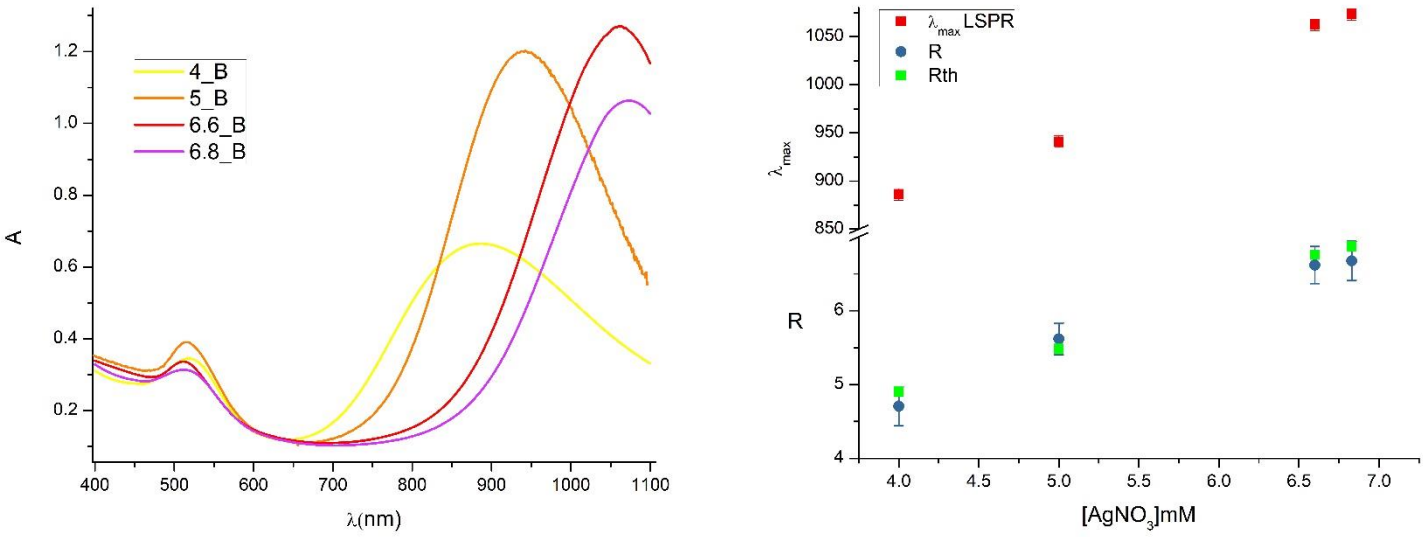

Figure 56 on the right UV-VIS-NIR spectra of the sample reported in table 20, on the right peak position for LSPR and experimental (blue) and theoretical (green) aspect ratio values

As it can be seen in Figure 56 and Figure 58, the linear relationship between λ_{max} of LSPR peak and the silver concentration is confirmed (R2=0.998), and it is due to the linear relationship between the Au:Ag ratio in the growth solution and the obtained GNRSs' aspect ratio (higher silver concentration determines an increase in length and a slightly decrease in the diameter, as it has been observed previously). Moreover, the experimental value of R does not differ from the theoretical values calculated based on equation 6. Link et al. derived the equation by the application of the Gans' theory together with the known dielectric function of the gold. Considering the resonance condition for the longitudinal mode (equation 5 with an appropriated geometric factor) and the fact that the real part of the gold dielectric function is wavelength dependent and nearly

linear, they determined the following equation, considering a wavelength region between 500-800 nm and GNRSs' size less than 1/10 of the wavelength of the interacting light:

$$\lambda_{max} = (53.71\,R - 42.29)\varepsilon_m + 495.14$$

They determined that the equation fits their experimental data if ε_m=1.77, a value in good agreement with the dielectric constant of water, namely the solvent, and this means that water is widely contentained in the surfactant's structures around the nanorods (electrochemically synthetized with CTAB and tetraoctylammonium bromide)(Link, Mohamed, and El-Sayed 1999). Since our R results fit theoretical values calculated from the maximum position of the respective LSPR bands and considering ε_m=1.77, it means that also for longer wavelengths the same equation and that even for our synthesis the water content in the GNRSs' organic layer is significative.

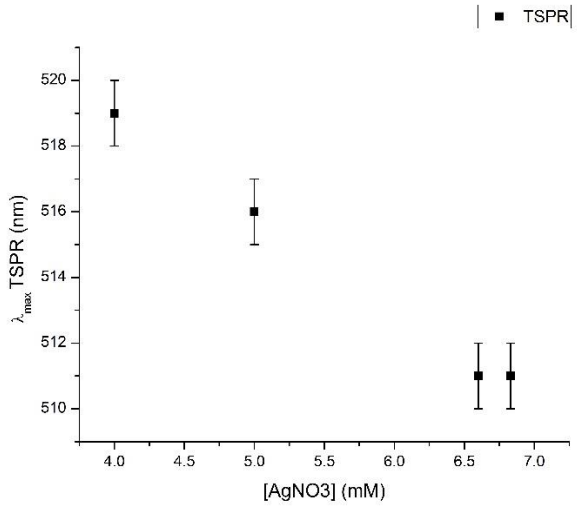

Figure 57 peak positions of TSPR band for the samples reported in Table 17

As it can be seen from Figure 57, the TSPR shift to shorter wavelengths when R increases even if it does not follow a linear trend. Indeed, in this spectral region the interband transition has a dominant effect. It makes the resonance condition to depend not only on the real part of the dielectric constant of Au[4] but also to the imaginary part, that causing the loss of linearity between R and the TSPR's peak position (K. S. Lee and El-Sayed 2005).

A comparison between UV-VIS-NIR spectra of A samples below AgBr precipitation and B samples are reported in Figure 60, while their data are compared in Figure 61.

[4] The real component of the gold dielectric constant is nearly linearly dependent on wavelength causing a linear relationship between R and LSPR when is the only relevant component for the resonance condition

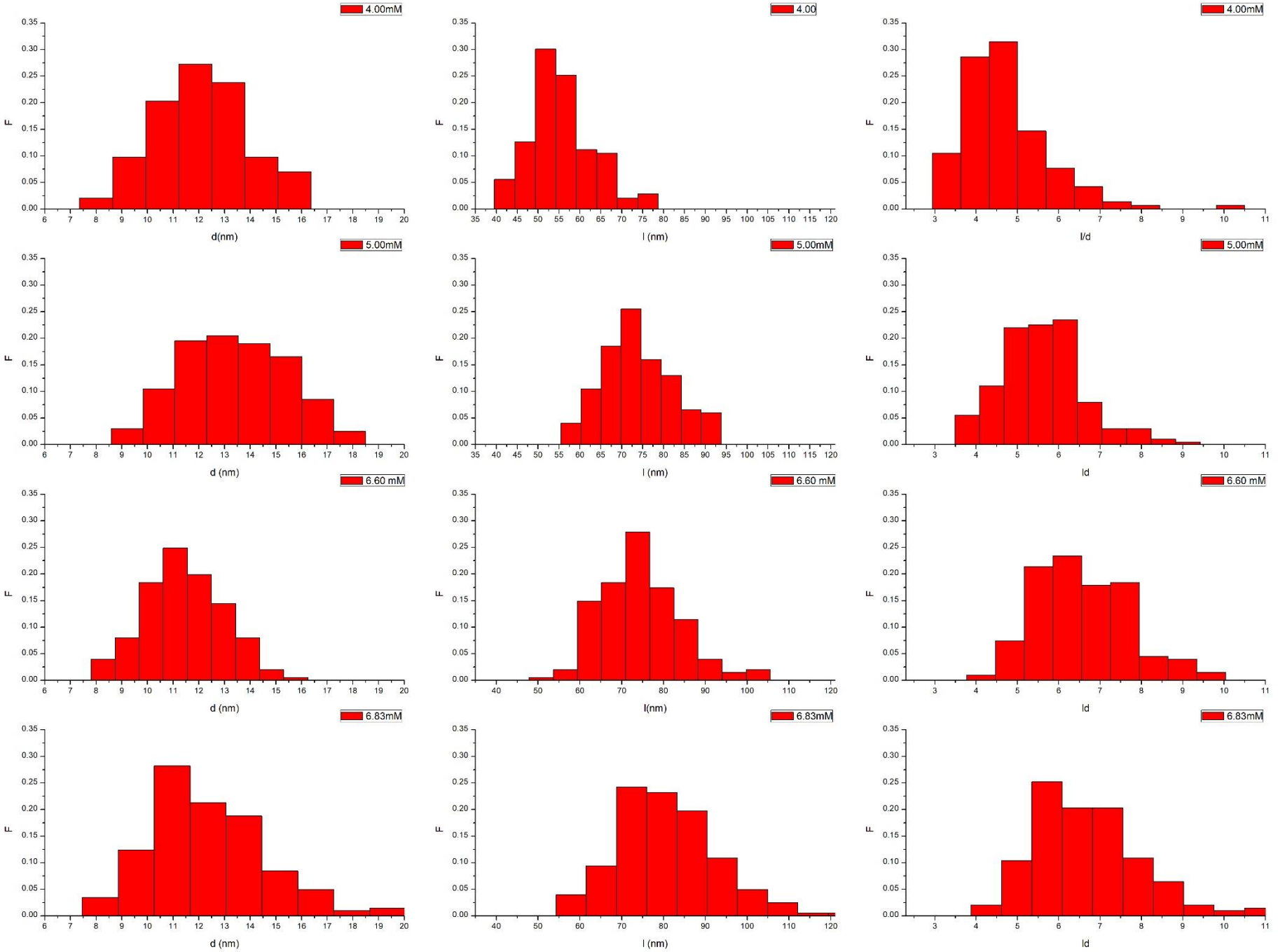

Figure 58 diameter, length and aspect ratio distributions of the samples reported in Table 19

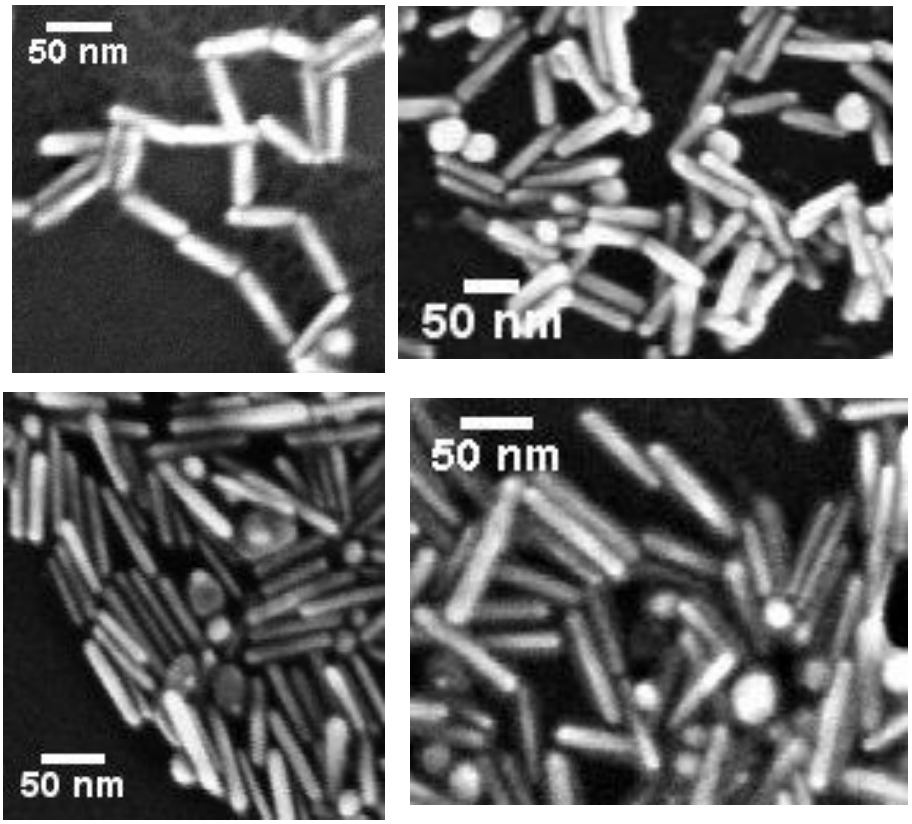

Figure 59 SEM images of sample 4_B top left, 5_B top right, 6.6_B lower left, 6.8_B lower left

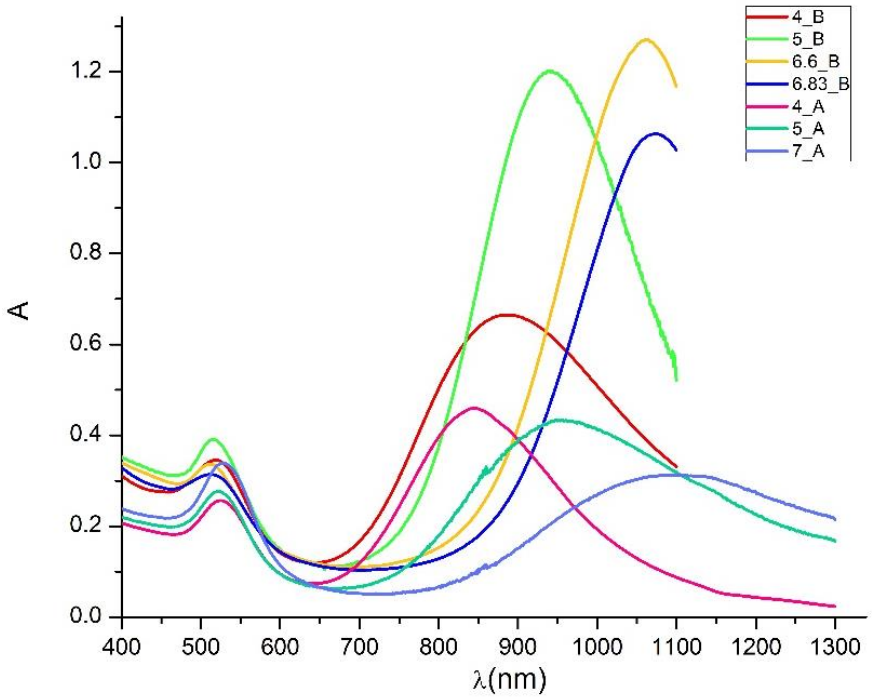

Figure 60 UV-VIS-NIR spectra of the B samples and 4_A,5_A,7_A samples

Table 21 values of ratio L/T, LSPR peaks' intensities, absorbance at 400 nm and percentage of shape impurities (nanospheres) for the samples reported on the left

sample	L/T	I LSPR	A_{400}	% GNSs
4_B	1.8	0.50	0.30	5
5_B	2.8	1.09	0.35	15
6.6_B	3.7	1.13	0.34	11
6.8_B	3.2	1.02	0.33	17
4_A	1.8	0.39	0.21	17
5_A	1.6	0.37	0.22	44
7_A	0.9	0.26	0.24	61

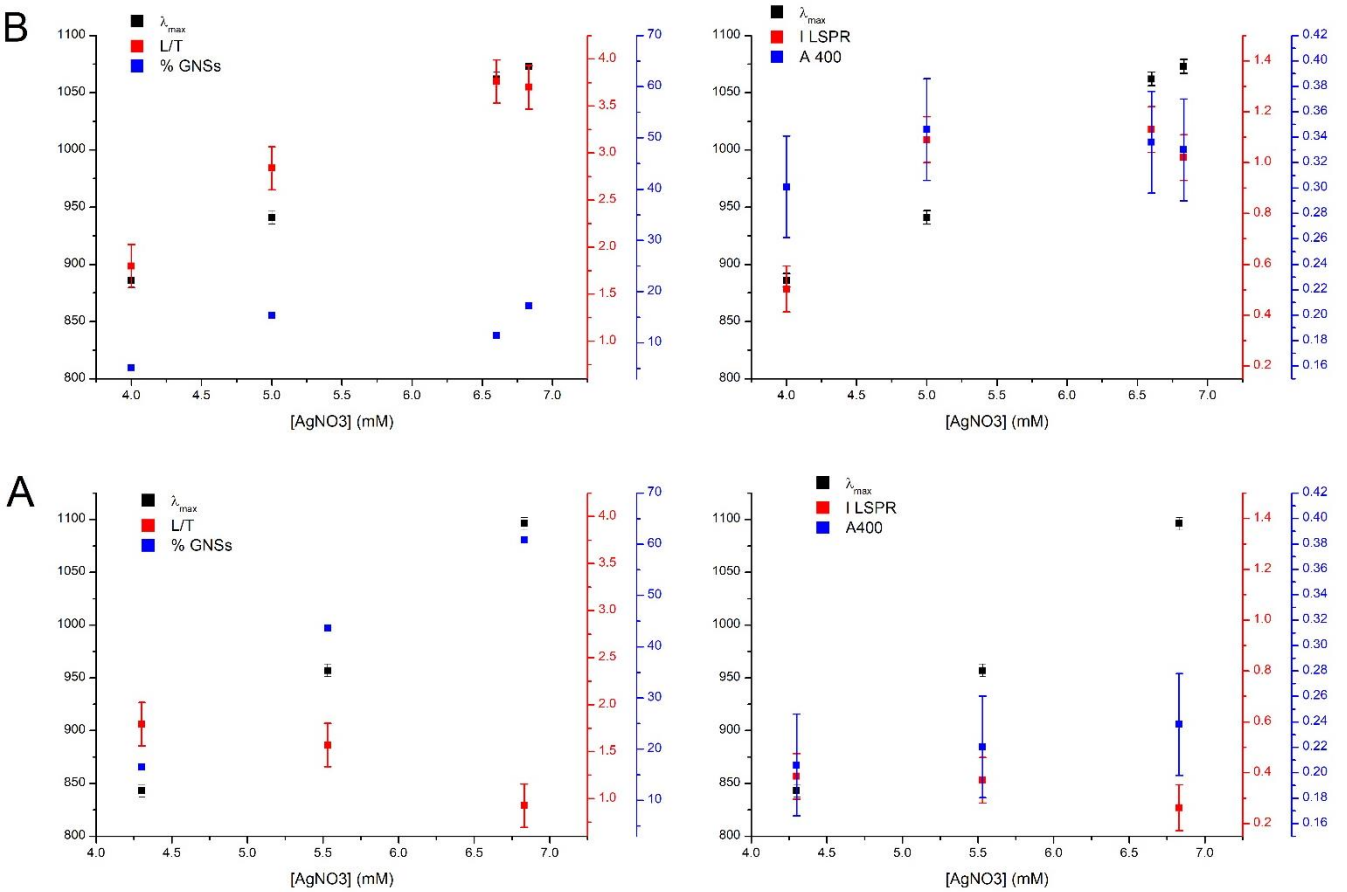

Figure 61 In the upper part data refer to B samples while in the lower refer to the A samples below AgBr visible precipitation. In all the graphs peak position of LSPR is reported as a function of the AgNO3 concentration in the stock solution as a referment. On the left is showed how ratio L/T and the percentage of shape impurities change with the increase in the silver ions concentration and relative shift in λmax LSPR, the same is done on the right for the absorption value at 400nm and the intensities of LSPR peaks . the error bars are taken from the studies reported in paragraph 3.3.1

As it can be seen in Figure 61, in the case of the A samples, the amount of shape impurities increases with the increase in the $AgNO_3$ concentration. Even though, the percentage of GNSs is calculated from TEM and SEM images (more than 2000 particles were counted for every sample) that are not so much reliable as a representation of the whole sample characteristics, these data are in line with the ratio between intensities of the TSPR and LSPR peaks. Indeed, the decrease in the value of L/T

determined in A samples means an increase of shape impurities, otherwise L/T value should increase for increasing aspect ratios (K. S. Lee and El-Sayed 2005) as it is shown for the B samples, where the percentage of GNRSs remains approximately similar at increasing $AgNO_3$ concentration. The trend showed for A samples is common, namely is widely reported that, even if $AgNO_3$ is necessary for obtaining anisotropic particles, its increase causes an increase in the amount of shape impurities. This has been attributed to the higher ionic strength associated with higher $AgNO_3$ concentration (Su, Yang, and Zhu 2015) or to the Ag^+ higher capability to passivate growing seeds that reduces the driving force for single crystal structure formation and then causes lower anisotropic particles development (Tong et al. 2017). The increase of shape impurities in A samples causes also a decrease in the intensities of LSPR peaks. The yield of GNRSs is definitely higher in the B samples since even the absorption values at 400 nm is increased, this means that in this set of samples both reduction and shape yield are higher.

It is reported that lowering CTAB concentration in the growth solution causes an increase in the fraction of shape impurities , for this reason the traditional protocol require CTAB 0.1M (C.J. Murphy et al. 2005). In our growth solution, the concentration of CTAB was halved thanks to the addition of 5BrSA. Considering that, our results suggest that a proper initial inclusion of 5BrSA in CTAB micelles, that can be better obtained with the initial heating and longer stirring of the CTAB and 5BrSA solution, is capable to remove the shape impurity problem deriving from the lower CTAB concentration since shape impurities are lower in B samples and do not increase with $AgNO_3$ concentration. As regard to the higher reduction yield, this may suggest the influence of 5BrSA reduction property in the growth of GNRSs, since when the reagent is better included in the micelle it allows to increase the reduction of gold salt.

3.8 Reproducibility

In order to evaluate the reproducibility of the synthetic process, four solutions were prepared at $AgNO_3$ concentration equal to 5.5mM in the stock solution (0.159 mM in the growth solution and Au:Ag equal to 3.03).This concentration was chosen since it is the central value in the considered concentration range, so if the reproducibility is $AgNO_3$ concentration dependent, it will be possible to obtain an average value. Moreover it is reported in literature that the standard protocol with $AgNO_3$ 4mM should allow to obtain GNRSs with LSPR peak at about 980 nm(Y. Huang et al. 2018), while without increasing the silver ion concentration it was not possible to obtain it. From the linear trend determined from B samples, LSPR peak at about 980 nm can be predicted to be obtained with a concentration of $AgNO_3$ stock solution equal to 5.5mM.

The most important parameter that has to be considered in the reproducibility evaluation is the peak position of LSPR. In Table 22 the LSPR peak positions are reported, while the obtained spectra are reported in Figure 62.

The mean value of LSPR peak position is 987±44 nm (considering a confidence interval at 95% of probability). As it can be seen from Figure 62, the mean value coincides with the expected value of the linear fit determined for B samples. The determined confidence interval was extended to the whole $AgNO_3$ concentration range. In Figure 62 it can be seen that, considering this value dispersion, all the samples obtained in this work (some of them are not previously discussed) show LSPR peak positions that do not significantly differ from the linear trend determined for B samples. Considering these results, it can be said that the determined linear trend is a good representation of the

relationship between $AgNO_3$ concentration and the obtained GNRSs' LSPR peak position and can be used to predict the $AgNO_3$ required concentration.

Table 22 LSPR peak position for the sample reported on the left

sample	λ_{max} LSPR
1_R	970
2_R	957
3_R	1014
4_R	1007

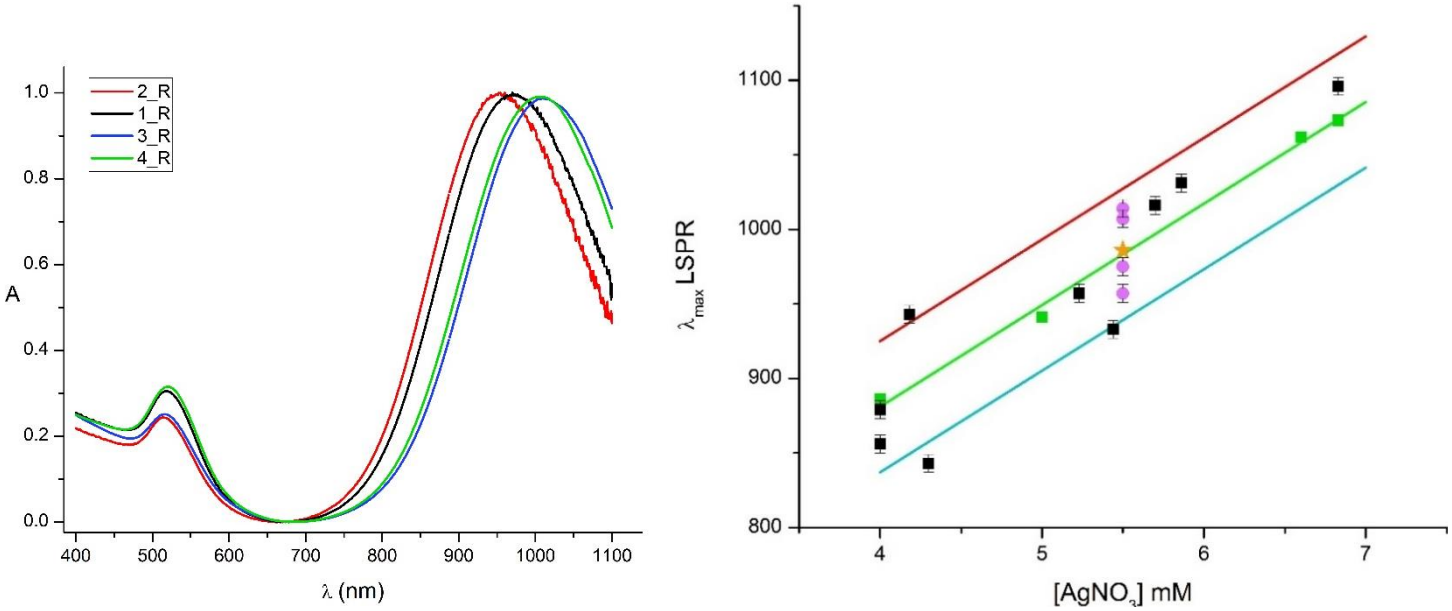

Figure 62 on the left the UV-VIS-NIR spectra of the solutions reported in Table 22 (absorbance values were normalized). On the right, it can be seen all the values of LSPR peak positions obtained by synthesis with different $AgNO_3$ concentrations that have been made in this work. Green points correspond to B samples and the green line is their linear fit. The area determined between the red and the blue line corresponds to 95% of confidence interval determined by SD of purple points (5.5mM), the star is the mean value of the purple points. The error bars reported are taken from paragraph 3.3.1.

Even though samples prepared in the same period and conditions show a good agreement between their LSPR peak position, such as the B samples, the dispersion that has been determined showed a quite poor reproducibility for the synthesis. The poor reproducibility is a widely reported problem for the GNRSs synthesis, and as already said, the protocol for GNRSs outside 700-900 nm of LSPR range are still far from ideal (Ye et al. 2012; Scarabelli et al. 2015). However, it can be improved by the adoption of some precautions. One very important factor that can influence the reproducibility of the synthesis is the water quality. Indeed, it is reported that the quality of the water is the main sources of irreproducibility. In this work Mili-Q water has been used for both the synthesis and the cleaning of glassware (after treatment with aqua regia), unfortunately it is deionized and filtered but not distilled. This means that contaminant traces cannot be excluded, and moreover after the filtration the pH could be slightly different, and it is a crucial parameter in determining the final aspect ratio (Scarabelli et al. 2015). Another critical issue is the cleaning of the entire lab environment where attention should be paid to reduce dust as much as possible (Henson et al. 2017; Scarabelli et al. 2015). Vials should be closed with caps, but it is important to assure the absence of metal in them, in order to avoid contaminations. Other important factors are: reagent age and

storage conditions, different vessel used in the synthesis (size, shape), different spin and heating efficiency (Henson et al. 2017).

So, the reproducibility can be improved by checking water quality and the lab environment, utilizing standard vials with opportune caps, working with standard heating and stirring efficiency, checking the quality of the reagents.

The difference in the required $AgNO_3$ concentration between what has been determined here and what Huang et al. have determined could be due to the use of different reagents, indeed it has been reported that different supplier and also different lots of the same supplier can cause variations in the obtained position of the LSPR (Henson et al. 2017).

3.9 Aging

Aqueous solution of GNRSs exhibit a gradual blueshift in LSPR. Na_2S added in the quenching should help to reduce this shift. It is particular important to reduce the shift since the optical properties of the solution depends upon LSPR band position, hence applications of GNRSs require particles stability. To evaluate if GNRSs with different R show different shift and its evolution during the time, B samples and two R samples were measured. As it can be seen in Table 23 and in Figure 63 and Figure 64 it seems that the maximum shift is already reached after 1 week, than even 4 months later it seems to be unchanged, moreover it seems to be not dependent on R since all the samples shift about 10 nm.

Table 23 shift of the LSPR of the GNRSs aqueous solution after 1 week, 2 months and 4 months for the reported samples on the left.

		ΔLSPR		
sample	R	1week	2months	4 months
4_B	4.71		10	10
5_B	5.62		8	8
2_R	5.76	10	10	
3_R	6.32	9	9	
6.6_B	6.62		10	10
6.68_B	6.68		9	9

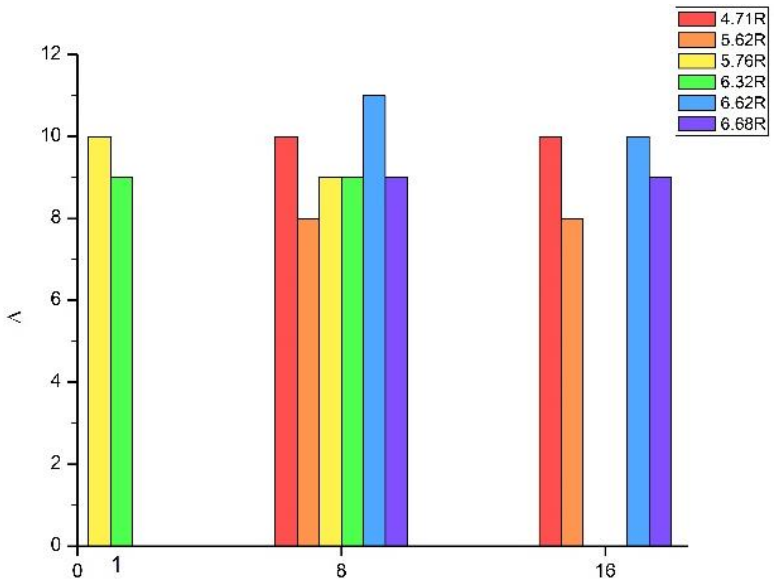

Figure 63 shift values of LSPR for the considered samples

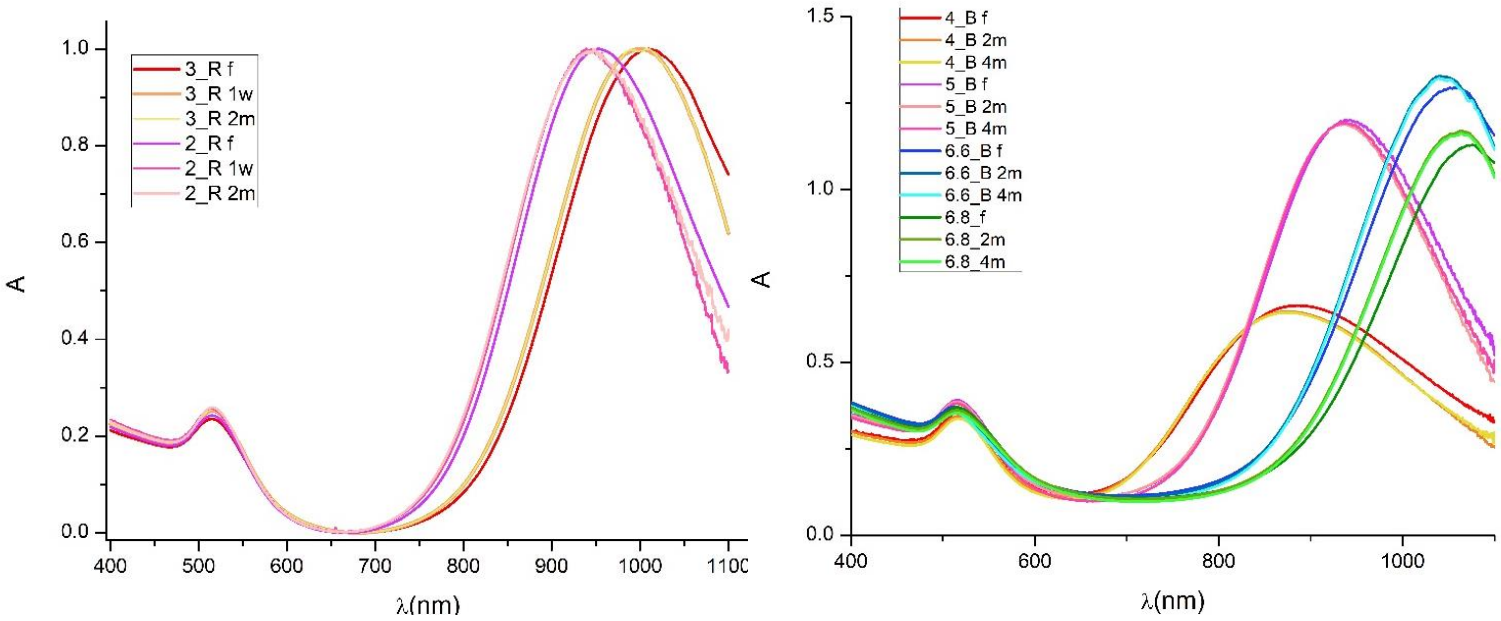

Figure 64 UV-VIS-NIR spectra of R samples 1 week and 2 months after their quenching on the left (spectra are normalized), spectra of B samples 2 and 4 months after their quenching on the right.

In order to understand the efficacy of the quenching performed with a S/M ratio of 4, the aliquots used for the studies reported in paragraph 3.3.1 were measured after 2 months. As it can be seen from Table 24, among aliquots quenched with a different S/M ratio the one corrisponding to S/M=4 does not show a significant reduction of the shift. Moreover, comparable shifts are also obtained for Q and CR aliquots and CR aliquots. This means that the quenching process with Na2S does not determine a significative reduction in the effects of the aging.

Table 24 shift of LSPR after 2 months of aliquots treated with different S/M ratio on the left and a comparison between the shift after 2 months of aliquots centrifuged and quenched and only quenched on the right

S/M	ΔLSPR
2	12
4	10
6	10

	ΔLSPR	
sample	CR	Q & CR
4_B	7	10
5_B	4	7

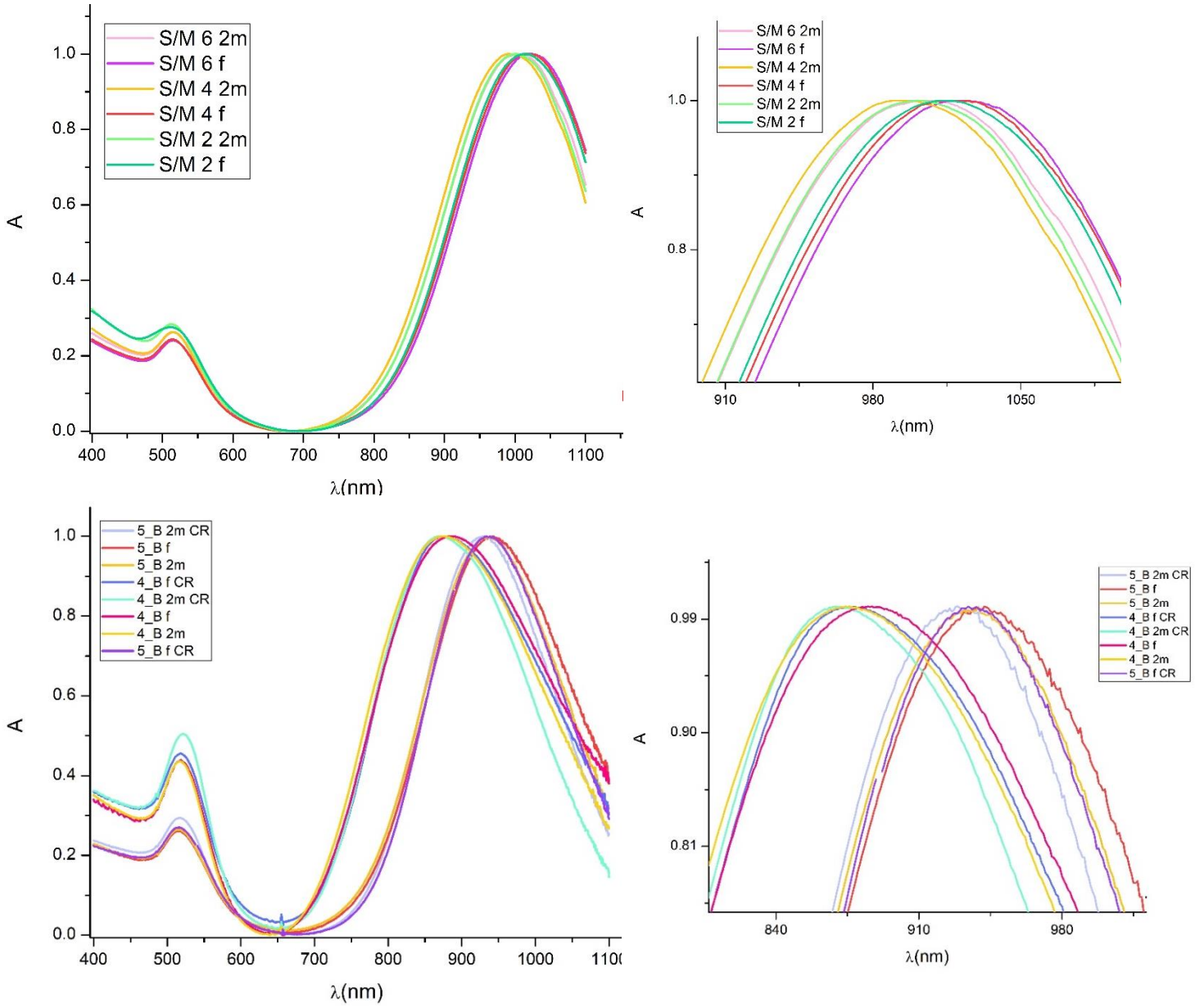

Figure 65 UV-VIS-NIR spectra of aliquots treated with different S/M ratio fresh and after 2months on the top and a comparison between aliquots centrifuged and quenched and only quenched fresh and after 2 months on the bottom

These results suggest that the shift in our GNRSs aqueous solutions could be not due to the presence of unreacted gold and silver ions, but it can be a consequence of GNRSs structure change to reach a more thermodynamically stable arrangement. Indeed, if the shift was caused by the unremoved reagent the Na_2S would be able to decrease it since it is capable to remove the unreacted ions from the reaction mixture, moreover the shift due to the presence of the unremoved reagents is reported to be around 50 nm, while the shift determined in our samples is not so far from the one reported for the best Na_2S treatment (5nm).

Quenching with Na_2S was determined to be effective for GNRSs solution with smaller R and reaction conditions as the same as the one reported in Table 13(Zweifel and Wei 2005). It is possible that the halved CTAB concentration allows an easier purification, so problems derived from a poor purification are reduced in our reaction conditions.

3.10 Determination of reduction yield

To evaluate the reduction yield of the GNRSs synthesis, two solutions identified as 4_Y and 5.5_Y were measured by ICP-OES, they were respectively obtained with $AgNO_3$ stock solutions 4mM and 5.5mM, and their UV-VIS-NIR spectra are reported in Figure 66.

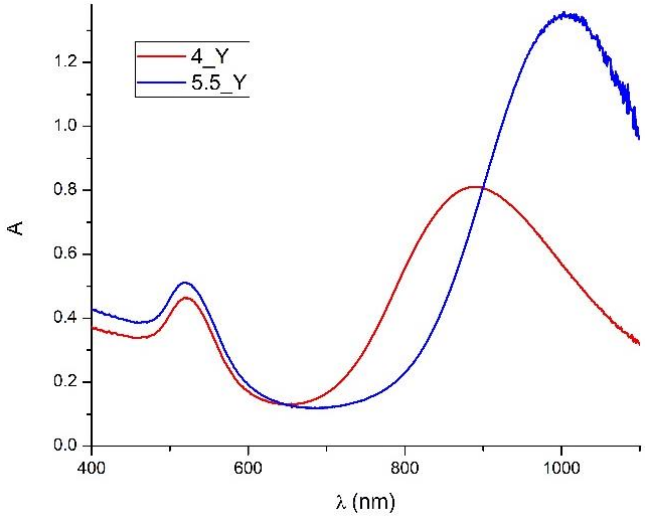

Figure 66 UV-VIS-NIR spectra of the sample 4_Y and 5.5_Y

The considered samples after the quenching (3 days after the seed addition) were carefully centrifuged and redispersed. The calibration was conducted with gold solutions with concentration from 1 ppm to 21 ppm (the maximum selected value corresponds to a yield of 100%). The solution used for the calibration were prepared from both standard gold solution (1000 ppm) and solution (43 ppm) obtained from the salt $HAuCl_4$ $3H_2O$ used for the GNRSs sinthesys.

1 ml of aqua regia has been added to 2ml of GNRSs sample obtaining a final concentration of 30% v/v as the one required in the method for the sample digestion (Coombs 2016). After 1h of digestion (Su, Yang, and Zhu 2015) solutions were diluted (25ml) to obtain a final aqua regia concentration of 10%, which better fits instrument requirement. Instrument was set as reported in the method (Coombs 2016), all the measures were performed at wavelength of 267.595 nm and 242.795nm, which can be both used for gold determination. Both the calibration obtained with salt and standard solutions working at 267.595 nm allow to obtain a better R^2 as it can be seen from Table 25, for this reason the reported data refers only to the best selected wavelength.

Table 25 quantification and detection limit and R^2 values obtained for the calibration curved obtained as reported on the top of the table

	standard		salt	
	λ(nm) 267.595	λ(nm) 242.795	λ (nm) 267.595	λ (nm) 242.795
LOD (ppm)	0.02	0.03	0.03	0.09
LOQ (ppm)	0.05	0.10	0.11	0.31
R^2	0.99976	0.9988	0.99983	0.9989

As it can be seen in Figure 67, the calibration curves obtained with salt solutions show lower values, this could be due to the hydration of the salt. It proves the previously discussed influence of reagent conservation in synthesis reproducibility since the hydration may increase gradually during the time, even if the reagent was always kept in the desiccator. Indeed, based on the measure at 267 nm, which has been selected as the best wavelength, salt values are 28% lower than the standard solution and this for sure affected the growth of GNRSs, just think of the importance of the ratio Au:Ag. For this reason, the most convenient way to use $HauCl_4$ reagent is to prepare a stock solution with the entire content of the sealed bottle, weighing the full and empty container to calculate the exact mass. The prepared stock solution has to be kept in the refrigerator and substituted as soon as visible changes appears (presence of insoluble material)(Scarabelli et al. 2015).

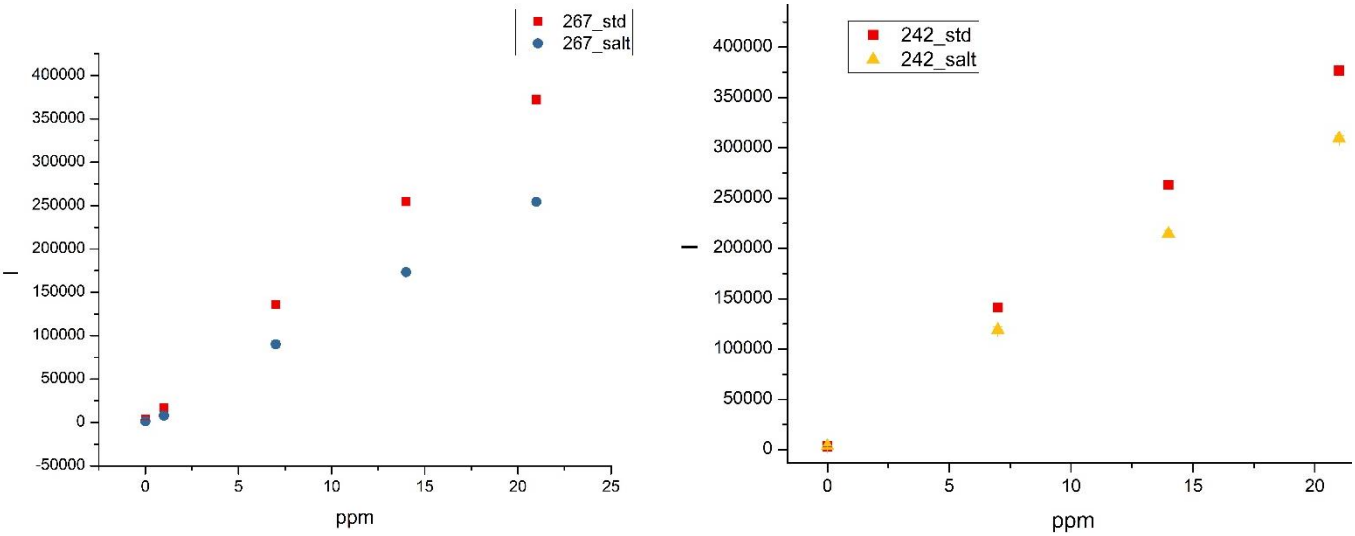

Figure 67 calibration curves obtained with standard and salt solution at different wavelength

In Table 26 are compared the yield obtained by ICP-OES and derived from the absorbance value at 400nm. Indeed, it is reported that this absorbance value vary linearly with Au^0 concentration with a slope of 2.4 (A*f*(mM Au^0)) regardless the shape and the size of the nanoparticles (Scarabelli et al. 2015).

Table 26 yield determined by ICP-OES and by the value of absorbance at 400nm

	% Yield	
sample	ICP_OES	A_{400}
4_Y	14.6±0.4	31±4
5_Y	15.8±0.4	36±4

The yield obtained by ICP measures are in line with the expected yield of GNRSs grown in silver containing solution, even though considering the hydration of the salt previously discussed, the value can be underestimated. However, the discrepancy between yield determined by absorbance value and ICP could be due to the formation of metallo-micelles containing CTA-$AuBr_4$ complex that cannot be fully digested with the acid digestion causing a significative underestimation of gold content as reported in the study of Park. It has been determined that with a microwave digestion the determined gold content was about double than the one determined with only the acid treatments (for ppm range comparable with our study) (Park et al. 2014). Hence considering that it

is reasonable to consider that the effective yield is the one determined by the absorbance value but further ICP measure with different samples digestion should be performed to confirm that.

4 CONCLUSIONS

In this work it has been determined that two main phases can be distinguished during one week of GNRSs growth. During the whole growth time the reduction of gold continues and both the dimensions grow. Contrary to what has been supposed by Ye et al. a blue shift is obtained when the growth is maintained for one week. Even if with different kinetic and morphological GNRSs evolution, the mechanism determined in our system is in line with the one reported by Park et al. and the differences can be attributed to the different surfactant system.

The quality of the seed particles has been proved as a key factor in obtaining high quality GNRSs and in particular $NaBH_4$ reduction efficiency must be carefully checked.

The aromatic additive has been proved to be involved in the formation of the organic layer presents in the surface of the particles, but it also been proved to be capable of gold precursor reduction even if the ascorbic acid remains fundamental for obtaining Au^0.

The presence of $AgNO_3$ was determined fundamental for obtaining anisotropic nanoparticles, confirming the studies of Walsh et al. A mean value of R equal to 2 ($AgNO_3$ 16µM in the growth solution), was found to be the minimum for obtaining in the UV-VIS spectra of the particles a LSPR band separated from TSPR band. We proved that LSPR band shifts linearly at increasing $AgNO_3$ concentration until AgBr precipitation occurs due to a linear increase in R value. Moreover, the relationship between R and λ_{max} LSPR was found to follow the theoretical relationship determined for shorter GNRSs, hence it allows to evaluate R values without the necessity of SEM/TEM images.

Studies on GNRSs aging determined that a blue shift occurs within one week and then it remains the same even after 4 months. The shift is moderate, and it does not depend on R or Na_2S concentration, this demonstrates the easier purification permitted by the lower CTAB concentration in the growth medium.

We determined that the initial step of CTAB and 5BrSA solution preparation must be performed in the water bath at 50°C, since this allows to improve the quality of the obtained particles.

The reproducibility of the synthesis is quite low, further studies should be performed to improve it by the employment of preparation and conservation of different stock solutions, the analysis of the used water, the use of standard glassware to perform the reaction.

The yield of the reaction is probably higher than the standard reaction in presence of silver nitrate, anyway further ICP studies with different sample digestion should be performed to confirm it.

5 BIBLIOGRAPHY

Buchwalder, Christian, Katayoun Saatchi, and Urs O. Häfeli. 2014. “Nanomaterial-Based Bioimaging Probes.” In *Bio- and Bioinspired Nanomaterials*, edited by Claudio Rosicini Daniel Ruiz_molina, Fernando Novio, 9783527335:201–28. https://doi.org/10.1002/9783527675821.ch08.

CFAMM, Central Facility for Advanced Microscopy and Microanalysis. 2017. “Introduction to Energy Dispersive X-Ray Spectrometry (EDS).” University of California Riverside. 2017. https://doi.org/http://dx.doi.org/10.1590/S0104-66322011000100011.

Coombs, Kayla. 2016. “Rapid Determination of Gold in Geological Samples Using the Agilent 4210 MP-AES.” 5991–7103EN.

Cotton, F. A., and G. Wilkinson. 1988. *Advanced Inorganic Chemistry*. Edited by John Wiley & Sons Ltd. 5th ed. London-New York.

Errant gene therapeutics, EGT. 2019. “Gene Therapy.” 2019. https://errantgene.com/science-technology/gene-therapy/.

Eustis, Susie, and Mostafa A. El-Sayed. 2006a. “Determination of the Aspect Ratio Statistical Distribution of Gold Nanorods in Solution from a Theoretical Fit of the Observed Inhomogeneously Broadened Longitudinal Plasmon Resonance Absorption Spectrum.” *Journal of Applied Physics* 100 (4). https://doi.org/10.1063/1.2244520.

———. 2006b. “Why Gold Nanoparticles Are More Precious than Pretty Gold: Noble Metal Surface Plasmon Resonance and Its Enhancement of the Radiative and Nonradiative Properties of Nanocrystals of Different Shapes.” *Chemical Society Reviews* 35 (3): 209–17. https://doi.org/10.1039/b514191e.

Gómez-Graña, Sergio, Fabien Hubert, Fabienne Testard, Andrés Guerrero-Martínez, Isabelle Grillo, Luis M. Liz-Marzán, and Olivier Spalla. 2012. “Surfactant (Bi) Layers on Gold Nanorods.” *Langmuir* 28 (2): 1453–59. https://doi.org/10.1021/la203451p.

Guyot-sionnest, Philippe, and Mingzhao Liu. 2005. “Mechanism of Silver (I) -Assisted Growth of Gold Nanorods and Bipyramids Mechanism of Silver (I) -Assisted Growth of Gold Nanorods and Bipyramids.” *Journal of Physical Chemistry B* 109 (October): 22192–200. https://doi.org/10.1021/jp054808n.

Henson, By Brantley C, Justin T Harris, Kimberly A Homan, and Material Matters. 2017. “Synthesis of Gold Nanorods : Avoiding Common Pitfalls Six Common Pitfalls in Gold Nanorod Synthesis.” *Material Matters* 12 (2): 1–8.

Huang, Xiaohua, Svetlana Neretina, and Mostafa A. El-Sayed. 2009. “Gold Nanorods: From Synthesis and Properties to Biological and Biomedical Applications.” *Advanced Materials* 21 (48): 4880–4910. https://doi.org/10.1002/adma.200802789.

Huang, Yue, Artiom Skripka, Lucía Labrador-Páez, Francisco Sanz-Rodríguez, Patricia Haro-González, Daniel Jaque, Federico Rosei, and Fiorenzo Vetrone. 2018. “Upconverting Nanocomposites with Combined Photothermal and Photodynamic Effects.” *Nanoscale* 10 (2): 791–99. https://doi.org/10.1039/c7nr05499h.

Jackson, Stephen R., James R. McBride, Sandra J. Rosenthal, and David W. Wright. 2014. “Where’s

the Silver? Imaging Trace Silver Coverage on the Surface of Gold Nanorods." *Journal of the American Chemical Society* 136 (14). https://doi.org/10.1021/ja501676y.

Jana, Nikhil R. 2005. "Gram-Scale Synthesis of Soluble, near-Monodisperse Gold Nanorods and Other Anisotropic Nanoparticles." *Small* 1 (8–9): 875–82. https://doi.org/10.1002/smll.200500014.

Joshi, Mangala, A. Bhattacharyya, and S. Wazed Ali. 2008. "Characterization Techniques for Nanotechnology Applications in Textiles." *Indian Journal of Fibre and Textile Research* 33 (3): 304–17. https://doi.org/10.1039/c0cp00504e.

Kumar, S., K. S. Gandhi, and R Kumar. 2007. "Modeling of Formation of Gold Nanoparticles by Citrate Method." *Industrial and Engineering Chemistry Research* 46 (10): 3128–36. https://doi.org/10.1021/ie060672j.

Lee, Kyeong Seok, and Mostafa A. El-Sayed. 2005. "Dependence of the Enhanced Optical Scattering Efficiency Relative to That of Absorption for Gold Metal Nanorods on Aspect Ratio, Size, End-Cap Shape, and Medium Refractive Index." *Journal of Physical Chemistry B* 109 (43): 20331–38. https://doi.org/10.1021/jp054385p.

Lee, Seunghyun, Lindsey J.E. Anderson, Courtney M. Payne, and Jason H. Hafner. 2011. "Structural Transition in the Surfactant Layer That Surrounds Gold Nanorods as Observed by Analytical Surface-Enhanced Raman Spectroscopy." *Langmuir* 27 (24): 14748–56. https://doi.org/10.1021/la202918n.

Lin, Z., J. J. Cai, L. E. Scriven, and H. T. Davis. 1994. "Spherical-to-Wormlike Micelle Transition in CTAB Solutions." *Journal of Physical Chemistry* 98 (23): 5984–93. https://doi.org/10.1021/j100074a027.

Link, S., M. B. Mohamed, and M. A. El-Sayed. 1999. "Simulation of the Optical Absorption Spectra of Gold Nanorods as a Function of Their Aspect Ratio and the Effect of the Medium Dielectric Constant." *The Journal of Physical Chemistry B* 103 (16): 3073–77. https://doi.org/10.1021/jp990183f.

Loredana Latterini, Luigi Trapani. 2015. "Phototermal ERffect of Gold Nanostructures for Application in Bioimaging and Therapy." In *Bio- and BIOinspired Nanomaterials*, edited by Claudio Rosicini Daniel Ruiz-Molina, Fernando Novio, 173–200.

Moores, Audrey, and Frédéric Goettmann. 2006. "The Plasmon Band in Noble Metal Nanoparticles: An Introduction to Theory and Applications." *New Journal of Chemistry* 30 (8): 1121–32. https://doi.org/10.1039/b604038c.

Mulvaney, Paul, Jorge Pérez-Juste, Luis M. Liz-Marzán, Steven Carnie, and Derek Y.C. Chan. 2004. "Electric-Field-Directed Growth of Gold Nanorods in Aqueous Surfactant Solutions." *Advanced Functional Materials* 14 (6): 571–79. https://doi.org/10.1002/adfm.200305068.

Murphy, C.J., J.X. Gao, T.K. San, L. Gou, T. Li, A.M. Gole, C.J. Orendorff, and S.E. Hunyadi. 2005. "Anisotropic Metal Nanoparticles: Synthesis, Assembly, and Optical Applications." *Journal of Physical Chemistry B* 109 (29): 13857–70. //000230698100005.

Murphy, Catherine J., Lucas B. Thompson, Alaaldin M. Alkilany, Patrick N. Sisco, Stefano P. Boulos, Sean T. Sivapalan, Jie An Yang, Davin J. Chernak, and Jingyu Huang. 2010. "The Many Faces of Gold Nanorods." *Journal of Physical Chemistry Letters* 1 (19): 2867–75.

https://doi.org/10.1021/jz100992x.

Murphy, Catherine J, Nikhil R Jana, and Laha Gearheart. 2001. “Seed-Mediated Growth Approach for Shape-Controlled Synthesis of Spheroidal and Rod-like Gold Nanoparticles Using a Surfactant Template.” *Advanced Materials*, no. 18: 1389–93.

Nikoobakht, B., M. El-Sayed, A., Z. L. Wang, and R. P. Gao. 2000. “Surface Reconstruction of the Unstable {110} Surface in Gold Nanorods.” *The Journal of Physical Chemistry B* 104 (23): 5417–20. https://doi.org/10.1021/jp000800w.

Nikoobakht, and Mostafa A. El-Sayed. 2003. “Preparation and Growth Mechanism of Gold Nanorods (NRs) Using Seed - Mediated Growth Method.” *Chemistry of Materials* 15 (16): 1957–62. https://doi.org/Doi 10.1021/Cm020732l.

Orendorff, Christopher J., and Catherine J. Murphy. 2006. “Quantitation of Metal Content in the Silver-Assisted Growth of Gold Nanorods.” *Journal of Physical Chemistry B* 110 (9): 3990–94. https://doi.org/10.1021/jp0570972.

P.S. Goyal, B.A. Dasannacharya, V.K. Kelkar, Manohar C., K. Srinivasa Rao, and B.S. Valaulikar. 1991. “Shapes and Sizes of Micelles in CTAB Solutions.” *Physica B: Condensed Matter* 174: 196–99.

Park, Kyoungweon, Sushmita Biswas, Sushil Kanel, Dhriti Nepal, and Richard A. Vaia. 2014. “Engineering the Optical Properties of Gold Nanorods: Independent Tuning of Surface Plasmon Energy, Extinction Coefficient, and Scattering Cross Section.” *Journal of Physical Chemistry C* 118 (11): 5918–26. https://doi.org/10.1021/jp5013279.

Park, Kyoungweon, Lawrence F. Drummy, Robert C. Wadams, Hilmar Koerner, Dhriti Nepal, Laura Fabris, and Richard A. Vaia. 2013. “Growth Mechanism of Gold Nanorods.” *Chemistry of Materials* 25 (4): 555–63. https://doi.org/10.1021/cm303659q.

Phenom-World BV. 2017. “Different Types of SEM Imaging – BSE and Secondary Electron Imaging.” *AZO Materials*. https://www.azom.com/article.aspx?ArticleID=14309.

Rodríguez-Fernández, Jessica, Jorge Pérez-Juste, F. Javier García De Abajo, and Luis M. Liz-Marzán. 2006. “Seeded Growth of Submicron Au Colloids with Quadrupole Plasmon Resonance Modes.” *Langmuir* 22 (16): 7007–10. https://doi.org/10.1021/la060990n.

Sau, Tapan K, and Catherine J Murphy. 2004. “Seeded High Yield Synthesis of Short Au Nanorods in Aqueous Solution.” *Langmuir* 20 (11): 6414–20. https://doi.org/10.1021/la049463z.

Scarabelli, Leonardo, Marek Grzelczak, and Luis M. Liz-Marzán. 2013. “Tuning Gold Nanorod Synthesis through Prereduction with Salicylic Acid.” *Chemistry of Materials* 25 (21): 4232–38. https://doi.org/10.1021/cm402177b.

Scarabelli, Leonardo, Ana Sánchez-Iglesias, Jorge Pérez-Juste, and Luis M. Liz-Marzán. 2015. “A ‘Tips and Tricks’ Practical Guide to the Synthesis of Gold Nanorods.” *Journal of Physical Chemistry Letters* 6 (21): 4270–79. https://doi.org/10.1021/acs.jpclett.5b02123.

Silva, José Adriano Da, and Mario R. Meneghetti. 2018. “New Aspects of the Gold Nanorod Formation Mechanism via Seed-Mediated Methods Revealed by Molecular Dynamics Simulations.” *Langmuir* 34 (1): 366–75. https://doi.org/10.1021/acs.langmuir.7b03703.

Sönnichsen, C., T. Franzl, T. Wilk, G. von Plessen, J. Feldmann, O. Wilson, and P. Mulvaney. 2002. “Drastic Reduction of Plasmon Damping in Gold Nanorods.” *Physical Review Letters* 88 (7):

774021–24. https://doi.org/10.1103/PhysRevLett.88.077402.

Stone, John, Stephen Jackson, and David Wright. 2011. “Biological Applications of Gold Nanorods.” *Wiley Interdisciplinary Reviews: Nanomedicine and Nanobiotechnology* 3 (1): 100–109. https://doi.org/10.1002/wnan.120.

Su, Gaoxing, Chi Yang, and Jun Jie Zhu. 2015. “Fabrication of Gold Nanorods with Tunable Longitudinal Surface Plasmon Resonance Peaks by Reductive Dopamine.” *Langmuir* 31 (2): 817–23. https://doi.org/10.1021/la504041f.

Tong, Wenming, Michael J Walsh, Paul Mulvaney, Joanne Etheridge, and Alison M Funston. 2017. “Control of Symmetry Breaking Size and Aspect Ratio in Gold Nanorods: Underlying Role of Silver Nitrate.” *Journal of Physical Chemistry C*, no. 121: 3549−3559. https://doi.org/10.1021/acs.jpcc.6b10343.

Usher, Al, D. C. McPhail, and Joël Brugger. 2009. “A Spectrophotometric Study of Aqueous Au(III) Halide-Hydroxide Complexes at 25-80 °C.” *Geochimica et Cosmochimica Acta* 73 (11): 3359–80. https://doi.org/10.1016/j.gca.2009.01.036.

Vincenzo Amendola, Roberto Pilot, Marco Frasconi, Onofrio M Maragò, and Maria Antonia Iatì. 2017. “Surface Plasmon Resonance in Gold Nanoparticles : A Review.” *Journal of Physics: Condensed Matter* 29: 48. https://doi.org/https://doi.org/10.1088/1361-648X/aa60f3.

Walsh, MJ, SJ Barrow, and Wenming Tong. 2015. “Symmetry Breaking and Silver in Gold Nanorod Growth - Supporting Information.” *ACS Nano*, no. 1: 1–9. http://pubs.acs.org/doi/abs/10.1021/nn506155r.

Xia, Younan, Xiaohu Xia, and Hsin Chieh Peng. 2015. “Shape-Controlled Synthesis of Colloidal Metal Nanocrystals: Thermodynamic versus Kinetic Products.” *Journal of the American Chemical Society* 137 (25): 7947–66. https://doi.org/10.1021/jacs.5b04641.

Yang, Wen Hui, George C. Schatz, and Richard P. Van Duyne. 1995. “Discrete Dipole Approximation for Calculating Extinction and Raman Intensities for Small Particles with Arbitrary Shapes.” *The Journal of Chemical Physics* 103 (3): 869–75. https://doi.org/10.1063/1.469787.

Ye, Xingchen, Linghua Jin, Humeyra Caglayan, Jun Chen, Guozhong Xing, Chen Zheng, Vicky Doan-Nguyen, et al. 2012. “Improved Size-Tunable Synthesis of Monodisperse Gold Nanorods through the Use of Aromatic Additives.” *ACS Nano* 6 (3): 2804–17. https://doi.org/10.1021/nn300315j.

Yousaf, Syeda Amber, and Salamat Ali. 2007. “Why Nanoscience and Nanotechnology? What Is There for Us? Introduction to Nanoscience.” *Journal of Faculty of Engineering & Technology*, no. January: 11–20. http://pu.edu.pk/images/journal/jfet/previous-pdf/FET07_02_Why Nanoscience and Nanotechnology f.pdf.

Yu, Chenxu, and Joseph Irudayaraj. 2007. “Quantitative Evaluation of Sensitivity and Selectivity of Multiplex NanoSPR Biosensor Assays.” *Biophysical Journal* 93 (10): 3684–92. https://doi.org/10.1529/biophysj.107.110064.

Zweifel, Daniel A., and Alexander Wei. 2005. “Sulfide-Arrested Growth of Gold Nanorods.” *Chemistry of Materials* 17 (16): 4256–61. https://doi.org/10.1021/cm0506858.